PREPARATION AND CHARACTERISATION OF GRAPHITISABLE CARBON FROM COAL SOLUTION

By

Bethuel Lesole Kgobane

Thesis submitted in partial fulfilment of the requirements for the degree

DOCTOR OF PHILOSOPHY

To the faculty of Natural and Agricultural Sciences
Department of Chemistry
Institute of Applied Materials
University of Pretoria
Republic of South Africa

Promoter:
Prof D Morgan
August 2006

DEDICATION

This research work is dedicated to my late brother Thabo Martin Makoe, my mother, grandmother, Kagiso, and the rest of the family for their unwavering support through thick and thin.

ACKNOWLEDGEMENT

I am greatly indebted to my research supervisor, Prof. D Morgan, for his invaluable guidance and encouragement, which made this work possible. I would like to extend my appreciation to the steering committee for this project and to the Director of the Institute of Applied Materials, Prof. W Focke, for their valuable suggestions and recommendations. Special thanks go to Pravina Maharaj for her moral and administrative support.

Special thanks are extended to Prof. R Merkle for teaching and allowing me the use of the optical microscope, to the Geology Department for providing polishing facilities, to Dr Verryn for XRD analysis of the results, to Prof. D de Waal and Mrs L C Prinsloo for teaching and allowing me the use of the Raman microscope, and to the Petrology Section of Coal and Mineral Technologies (Pty) Ltd at the SABS, in particular Mrs V Du Cann for analysis of the coal samples. Further appreciation goes to the Department of Chemical Engineering for miscellaneous support. Many thanks go to Prof. R Falcon for her valuable suggestions for this thesis.

The financial support for this research, from the National Research Foundation (NRF), Eskom-PBMR, Suprachem and the Department of Chemistry is gratefully acknowledged. My sincere thanks also go to Kumba Resources Ltd for providing the coal samples. I further extend special thanks to Ferro Industrial Chemicals Ltd and SA Dow (Pty) Ltd for providing the carbon additives.

I wish to take this opportunity to thank all my friends at the University of Pretoria for their warmth and hospitality, which made my work at the University a wonderful experience. Sincere thanks goes to Mr M Mthembi for his contribution to the work and to all co-researchers in the Institute of Applied Materials who were so kind and supportive in my work. Lastly, I would like to acknowledge the support of Dr T Mathe, Mr M Phaladi and my family throughout this process.

ABSTRACT

The energy demands by the industrial world are continuing to rise, while the rate of new oil discoveries is falling. Within the next 30 years, available petroleum supplies are likely to fail to meet the demand, and oil will no longer be able to serve as the world's major energy source. Coal, being relatively abundant worldwide and potentially adaptable for use in existing plants that have been engineered for petroleum use, can serve as an inexpensive substitute for, or successor to, the more expensive oil fuels in use today. Graphitisable carbon is one of the high-value products from petroleum as its value lies partly in the nuclear industry. Making graphitisable isotropic carbon from well-purified coal is therefore a primary motivation for this study. However, its purity is far too low.

Substantial purification is obtained by dissolving the organic part of coal in dimethylformamide with the addition of a little alkali. Results indicated that more than 90 % of the organic part of a 10 % ash flotation product dissolved in N, N-dimethylformamide on addition of 10 % NaOH. The bulk of the impurities are removed by centrifugation and the dissolved organic material is recovered by water precipitation. Subsequently, the ash level is lowered from 10 % in the coal to < 1.60 % in the coal extracts at a washing efficiency of 33 %. The addition of Na_2S (the molar ratio of NaOH to Na_2S was 1:1) lowered the ash level further to 0.70 %.

The coal extract solution obtained showed an absorbance of 1.00 with an organic content of 8 %. However, addition of sodium sulphide to the extraction medium at 25 ± 1 ^{o}C lowered the organic content to 5.6 %. At high temperature of 90 ± 2 ^{o}C, the organic content was further lowered to 2.6 % with subsequent loss in colour.

The coal extract obtained by water precipitation showed low C/H atomic ratio on the addition of S^{-2}. Nucleophiles such as cyanide, thiosulphate made no substantial change to the hydrogen content nor the degree of extraction.

On coking by step heating under nitrogen to 480 ^{o}C at a rate of 10 ^{o}C min^{-1} for 1 h, then to 900 ^{o}C with a soaking period of 2 h, the coal extracts melt, then reorganise into a liquid crystal phase around 500 ^{o}C, which then solidifies into a semi-coke on further heat treatment. The heat-treatment of the coal extracts produced 75 % carbon yield. When polished specimens of the cokes were observed by reflectance microscopy, flow textures with domain sizes of a few to many microns were observed. Isotropic, poorly graphitising cokes showed little or no structure. Anisotropic cokes were produced when these domains of liquid crystal grew and coalesced. The cokes were found to be highly graphitisable. However, in the heat-treated coal extracts prepared at high temperature, the liquid crystal domains were graphitisable but appeared not to have coalesced. Nevertheless, the random orientation of the domains allowed isotropic blocks to be formed with extremely low crystallinity. The precursors that form these liquid crystals are generally materials known to have a high aromatic carbon content. The precursors that form these liquid crystals are generally materials with a high purity and aromatic carbon content, and low in heteroatoms.

Optical microscopy of the polished samples prepared at 90 ± 2 ^{o}C revealed surfaces with much less ordered coke, having smaller crystalline domains than the heat–treated coal extracts derived at room temperature. Essentially, isotropic graphites were obtained. Addition of S^{-2} produced an extensive flowing texture, and a highly crystalline domain cokes. The carbon yield lowered. The graphitisability of the carbon improved. The X-ray diffraction data on the graphitised carbon showed that the degree of graphitisation decreased in the following order: high S^{-2} coal extracts derived at room temperature (GSF-25RT) > high S^{-2} coal extracts derived at high temperature (GSF-25HT) and no S^{-2} coal extracts derived at room temperature (GSF-0RT) > no S^{-2} coal extracts derived at

high temperature (GSF-0HT), corresponding to 79 > 75 % and 67 > 25 % respectively. The interlayer spacing (d_{002} -value) of the graphites follows the order GSF-25RT (3.37Å) < GSF- 25HT (3.38 Å) and GSF-0RT (3.38 Å) < GSF-0HT (3.42 Å). Subsequently, the Raman spectroscopy, consistent with the X-ray diffraction data, showed the ratio of the d-peak (degenerate) to g-peak (graphitic) in the order: GSF-0HT < GSF-0RT and GSF-25HT < GSF-25RT, corresponding to 1.26 <1.75 < and 6.7 < 7.0 respectively.

Because the quality of the coke depends on the nature and quality of the starting material, addition of the carbon additives in the starting material prior heat-treatment affected the flow texture of the coke. The carbon black, which has a spherical shape, forms aggregates that disperse much more easily than the flat chains of aggregates of acetylene black. The difficulty in dispersing the carbon additives was, however, overcome by using a high-shear mixer. Analysis of the coal extracts revealed that the hydrogen content in the coal extracts decreased linearly on addition of the carbon additives, favoring dehydrogenative polymerisation. The addition of carbon additives in the coal extract solution produced an isotropic carbon on heat treatment. Optical microscopy of the resin-mounted cokes revealed decreasing size of the crystalline domain with increasing dosage of the carbon additives. The optimum amount of carbon additives required was found no to exceed 0.44 %. Beyond this threshold, the anisotropy of the cokes could not be observed through the resolution of the optical microscope. In addition, the amounts of volatiles released were found to decrease with increasing dosage of the carbon additives.

At low dosage of the carbon additives, the heat-treated coal extracts produced graphitisable isotropic carbon with low level of crystallinity. However, at high dosage of the carbon additives, the cokes did not graphitise. The temperature of graphitisation decreased from 2976 to 2952 ^{o}C with increasing dosage of the carbon additives. The decreasing order of graphitisation was 69 > 61 > 62 %, corresponding to 0.44 > 0.88 > 1.60 acetylene black. With the addition of carbon

black, the decreasing order of graphitisation was 57.7 > 56.5 > 51.5 %, corresponding to 0.44 > 0.88 > 1.60 wt % respectively. The interlayer spacing $d_{002,}$ increased in the same order, suggesting a shift towards a turbostratic and formation of a poorly graphitised, and turbostratic carbon. Raman spectroscopy revealed that the intensity ratio R of the g to the d peak decreased with increasing dosage of the carbon additive.

Cokes produced from the coal extracts prepared at 25 ^{o}C but without S^{-2} showed also a remarkable degree of flow texture. Its crystalline domain units were relatively small. The resin-mounted coke samples observed under an optical microscope (objective x 25) showed reduced flow texture with the addition of carbon black. The graphitisability of the resultant cokes also decreased on addition of carbon black. The optimum dosage observed for reducing the flow texture without reducing the crystallinity was found to be < 0.22 %.

Improved degree of graphitisation of the carbon was studied on addition of iron (lll) compounds. Iron (lll) compounds showed a promising improvement in the graphitisability of the carbon when added in small amounts. The intracellular hard carbon is converted to soft carbon, thereby improving the degree of graphitisation. The overall effect was a more isotropic graphitic carbon but the degree of graphitisation obtained was far too low: on addition of 1 % and 3 % (by wt) of iron (lll), the compounds were 21 % and 27 % respectively. Oxygen intrusion into the precursor's coal material prior to heat treatment is thought to have inhibited the degree of graphitisation. Increasing the amounts of the iron (lll) compound and prohibiting the intrusion of oxygen during mixing could improve the graphitisability of carbon. However, the optimum amount to be used remains an important subject to be explored in future.

TABLE OF CONTENTS

Chapter 3

Chapter 4

Chapter 5

CHAPTER 6

Chapter 9

LIST OF FIGURES

LIST OF TABLES

TABLE PAGE NO

LIST OF SCHEMES

LIST OF ABBREVIATIONS

CSIR	Council for Scientific and Industrial Research
CY	Carbon yield
DBP	Dibutylphthalate
DMA	Dimethylacetamide
DMF	dimethylformamide
DMSO	Dimethylsulphoxide
ddpm	Dial divisions per minute
FIC	Fibre-bundle image compression
FWHM	Full width at half maximum
HMPA	Hexamethyl phosphoramide
ISO	International Organization for Standardisation
NMP	N-methyl-pyrrolidinone
NMR	Nuclear magnetic resonance spectroscopy
NRF	National Research Foundation
PBMR	Pebble Bed Modular Reactor
pm	Picometer
ppm	Parts per million
SABS	South African Bureau of Standards
SEM	Scanning electron microscope
TGA	Thermogravimetric analysis
TMU	Teramethyl urea
UV	Ultra-violet

SAMPLE CODES

Each photomicrograph is labelled with a code, e.g. RSF-25 RT, which signifies that it is representative of the sulphide-derived Refcoal (R), containing 25 g Na_2S (NaOH:Nu^{-1} molar ratio of 1:1) and obtained at room temperature (RT). For the corresponding coke and graphite, the codes are CSF-25 RT and GSF-25 RT respectively. The other labels follow the same pattern. Room-temperature extraction means extraction at 25 ± 1 °C, while high-temperature means extraction at 90 ± 2 °C. Some of the selected codes are listed below:

RCN-00RT	Refcoal without cyanide and prepared at room temperature
RCN-06RT	Refcoal with cyanide content of 6g and prepared at room temperature
RCT-00RT	Refcoal without thiosulphate and prepared at room temperature
RCT-06RT	Refcoal with thiosulphate content of 6 g and prepared at room temperature
CSF-0HT	Coke with no sulphide obtained from high temperature prepared coal extracts
CSF-0RT	Coke with no sulphide obtained from room temperature prepared coal extracts
CSF-25HT	Coke with sulphide content of 25g obtained from high temperature prepared coal extracts
CSF-25RT	Coke with sulphide content of 25g obtained from room temperature prepared coal extracts
GSF-0.0HT	Graphite without sulphide and obtained from high temperature prepared coal extracts
GSF-25HT	Graphite with sulphide content of 25g and obtained from high temperature prepared coal extracts
GSF-0.0RT	Graphite without sulphide and obtained from room temperature prepared coal extracts

GSF-25RT	Graphite with sulphide content of 25g obtained from high temperature prepared coal extracts
GSF-0.44CB	Graphite withcarbon black of 0.44 % and prepared from room temperature derived suphide coal extracts
GSF-0.88CB	Graphite with carbon black of 0.88 % and prepared from room temperature derived suphide coal extracts.
GSF-0.44 AB	Graphite with acetylene black of 0.44 % and prepared from room temperature derived suphide coal extracts
GSF-0.88AB	Graphite with acetylene black of 0.88 % and prepared from room temperature derived suphide coal extracts
CCB-0.15	Coke prepaped from the room temperature derived coal extracts with the addition of 0.15 % carbon black
GCB-0.22	Graphite prepared from room temperature derived coal extracts with the addition of 0.22 % carbon black
Gfe-1	Graphite prepared from the room temperature derived coal extracts with the addition of 1 % of iron (lll) compound
Gfe -3	Graphite prepared from the room temperature derived coal extracts with the addition of 3 % of iron (lll) compound

CHAPTER 1

INTRODUCTION

Eskom South Africa, in collaboration with other international energy corporations, has ventured into the Pebble Bed Modular Reactor (PBMR) project to boost its electricity supply. The PBMR is a type of High-Temperature Gas Reactor (HTGR), which means that its core is gas-cooled [1, 2]. Helium gas removes the heat generated by the nuclear fission from the reactor core, in contrast to other conventional water-cooled energy reactors. The technology was extensively tested in Germany in the 1960s and 1970s and elsewhere. With the ever-increasing demand for electricity in the developing world, it is hoped that the PBMR will be the ultimate effective solution to overcoming some of the electricity supply problems currently experienced in areas far remote from the coalfields where the demand for electricity is huge. Eskom believes that it would create a market, both within South Africa and in the rest of the world, for 30 reactors per year within the next two decades. Such a project venture in nuclear energy would be a powerful strategy in the realisation of clean energy for the African Renaissance, and for the New Partnership for African Development (NePAD) as a whole [3].

The PBMR consists of a structure made of synthetic graphite blocks (the reflectors), contained within a steel pressurised vessel. Depending on their position within the structure, the blocks are of differing qualities, with the inner ones able to withstand the high temperatures (up to 950 ^{o}C) and high neutron fluxes experienced during operation. The outer blocks are loaded with boron carbide, which acts as a neutron shield, to prevent activation of the steel shell.

The fuel consists of spheres of graphite (the pebbles), 60 mm in diameter, which contains many uranium dioxide beads, evenly distributed throughout (Fig. 1.1). The uranium dioxide spheres are coated to contain the fission products. The

coatings, applied by means of chemical vapour deposition, consist of, firstly, two layers of carbon with differing porosities, then the main barrier layer of silicon carbide, then a third carbon layer.

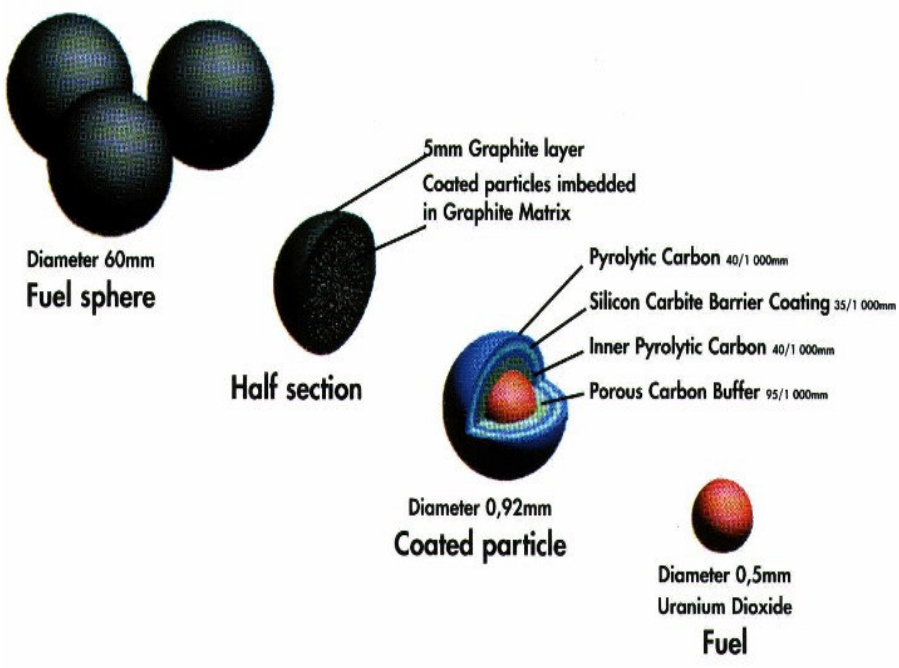

Figure 1.1: Fuel element design for PBMR [3]

The coated beads are mixed with a fine powder consisting of 75 % natural graphite and 25 % synthetic graphite, as well as a binder resin, and are then moulded into the spherical shape. After being hardened at about 1900 ^{o}C, the pebbles are ready for use. The uranium used in the start-up fuel is 4 % enriched and the equilibrium fuel has a uranium enrichment of 8 % [3].

During normal operation, 440 000 pebbles, of which 310 000 contain uranium oxide and 130 000 are pure graphite spheres that serve as additional nuclear moderators, are loaded into the top of the reactor and discharged at the bottom where their degree of “burn-up” is measured. The pebbles are then either returned to the reactor or, if fully used, retained within the reactor building to allow most of the decay of the short-lived fission products to take place. To

remove the heat generated by the nuclear reaction, helium gas at 450 ^{o}C is passed through the pressure vessel from the top. It passes between the fuel pebbles and then leaves the bottom of the reactor vessel at about 900 ^{o}C. The hot gas then passes through a conventional gas system to drive electric generators, giving a useful capacity of about 165 MWe. The helium used as a coolant for the PBMR is corrosion-resistant and has good heating properties (having a specific heat that is much greater than CO_2), it does not condense and can therefore operate at any temperature, it has a negligible neutron-adsorption cross-section and can be used in a direct cycle, driving a gas turbine with high efficiency [2]. The modular nature of the system would allow ten such reactor/generators to be built on a site, sharing services and a single control room.

The reactor is described as being inherently safe because the silicon carbide layer around the uranium oxide beads is able to contain essentially all the fission products up to a temperature of 2 000 ^{o}C [1, 2]. If the coolant helium stopped flowing, the reactor would warm up to about 1 350 ^{o}C, at which point the negative coefficient of criticality would bring the nuclear chain reaction to a close. The fission products (equation 1.1) resulting from radioactive decay would continue to heat the fuel until, at a temperature of approximately 1600 ^{o}C, the heat losses through the reactor shell would balance the heat production, and the core would begin to cool.

$$ {}_{92}U^{235} + {}_{0}n^{1} \rightarrow {}_{92}U^{236*} \rightarrow F_1 + F_2 + n + \text{energy} \qquad (1.1) $$

It is therefore impossible for the reactivity of the fission products to be lost. In addition, the thermal mass of the reactor core is such that temperature changes occur slowly, over several days, allowing problems to be solved under conditions that would not engender panic.

The graphite used for the construction of the reactor core contributes to the safety of the design due to its very high sublimation point, in an inert atmosphere,

of more than 3 000^{o}C and its slow rate of oxidation, even at the operating temperature, in air. The graphite is required to be of high purity and physical or structural integrity. Graphite is chosen as a moderator in nuclear fission reactors because it is the most readily available material with a low thermal neutron-capture cross-section, allowing efficient use of the neutrons generated [4, 5]. The thermal neutron-capture cross-section is usually expressed in terms of an equivalent boron concentration by summing the concentrations of the individual impurities (elements, weighted by their thermal neutron-capture cross-section).
The physical structure of the graphite is of crucial importance for efficient operation and a long life. The graphite blocks must be highly isotropic to give the best dimensional stability under irradiation and to obtain uniform thermal expansion in all directions [6 - 8]. The synthetic graphite used to manufacture the fuel pebbles must be very fine, but graphite, again due to its anisotropic structure, is very difficult to mill, tending merely to flake along the planes of crystal weakness. Essentially, all of the graphites employed in fission reactors as moderators and most, but not all, of the graphites used in fusion systems are derived from blocks manufactured from petroleum or pitch cokes. Cokes employed to manufacture conventional nuclear graphites are classified as needle cokes from petroleum, pitch cokes, or Gilsonite pitch cokes from the asphalt of Santa Maria cokes. Both needle cokes and pitch cokes yield anisotropic graphite blocks, while Gilsonite pitch cokes and Santa Maria cokes yield isotropic blocks [8].

Coke made by pyrolysis of the coal extracts does not always graphitise on heating to 3 000 ^{o}C as a pre-ordering of the atoms is necessary. The coke is formed when the precursor, on heating, liquefies and forms domains of discoidal liquid crystal prior to cross-linking, with the loss of volatile material. Anisotropic needle cokes are prepared when the domains of liquid crystal grow and coalesce into a semi-coke on heat treatment. These are highly graphitisable, but difficult to convert into isotropic blocks. Cokes in which the liquid-crystal domains do not coalesce may be graphitisable, but the random orientation of the domains does

not allow isotropic blocks to be formed. Precursors that form these liquid crystals are generally materials with high aromatic carbon content.

At graphitisation temperature carbon looses most of its impurities, except for carbide elements, boron in particular, which tend to come off too slowly at high temperatures. Sulphur, if present in high proportion, comes off whilst adversely disrupting the structure, causing “puffing”. The lower the original load of impurities, the purer the final product.

1.2 Aim of the study

Coal is a relatively abundant mineral solid fuel worldwide and potentially adaptable for use in existing plants that have been engineered for petroleum use. When purified, coal can serve as an inexpensive substitute for, or successor to, the more expensive oil fuels in use today. The molecules present in coal have the required structures to substitute petroleum and yield cokes that graphitise well. It was therefore the aim of this study to:

- Examine the cokes prepared from coal purified by Refcoal process
- Evaluate the graphitised cokes (see Scheme 1.1).

1.3 Contents of the study

The dissertation consists of nine chapters. Chapter 1 has already given the background to the purpose of this study. Chapter 2 discusses the relevant literature on coal and its purification. Chapter 3 looks at the chemistry of the carbonisation of the coal. Chapter 4 examines the graphitisation process. Chapter 5 discusses the methods of graphite characterisation. Chapter 6 investigates the instrumentation that can be used for analysing graphitisable carbons. Chapter 7 details the experimental methods. Chapter 8 discusses the experimental results and the last two Chapters (9 and 10) the conclusions and the references respectively.

Scheme 1.1: Project outline of coal purification process, through coke formation to graphitisable carbon [9,10]

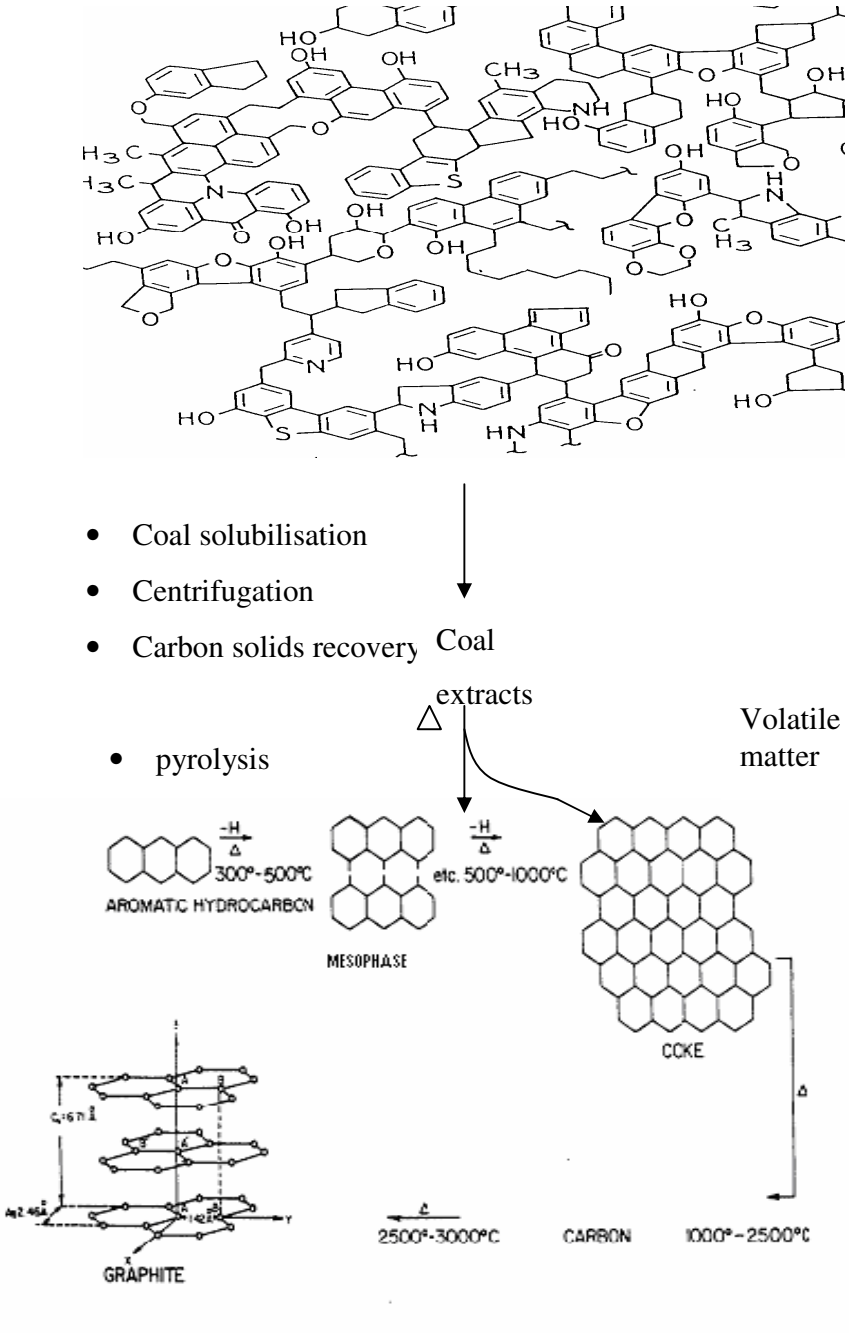

CHAPTER 2

COAL

The quality of coke and the graphite subsequently produced is determined primarily by the purity of the starting material and its biochemical formation. This chapter seeks to explain some of the previous areas studied that have a great impact on the science of coal and its purification. Previous work on coal solubilisation is discussed. The biochemical formation and the hypothesised structure of coal detailed are important to understanding the choice of the solvent-reagent suit needed to improve the purity of coal. The effects of solvents and additives on coal solubilisation are also discussed.

2.1 Coalification process

Coal is defined as a readily combustible rock containing more than 50 % by weight and more than 70 % by volume of carbonaceous material [11]. This carbonaceous material resulted from the accumulation and slow decay of plant remains under water. It involves a continuous series of alterations through the coalification process from living material > lignite > subbituminous coal > anthracite. Such succession in properties through the coalification process is called 'metamorphism', which occurred over a long period of time. The changes in the plant materials are reported to involve a *biochemical* process of diagenesis and a *geochemical* process of metamorphism [12].

The degree of coalification or 'rank' of coal increases progressively from lignite, through low-rank coal to high-rank coal, and to anthracite. This transformation of the vegetable matter into peat and then into coal of different ranks is apparently the result of decomposition due initially to bacterial action and dehydration, then to devolatilisation and densification due to chemical and geodynamic processes [11].

2.1.1 Biochemical coalification

Biochemical coalification is associated with changes within the plant residues in the sedimentary basin at low temperature and pressure to form macerals. It is described by processes defined by the availability of oxygen, viz. disintegration, mouldering, peatification and putrefaction. *Disintegration* of plant material into water and carbon dioxide occurs under normal conditions of freely available oxygen. If conditions change, some resisting plant remains are conserved into liptobiolites consisting largely of relatively stable exinite macerals [13, 14]. *Mouldering* is the process during which coal is produced in an environment of diminished oxygen supply. Bacterial and fungal activities cause the material to become enriched in carbon and oxygen, but poorer in hydrogen. The abundance of sclerotinite in South African coals suggests that mould was of importance in their formation. *Peatification* takes place by way of bacterial decomposition and weakly oxidising conditions, resulting in the formation of humic acid. In the acidic reducing environment, vitrinite and accompanying pyrite are formed, while inertinite macerals are derived from the exposure of plant remains to a lower level of acidity and stronger oxidising conditions [13, 14, 15]. Swamp fires have resulted in the formation of certain varieties of fusinite and semi-fusinite macerals, and these represent fossil charcoal. *Putrefaction* (fermentation) occurs under reducing conditions. A relatively deep water cover is also a necessary condition for this process in which anaerobic bacteria remove the oxygen of the vegetable matter, converting it into hydrogen-rich material [13, 14].

2.2.2 Geochemical coalification

Geochemical coalification precedes biochemical coalification in the absence of microorganisms. The progressive development of peat occurs with increasing build-up of deposition and coverage by incoming sediments. The plant undergoes changes known as carbonification or geochemical coalification, resulting in a coal rank increase [13]. Accompanying such rank increase is a

decrease in porosity due to an increasing overburden pressure with depth. According to Stach *et al*. (14), the porosity of coal falls very rapidly in the early stages of coalification and serves as a good diagnostic indicator for peat and brown coals. Physico-structural and chemical changes take place as coalification progresses. The carbon content is reported to increase, and the oxygen and hydrogen contents decrease with the series. The reactivity of each series decreases from lignite to anthracite. While the moisture content decreases, the porosity falls. This is thought to serve as a diagenetic indicator for compressible peats and brown coal.

The difference in plant materials, the extent of their decomposition, and the subsequent action of pressure and heat during geochemical coalification determine the rank of the coal. The degree of coalification is estimated from optical properties such as the reflectivity of vitrinite, which is dependent on the chemical composition of the coal. Stach *et al.* (14) reported that Francis estimated that a period of eight million years is required for the production of bituminous coal from peat.

Physical change occurs as coalification progresses through bituminous coal to anthracite (Fig. 2.1). The top row of hexagons represents the aromatic nuclei, which slowly coalesce into larger clusters, while the lines, or aliphatic cross-links, are slowly removed during increasing coalification. The second row depicts the increasing orientation of elementary aromatic elements parallel to the bedding planes. Static pressure thus causes such physical changes as a decrease in porosity and the reorientation of the elementary aromatics, known as micelles [14]

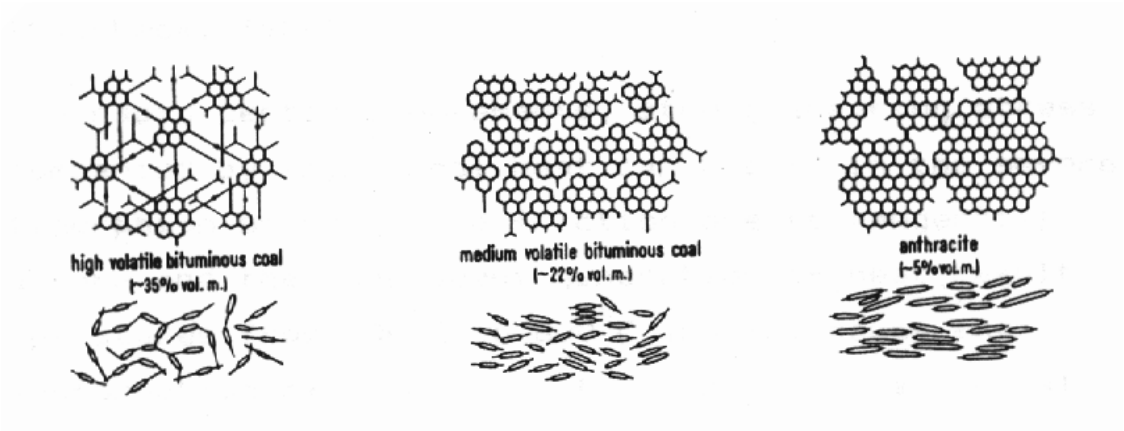

Figure 2.1: Physical changes in coalification from bituminous coal to anthracite [14]

Other physical changes are a decrease in the moisture content and an increase in the specific gravity as a result of increasing compaction with depth. Research has shown that tectonic pressure might not be the cause of the increased rank associated with regions of folds [16]. Instead, sediments and coal were buried to great depths in the foredeeps associated with ore-genesis before the onset of foldings. Consequently, the rocks were subjected to greater heating, resulting in an increase in rank. However, rapid tectonic movements occurring along the faults and over thrusts during earthquakes are reported to have occasionally caused a local rise in rank due to the concentration of frictional heat [16].

Such movements and frictional forces may result in the severe metamorphism of coal. The friction due to tangential pressure and the resultant heat generation were accompanied by a temperature rise from 300 ^{o}C to 800 ^{o}C, which may have caused the transformation of anthracite to graphite [14]. Chemical changes indicate the degree of increasing coalification in the transformation from wood to peat, lignite and bituminous coal, and to anthracite (see Table 2.1). An increase in carbon with an accompanying decrease in the hydrogen, oxygen and nitrogen contents are a reflection of metamorphism or rank increases.

Table 2.1
Coalification through time, pressure and heat
(dry ash-free values) [11]

	C	H	O	N
		%		
Wood	50.0	6.0	43.10	-
Peat	58.9	5.1	33.10	2.6
Lignite	71.0	4.4	23.10	1.2
Bituminous	81.4	5.4	10.10	1.9
Anthracite	92.9	3.1	2.40	0.9

The transformation of the vegetable matter into peat and then into coal of different ranks is reported to be the result of decomposition due to bacterial action, then dehydration, devolatilisation and densification due to chemical and geodynamic processes [11]. Factors such as heat, pressure and long periods of time determined the transformation from peat to lignite to subbituminous coal to bituminous coal, and then to anthracite. It is the porosity and moisture content of coal that decrease with pressure. In a progressive transformation of peat to anthracite, an increase in the amount of fixed carbon and a decrease in the amount of moisture, oxygen and volatile matter have been documented.

The different coalification behaviours of the individual macerals as based on the H/C and O/C ratios (Fig. 2.2) has been reported [14]. The carbon content increases rapidly with depth as the oxygen-rich substances, such as cellulose and hemi-cellulose, are decomposed microbiologically. The increase in carbon content is estimated by Stach *et al.* [14] to reach a maximum of 64 % with the fall in moisture content. Such changes in the coalification process are thought to be the result of increased compression.

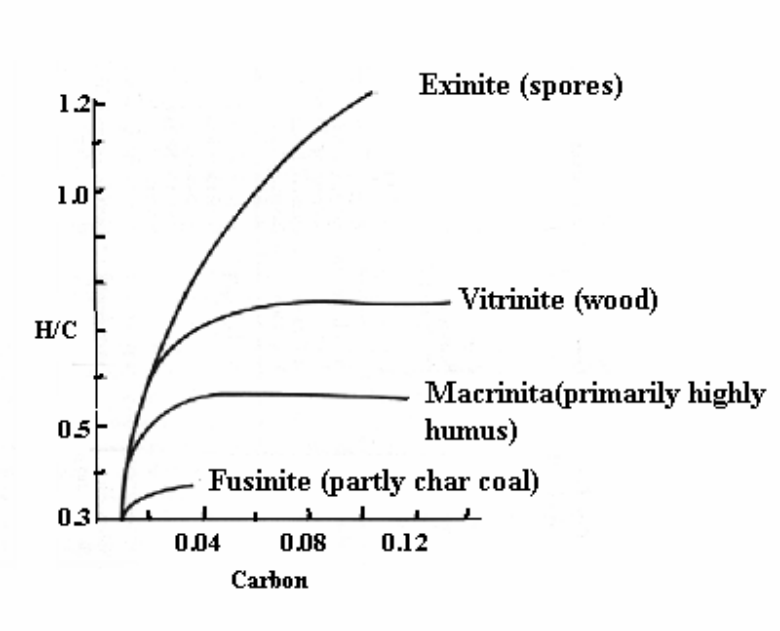

Figure 2.2: Coalification of different macerals based on H/C and O/C atomic ratio [14, 17]

2.2 Hypothetical structure of coal

Coal is thought to be a three-dimensional structure, crossed-linked, viscoelastic glassy macromolecular solid that is permeated by material of low molecular weight and the behaviour of which is similar to that of cross-linked polymeric networks [9, 11, 18, 19]. This theory attempts to describe properties such as the degree of cross-linking and the glass transition temperatures of the network nature of coal. Part of the evidence for this theory is that coal behaves as an elastic, not plastic, solid. This suggests that the cross-linkages are covalently fixed. Given *et al.* in the book edited by Marsh [20] reported a macromolecular/molecular two-phase system – the host/guest or rigid and mobile phase model. This model suggests that a substantial proportion of the organic part of coal – the mobile phase or "guest" – is composed of a phase of low molecular weight, physically trapped within an immobile phase or "ghost" of high molecular weight. The latter is extensively cross-linked.

The inorganic constituents, consisting partly of minerals such as kaolin ($Al_2Si_2O_5.(OH)_4$) and free silica entangled in a macromolecular structure of condensed aromatic rings, are hypothesised to form large units of 'bridges' or cross-linkages of aliphatic and/or ether groups, conferring on them a certain structural order [21, 22]. The removal of the cross-link bonds, viz. the bridges of hydrogen bonding (hydrogen bonding is reported to be a major force holding the minerals at the maceral boundaries) in the C-C and C-O bonds, provides some flexibility in a cross-linked structure. The result is differential swelling of the coal macerals as well as stresses that contribute to chemical comminution. The solvent-reagent mixture facilitates the reorganisation of aromatic units into a graphite-like structure during pyrolysis of the coal extracts [23, 24].

The mineral matter in coal has a detrimental effect on its utilisation for combustion, gasification, carbonisation, liquefaction, etc. purposes. The combustion of high-sulphur and high-ash coal leads to adverse environmental and other deleterious effects. Acid rain resulting from the emission of sulphur dioxide (SO_2) has a harmful effect on agriculture and destroys the ecological balance. The demineralisation of coal prior to its combustion and carbonisation is therefore important for environmental protection. The microscopically recognisable organic and inorganic constituents from the sedimentary rock are discrete fossilised plant fragments called 'macerals' [24].

Most of these minerals are in form of aluminosilicates, carbonates, sulphides and silica. The abundant oxygen in the macerals follows carbon and hydrogen and is found combined with other elements in coal to form various functional groups, such as carboxyl (CO_2H), carbonyl (C=O), and the methoxy ($-OCH_3$) and phenol (OH) groups (Fig. 2.3) [25, 26]. The mineral matter includes all inorganic non-carbonaceous material found in coal. This excludes carbon, nitrogen, sulphur and oxygen, and is estimated by an equation (equation 2.1) [11].

$$\% \text{ Mineral matter} = \% \text{ ash} + \% \text{ pyritic S in coal} + 0.8\,CO_2 \text{ in coal} - 1.1 \text{ x } SO_3 \text{ in coal} + 0.5 \text{ x } \% \text{ Cl in coal} \quad (2.1)$$

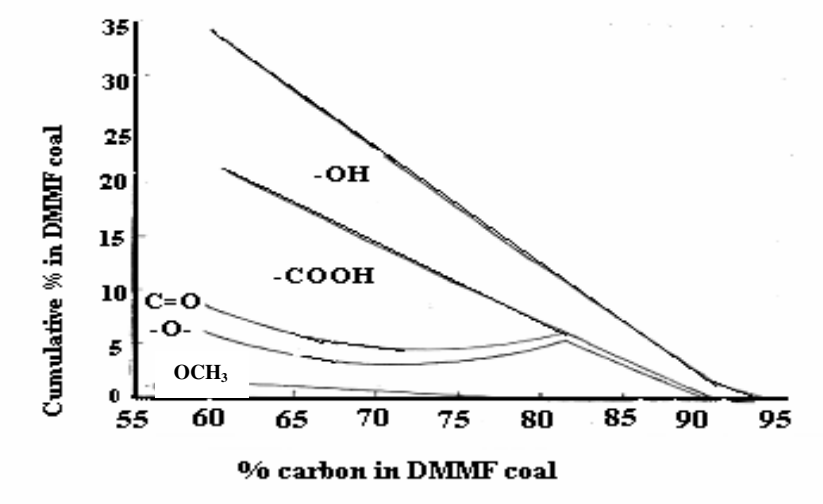

Figure 2.3: Distribution of oxygen functionality in coals [15]

The decreasing oxygen content of wood, peat, and lignite with increasing rank of coal, and expressed on a dry, mineral-matter-free basis, is shown in Table 2.2. Wood appears to be oxygen-rich, while anthracite is oxygen-poor but carbon-rich. The higher the oxygen content, the lower the carbon content.

Table 2.2

Chemical composition of wood, peat and various coals [27]

Carbonaceous materials	**C**	**H**	**O**	**N**
		%		
Wood	50	6.3	42.7	1.0
Peat	57	5.2	36.8	1.0
Lignite	65	4.0	30.0	1.0
Low-rank coal	79	5.5	14.0	1.5
Medium-rank coal	88	5.3	5.0	1.7
Anthracite	94	2.9	1.9	1.2

The surface area of coal is related to the plasticity of the coal and its agglomerating properties during heating. The release of volatile matter from the surface during heating becomes an important factor in the quality of coke.

2.3 Coal macerals

Macerals are petrographically distinct units of vitrinite, exinite and inertinite seen in thin and polished sections of coal and are analogous to minerals in ordinary rocks [12]. However, the physical and chemical properties change during geochemical coalification so that they cannot be considered as being identical with minerals [13]. Stach *et al*. [14] stated that Stopes first used the term 'maceral' for a constituent of coal isolated by maceration, from the Latin *macerare* meaning 'to soften'. The contrast between the macerals appeared when polished sections of a resin-mounted coal sample were observed under a microscope using an oil-immersion lens [13]. Though distinguishable under the microscope, their properties are different. However, the differences become smaller as the rank increases (Fig. 2.4).

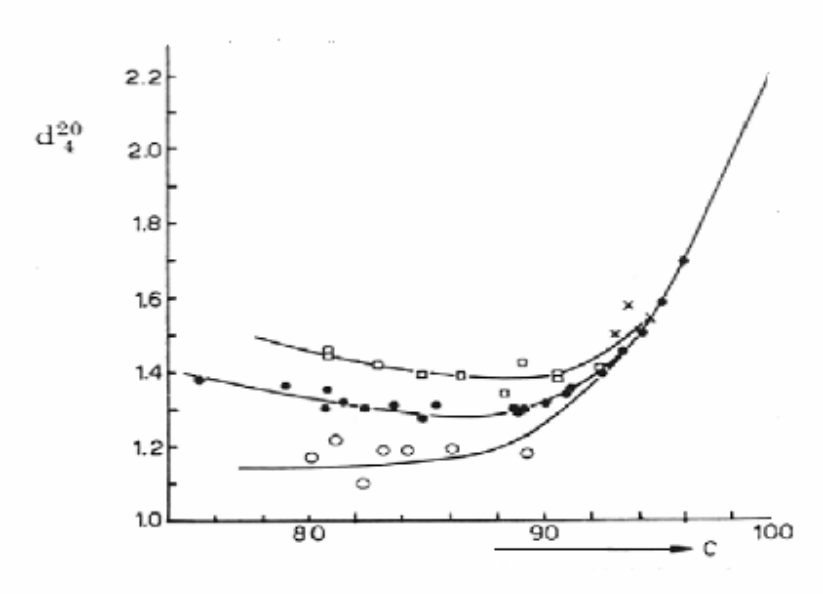

Figure 2.4: Densities of coal macerals

• Vitrinites, 0 Exinites, Micrinites, X Fusinites [16]

Vitrinite is a relatively hydrogen-rich maceral; it is composed of the humic material associated with peat formation and is formed from the coalification of lignin structures [12, 14]. It is a major petrographic constituent of coal in Britain, opaque and with a reflectance of 2.5 % – 6.0 % [27]. Vitrinite is a relatively reactive maceral and its softening point increases with the degree of oxidation, with a concomitant decrease in reactivity [28].

Exinite is also hydrogen-rich and originates from spores, cuticular matter, algae, resins and waxes. Carbonisation of this maceral is reported to give predominantly tar and gases. Unlike vitrinite and exinite, inertinite is found to be poor in hydrogen but rich in oxygen. During carbonisation, inertinite is thought to remain inactive, whereas vitrinite melts to varying degrees, while exinite produces tar on heat decomposition [14].

Macerals rarely occur by themselves but are usually associated with macerals of the same group or with other groups. These associations are known as microlithotypes [14]. The American Geological Institute (A.G.I.) [12] defined them as a typical association of macerals in humic coals, occurring in bands at least 50 microns wide. Macerals and microlithotypes comprise the four visible banded constituents in humic coals, called lithotypes. The lithotypes are classified according to their different physical and chemical properties and are named vitrain, clarain, durain and fusain. Vitrain is the bright, black lithotype, which breaks into roughly cubical forms and has a conchoidal fracture. In humic acid coals, vitrain is common and consists of the microlithotype group's vitrite and clarite.

Vitrite comprises vitrinite, while clarite is composed of vitrinite and exinite. The vitrinite content in each of the microlithotypes is in excess of 95 % [14]. Clarite is characterised as being semi-bright with a silky lustre and a sheetlike, irregular fracture. It contains fine bands of durain, which distinguishes it from vitrain [12].

The fine bands are less than 3 – 10 mm in thickness and can be composed of the microlithotype groups' vitrain, clarite, durite, trimacerite, as well as the microlithotype fusinite.

Durite contains at least 95 % of both exinite and inertinite, whereas fusite consists of more that 95 % fusinite. Trimacerite comprises the three maceral groups, as the name implies, namely vitrinite, exinite and inertinite, in varying proportions but always in excess of 5 % [14]. Durain forms the dull, matte lustre bands, grey to brownish-black in colour with granular fracture [12]. The bands are greater than 3 – 10 mm in thickness and usually consist of durite and trimacerite, and sometimes clarite, which is rich in exinite. Fusain has a silky lustre and a fibrous structure. It is friable and black, occurring in strands or fibres, and is soft when mineralised [12]. It is composed of microlithotype fusinite. The environment in which fusain is formed was very dry and owing to the strong resemblance between fusain and charcoal, it is also believed by van Krevelen (1951), as reported by Stach *et al.* [14], that fires could have resulted in the formation of this lithotype.

South African coals are predominantly of low rank, are inertinite-rich and possess a high mineral content [15]. Investigations into the maceral group content of the seams mined in South Africa has shown that the average distribution is as follows: vitrinite 49 %, exinite 4.4 %, inertinite 41.4 % , minerals 5.2 % and remaining is moisture [29]. The mineral distribution content of vitrinite and exinite are low compared with that of inertinite, which shows the opposite trend. In contrast, European coal shows the following maceral distribution: vitrinite 49 %, exinite 4.4 %, inertinite 14 % and minerals 3 % [15].

2.4 Reflectance of macerals

The reflectance of macerals or other particles in coal is described as the proportion of directly incident light (expressed as a percentage) that is reflected

from a plane of a polished surface under specific conditions of illumination. This property is related to the aromaticity of the organic compounds in the coal and it increases progressively for all the macerals as the rank of coal increases. Its measurement is taken by dry objectives or by the water or oil-immersion technique using oil with a refractive index of 1.518 at 23 °C and an incident light wavelength of 546 nm. The reflectance so obtained is calculated from equation (2.2) [30].

$$R = \frac{Rs \bullet A}{As} \qquad (2.2)$$

where

R = reflectance of coal maceral

R_s = reflectance of a calibration standard

A_s = deflection of galvanometer.

The reflectance, R, is related to the optical properties of other material and the immersion medium by the following Beer's equation (2.3)

$$R = \frac{(n - n)^2 + n^2 k^2}{(n - n_1^2) + n^2 k^2} \qquad (2.3)$$

Where

n = refractive index of reflecting material

k = absorption index of reflecting material

n_1 = refractive index of medium in which the measurements are made

2.5 Volatile matter

According to ISO (International Organization for Standardisation) Standard 562, volatile matter is described as the loss of mass when coal is heated to 900 °C in the absence of air with gaseous combustion products allowed to escape. The correct estimation is essential in correlating many other properties of coal, viz. rank, calorific value, total carbon and hydrogen, coke yield and petrographic composition [11].

With increasing rank, the oxygen-dominated cross-linkages are thought be replaced by a weaker hydrogen bonding. Heating of such coal breaks the hydrogen bonds to show a high degree of plasticity. With a further increase in rank, the hydrogen bonding is lost to produce a non-fusible, high-carbon-content and aromatic structure typical of anthracite. A variation in the fluidity of coals is correlated to the volatile matter released and to the strength of the hydrogen bonding in the reactive components of the coal (Fig. 2.5) [20].

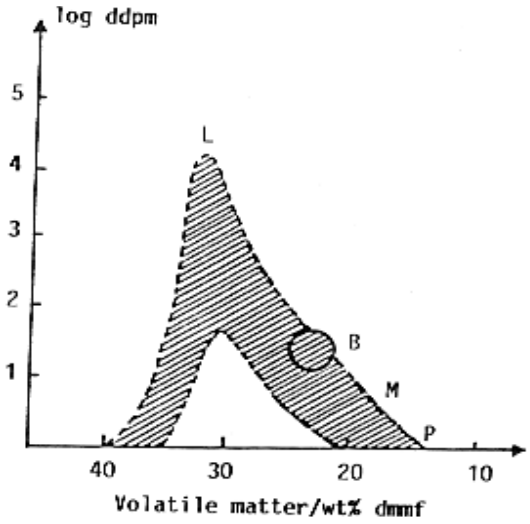

Figure 2.5: Variations in maximum fluidity (ddpm: Gieseler) with volatile matter [20]

2.6 Dissolution of coal

The conversion of coal into nuclear graphitic carbon requires relatively pure coal extracts. To provide for such purity, a suitable solvent is required in the extraction process, which separates a desired portion of coal into a solvent. The process may be achieved by physical or chemical methods [31]. The physical methods are based on the differences in the physical properties of the minerals and the carbonaceous part of coal. The chemical methods involve extraction of the

organic part in various solvents utilising various additives. It has been shown that coal extraction with organic solvents strongly affects the coking properties of the coal residue. Furthermore, dependence between the extraction yield and the coking properties of heat-treated coals has been reported [32, 33].

2.6.1 Theories on the mechanism of coal extraction

Theories on the routes for the disruption of the coal matrix have been reported. The use of reagents that attack the surface of coal has been documented. In this process, chemical transformation is thought to effectively “peel away” this surface to expose fresh surface to the reagent. The technique is believed to involve radical transformations of the coal structure, resulting in extensive carbon-carbon bond cleave-reagent reaction times, and greater possibilities for the selective cleavage of bonds [22].

In another theory, the reagent is thought to penetrate into the coal matrix and swell the coal. This is believed to allow a greater surface area, effectively longer coal–reagent times, and greater possibilities for the selective cleavage of bonds. Swelling is thought to put a strain on the coal matrix, leading to the rupture of hydrogen bonds and the reorientation of the coal matrix, which allows reorientation of the hydrogen bonding structure to occur. It is believed that an appropriate hydrogen-bonding agent, if allowed to penetrate the swollen coal structure, would be capable of “tying up” hydrogen bonding sites in the coal. It is the combined efforts of swelling and bond breaking that appear to allow included mineral matter to “drop out” of the coal structure while weakening the coal matrix. When treated with a suitable solvent, differential swelling of coal macerals leads to stresses that contribute to chemical comminution. Research showed that maximum swelling occurs when the Hilbrand solubility parameter of the solvent matches that of the coal. Solvents such as pyridine have been found to be the most effective swelling agents. Inertinite rich-coal was found to show reduced swelling compared with vitrinite-rich coal samples of similar rank. Toluene is the

solvent most commonly used in the dissolution of coal. It has been pointed out in the literature that the solvent should have a hydrogen-donor capability in order to stabilise the free radicals generated and thereby reduce undesirable re-polymerisation reactions [24]. Systems known to increase the solubility of the coal in different solvents were observed in petroleum pitches in which a low C/H ratio favoured solubility in different solvents and reduced condensation of the hydrogen-rich aromatic molecules [34].

The removal of such materials from the structural boundaries yields a more friable, “soft” coal structure. Moreover, the leaching of fine mineral particles from the coal matrix results in a more porous structure and improves the coal’s grindability. The prior removal of some mineral matter is reported to reduce the coal’s abrasiveness. The treated coal should be more amenable to crushing and such crushing should occur along maceral boundaries due to the combined effects of external hydrogen bonding and swelling.

Large amounts of impurities of comparable particle size distribution are likely to be released. This reduces the cost of follow-up because the coal structure is most susceptible to chemical attack during the swelling process. A wide variety of chemical reagents are capable of blocking the internal hydrogen bonding of the coal. However, for a chemical coal beneficiation system to be practical, this hydrogen bonding system must be readily available, inexpensive, be of sufficiently small molecular size, and not be expected to introduce unwanted chemical elements that will lead to corrosion or pollution problems with the processed, comminuted coal. These qualifications substantially limit the number of hydrogen bonding reagents [24] that could be used.

2.6.2 Parameters affecting solvent extraction

The extraction process is influenced by many factors which interact in solution with coal to effect dissolution. Some of these factors, e.g. temperature, will not be

discussed alone but in conjunction with other factors. The parameters that affect coal solubilisation, viz. nature of a solvent, moisture and oxygen, particle size, coal properties and other sulphide additives in demetallation, are detailed in this section.

2.6.2.1 The nature of the solvent and its effect on extraction

The extraction of coal has been correlated to some physical parameters of both the solvent and the coal. It has been shown that the properties of the solvent, viz. internal pressure, surface tension, dielectric constant or dipole moment, have little correlation with coal solubilisation. A distinction between solvents that are capable of breaking the intermolecular bonds in coal and those that stabilise coal fragments has been documented. The family of solvents containing an element with an unshared electron pair, such as nitrogen or oxygen, has been found suitable for coal solubilisation [35, 36]. Coal, being hypothesised as containing micelles with a size range of 1 to 300 microns, swells on adsorption of the solvent, and forms the micellar network of smaller units from the swelled structure. According to the Dryden model of coal solubilisation, the extent of coal extraction is proportional to the swelling structure. A solvent was considered suitable if it promoted swelling of the coal structure while simultaneously stabilising the coal micelles solution. Swelling promotes loosening and the availability of an unshared pair of electrons was considered to be an important factor. Experimental findings showed that coals that were heated to 200 – 400 ^{o}C in an inert atmosphere, cooled and then extracted with the solvent, gave a higher yield than untreated coal [37]. Studies on the influence of time on extraction showed a linear relationship between time and the yield of the coal extracts. Increased temperature was found to increase the yield and the smaller particles of coal produced a higher yield of coal extracts [36].

In hydro-dissolution, dissolution of coal is thought to result from an interaction of coal with a specific chemical structure of the solvent. Different solvents with

specific chemical structures showed different types of interactions with coal. The high power of a solvent containing amines (in extraction) is thought to be attributable to its chemical structure, which shows the presence of an unshared pair of electrons on the nitrogen. A solvent with a hydroxyl group attached to an aromatic ring and a hydro-aromatic ring was found to be more effective in coal extraction. A two-ring system containing a hydroxyl group attached to an aromatic ring and a hydro-aromatic ring was even more effective [36].

It has been shown that about 65 % of mineral matter and sulphur could be removed by treatment with 20 % sodium hydroxide from Turkey lignite coal. Mukherjee and Borthakur removed about 90 % of the mineral matter from coal using aqueous sodium hydroxide solution followed by acid treatment. A polar solvent appeared to break the polar interactions and allowed the swelling of coal [31].

Increased porosity was found to occur when coal was dissolved in methanol at 25 ^{o}C. With supercritical alcohols, the coal is hydrogenated and the result is a higher conversion [38, 39]. Alcohols show greater solubility for polar organic molecules and tend to form hydrogen bonding or dipolar attractive forces, which provides an opportunity for chemical interaction (nucleophilicity of the alcohol oxygen facilitates alkylation) [40].

Sapienza *et al*. [1979] treated coal with CO_2/H_2O and removed about 15 % of the ash. The carbon dioxide penetrates the coal structure more readily and extensively, diffuses along the lines of mineral inclusions and provides a method of simultaneous cleaning and fracturing. The synergistic interaction of these two inexpensive reagents causes the selective solubilisation of alkali and alkali earth mineral matter in the coal and the swelling of the coal matrix, which then weakens the coal structure [22]. Supercritical water when used as a solvent gave an extraction yield of 40 – 50 % at 380 ^{o}C [41].

Comprehensive investigations into the solvent extraction of Polish high-volatile sub-bituminous and bituminous coals in a batch-stirred autoclave were done using hydrogenated anthracene oil as a start-up solvent. Successive recycled solvents without hydrogen or catalysts showed a steady decrease in coal conversion and extraction yield (caused by a continuous decrease in the H-donor capacity of the recycled solvent). The successive recycled solvents enriched with catalytically hydrogenated coal extracts are thought to have affected the coal conversion and extraction yield by stabilising the chemical group compound of the successive recycled solvents [42].

An extraction yield of 27.4 % was obtained from a supercritical solvent mixture of 95 % p-xylene and 5 % tetralin at a temperature of 345 – 366 ^{o}C, and a pressure of 3.5 -6.9 MPa. An improved yield of 54 % (by mass) was obtained when coal was dissolved in supercritical water, stannous chloride or molybdenum trisulphide and the catalyst impregnated at a hydrogen pressure of 2.6 – 5.4 MPa, with a system pressure of 22.3 – 34.6 MPa [43].

An attempt to match coal solubilisation with the Hilbrand solubility parameter has been strongly opposed. However, Gutmann's donor/acceptor theory was found to be acceptable [44, 45, and 46]. Acid cleaning offers an advantage over typical gravity methods in the sense that the chemical composition of the mineral matter does not influence the acid's removal. The acid attack on the mineral occurring in the partings of coal is thought to form the basis of the disintegration process for breaking coal during mining [22].

Certain solvent additives improve the extraction yield of certain coals in some solvents. These additives are typically electron-donor or electron-acceptor compounds. The addition of various salts in the extraction of coals with carbon disulphide/N-methyl-2-pyrrolidinone (CS_2-NMP) solvent mixture (1:1 by vol.) showed that lithium and tetrabutylammonium salts (0.25 mol/kg-coal) of various anions considerably increased the extraction yield from 60 to 84 %. The yields

increased in the order $F^- > Cl^- > Br^- > I^-$, indicating that the anions with a small ion radius or large electronegativity are effective in enhancing the yield. The role of anions in the enhancement of coal solubility was based on the assumption that acid-base interactions between coal acidic sites and anions are responsible for the increment in the extraction yields [47]. However, without salts, CS_2-NMP mixed solvent gave slightly lower yields (63.7 – 69.7 wt %). The addition of a small amount (25 mg/g) of tetracyanoethylene improved the extraction yield to 85 wt %. Various additives, namely tetracyanoethylene and p-phenylenediamine improved the extraction yield. Tetracyanoquinodimethane (TCNE) was found to be effective for coals that had a large fraction of heavy extracts, increasing the extraction yields considerably. Characterisation of the fraction solubilised suggested that the enhancement of the extraction yield is attributed to suppression of the association between coal molecules [48, 49].

Previous work showed that extraction of coal with PhMe gave a conversion of approximately 30 wt %, while with water as solvent the conversion was 43 wt %. The addition of tetralin to the solvents gave higher conversions (69 wt % with PhMe and 57 wt % with water) [50].

2.6.2.2 The effect of moisture and oxygen

Moisture is an undesirable component in coal. Its existence in the solvent greatly reduces the solubility effect of the solvent on coal. In a continuous process, the solvent is recycled and the cumulative water content produced decreases the solubility effect of the solvent. In solvents immiscible with water, this effect is too great because water alone impedes the power of the solvent. Water alone is therefore not a good solvent for coal. Research conducted at West Virginia University showed that as little as 3 mole % (0.6 wt %) of water in coal cut the extraction yield by > 50 % in NMP. This makes the issue of moisture in coal very important. For this reason, the extraction process at the Institute of Applied Materials, University of Pretoria, ensures the absence of moisture in the reagents

used. The coal used is kept in nitrogen-purged plastic bags to minimise the amount of intrusion by moisture and oxygen. The little moisture that is present is driven off when the reactor containing the coal and solvent is heated to operating temperature [50].

2.6.2.3 The effect of particle size

There is a significant increase in the extraction yield with decreasing coal particle size. However, the rate of increase in the yield is too small to be accounted for, by assuming that a surface layer of constant thickness is completely extracted. In a study of the effect of coal particle size, 60 – 200 mesh size in extraction, an insignificant extraction yield was obtained. This finding is very important from the process economics point of view since with the conventional crushers, coals can be crushed down to 60 mesh size and require no grinding (this means an expensive operation would be required for this solvent extraction process) [51].

2.6.2.4 The coal properties affecting extraction

The extractability of coal decreases rapidly as the carbon composition of coal increases from 85 – 89 wt % (dry ash basis). The extractability then becomes almost negligible at 92 – 93 wt % carbon. This statement applies broadly to all temperatures and types of solvents. Of the petrological constituents, vitrain yields the most extract and fusain the least [33].

2.6.2.5 The effect of sulphide on extraction

The use of hydrogen sulphide in qualitative inorganic analysis has been well documented. Under controlled acidic media conditions, hydrogen sulphide precipitates heavy metals of group II (not related to periodic classification) (Hg^{2+}, Bi^{3+}, Cu^{2+}, As^{3+}, Sb^{3+}, Cd^{2+} and Pb^{2+}) to form insoluble metal sulphides. High acidity is believed to inhibit the dissociation of hydrogen sulphide, thereby

reducing the sulphide ion concentration. The group IV forms slightly soluble sulphides precipitates of Zn^{2+}, Mn^{2+}, Ni^{2+} and Co^{2+}. These are precipitated by the passage of hydrogen sulphide through an alkaline solution (ammonia solution). The hydroxide is reported to remove the acidic protons furnished by hydrogen sulphide to form water, thereby favouring the production of more sulphide ions, as in Scheme 2.1. This increase in sulphide ion concentration is believed to ensure that any group IV metal sulphides present are precipitated [52, 53].

2.7 Efficient coal solubilisation

The term 'supersolvent' is used to denote dipolar, aprotic solvents that are capable of dissolving a large fraction of the organic material in coal [36]. The general formula (equation 2.5), although complex, is identified with the solvents teramethyl urea (TMU), dimethylsulphoxide (DMSO), dimethylformamide (DMF), hexamethyl phosphoramide (HMPA), N, N-dimethyl acetamide (DMAA), and N-methyl-2-pyrrolidone (NMP) [36]. The solubilisation of coal in aprotic solvent by treatment with sodium hydroxide alone has been well documented [54, 55, 56]. Solubilisation was found to increase with an increase in reaction time, temperature, alkali concentration and decrease in particle size.

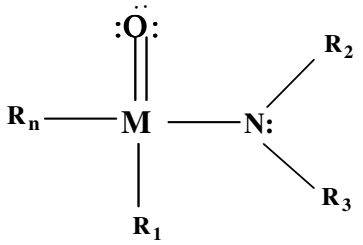

(2.5)

where

M = a carbon

R_2 and R_3 = hydrogen atoms or a lower alkyl group

R_1 and R_n = lower alkyl group and another group, a monocyclic group [56].

2.7.1 Extraction of coal with N-methylpyrrolidone

Coal, being a polynuclear aromatic structure, is hydrogen-deficient. The West Virginia University in the USA employs the hydrogen-rich solvent mixture of N-methylpyrrolidone (NMP) and carbon disulphide (CS_2) to obtain a carbon yield of about 87 % at 300 ^{o}C. The coal extracts produced may be suitable as precursors for the production of value-added carbon products. The dissolution of coal is reported to depend on the solvent type and on the physical and chemical properties of the solvent, and cannot be attributed to a simple diffusion-controlled process. Further, solvent extraction is dependent on time and temperature and, to a lesser extent, on the particle size of the coal, the solvent-to-coal ratio, and the oxygen and moisture content of the coal. However, a mounted coke sample in resin (produced from a heat-treated coal extract) showed isotropic texture with poor crystalline domains. NMP is a relatively expensive solvent [47, 57, 58].

2.7.2 Extraction of coal with N, N-dimethylformamide and alkali

Morgan [53] developed a coal solubilisation process referred to as the “Refcoal process”. This essentially involves mixing a polar aprotic solvent such as dimethylformamide (DMF) with coal. With the addition of a small amount of alkali to the extraction medium, solubilisation occurs. Dissolution conditions are mild – atmospheric pressure, and a temperature from room temperature to just below boiling point. The alkali moves into the solution by means of a phase-transfer catalyst and the coal appears to act in this capacity. The Refcoal process entails: 100 parts by mass of coal, 1 000 parts of the solvent and 10 parts of the base, mixed in an oil or water bath-jacketed reactor and stirred for 5 h under a nitrogen atmosphere. The progress of the extraction is monitored photometrically by taking small samples of the slurry at regular intervals. Most of the studies have been done on a flotation concentrate from Iscor’s Tshikondeni mine, with 8 % ash, when 90 – 92% of the organic material goes into the solution. The purified products are referred to as “Refcoal”, for “refined coal” [54].

CHAPTER 3

CARBONISATION

The graphitisability of the carbon is determined primarily by the quality of the carbonised starting carbon, coke. Enhancement and control of this coke quality can be achieved by the use of chemical additives. The overall effect is to bring about a certain degree of graphitisation or to promote a more graphitic structure. This chapter gives the literature background on some of the chemical processes associated with carbonisation. For a more complete understanding, some mention will also be made of non-graphitising carbons. Previous work on the effect of additives on carbonisation and the resultant coke texture is discussed.

The term 'carbonisation' is used in the literature generally to cover the pyrolysis of carbon-containing compounds at different temperatures and to different degrees of structural ordering. The definition adopted for the purpose of this work will be: *Carbonisation is the process of converting, by heating, carbon-containing compounds to carbon prior to the onset of three-dimensional ordering as detected by X-ray diffraction techniques*.

The types of carbon discussed in this text are the non-graphitising or hard carbon, and the graphitising or soft carbon. The distinction between the two carbons comes from the X-ray diffraction pattern of a hard or non-graphitising carbon, which does not develop the three-dimensional (hkl) lines of crystalline graphite upon heating as do the soft or graphitising carbons. Hard carbons can be carbonised to temperatures in excess of 2 000 ^{o}C without the development of the three-dimensional ordering, i.e. without graphitisation, whereas with soft carbons, graphitisation is a significant process at about 1 400 ^{o}C.

3.1 Mechanism of carbonisation

The mechanism by which a heated carbonaceous material decomposes and forms a char or carbon is of fundamental importance in understanding the production of carbons of all kinds. The process can be considered to occur in three broad stages. The first stage, which is termed the 'pre-carbonisation' stage, extends up to heat-treatment temperatures of the order of 400 ^{o}C and is accompanied by molecular rearrangement and initial condensation reactions. The second stage, which does not occur in hard carbons, is usually completed at about 600 ^{o}C and contains the bulk of the condensation reactions within a plastic stage; its completion is marked by the formation of a solid semi-coke. The third stage occurs after the formation of the solid semi-coke, during which volatilisation of most of the remainder of the non-carbon elements and some structural rearrangements occur. The three stages can overlap and vary according to the material concerned. However, it is in the second stage that the fundamental differences between hard and soft carbons are shown up. The existence of a plastic stage during the carbonisation of graphitising materials does not ensure a graphitising carbon [59].

3.1.1 The precarbonisation stage

The raw materials of graphite production, such as coal, coal-tar pitch and petroleum derivatives, are predominantly mixtures of aromatic, heterocyclic and multi-ring systems of various sizes. The final properties of the graphite produced are determined to a large extent by the chemical composition and reactivity of the molecular species and by the reaction intermediated. These properties usually help to follow the molecular changes occurring upon the pyrolysis of mixtures. However, it is impossible to follow the carbonisation of materials such as coal tar and petroleum pitches due to their extreme molecular complexity and due to the lack of operational techniques.

The formation of graphitic carbons from simple and polynuclear hydrocarbons has been studied in detail. The emphasis was on the nature of the resultant graphite. The studies correlated the molecular structure of the parent material with the final graphitic properties, but paid little attention to the intermediate stage. This section describes the literature dealing with possible reaction sequences proposed in the literature, particularly those that discuss graphitising carbons or those that compare and contrast the precarbonisation behaviour of graphitising and non-graphitising carbons [59].

Consideration was given to non-graphitising carbon in polyvinylidene chloride and to graphitising carbon in polyvinyl chloride. The carbonisation behaviour of polyvinylidene chloride was contrasted with that of polyvinyl chloride. Both were found to initially lose hydrogen chloride by a “zip” reaction and were thought to produce a fully conjugated polyene chain (alternate single and double bonds) by the successive release of adjacent hydrogen chloride groups along the polymer chain [58]. Subsequent reactions were found to lead to different products. Polyvinylidene chloride was found to lose more hydrogen chloride above 250 ^{o}C to give coke containing aromatic rings cross-linked by a polyene chain with little possibility of reorder and growth of the aromatic layers. Polyvinyl chloride, on the other hand, did not form aromatic regions until 400 ^{o}C, at which temperature there was a rapid evolution of hydrogen and the formation of the aromatic rings. Following the carbonisation of polyvinylidene chloride by infrared spectroscopy, it was found that the C-Cl and aliphatic C-H bonds disappeared as the carbonisation progressed, and double bonds and aromatic structures appeared [59].

The hydrogen chloride molecule released a hydrogen molecule by a “zip” reaction. This reaction was initiated by the formation of a radical, which was able to travel along the polymer, forming alternate single and double bonds. However, it was also able to eliminate hydrogen chloride from adjoining polymer chains, thus forming a cross-linkage, and also to form a cross-linkage by meeting

another radical on an adjacent chain and forming a bond. A rigid solid structure containing many cross-linkages was formed in the temperature range 150 – 190 ^{o}C, unlike the model of Winslow *et al.* [1980], which only formed cross-linkages through the loss of the second molecule of hydrogen chloride occurring at temperatures in excess of 250 – 700 ^{o}C [60]. Despite the various contradictions in the above-documented literature, the basic picture that emerges is that polyvinylidene chloride formed carbon containing aromatic rings that were cross-linked by polyene chains. These cross-linkages prevented the growth of the extensive aromatic layers that were a prerequisite for the formation of graphite. Polyvinyl chloride, on the other hand, formed aromatic rings which acted as nuclei and grew into the necessary extended aromatic layers at the expense of the surrounding aliphatic materials. The reason why polyvinyl chloride does not form cross-linkages in the initial zip reaction is not completely clear but it is thought to be due to a different type of reaction taking place. Subsequent work revealed that the loss of hydrogen chloride from polyvinylidene chloride was initiated by the formation of a radical, which then traversed the polymer chain forming either a polyene or a cross-linkage [60, 61]. The study of the effect of electron spin resonance on polyvinyl chloride and polyvinylidene chloride detected free radicals at temperatures as low as 90 ^{o}C, reaching a broad maximum at 300 – 400 ^{o}C. The temperature at which the maximum concentration was reached was 560 ^{o}C [62]. Despite their apparent similarities, polyvinyl chloride and polyvinylidene chloride form polyene chains in entirely different ways.

The precarbonisation stages of another graphitising carbon, acenaphthylene, and of a non-graphitising carbon, bifluorenyl, were followed using spectroscopic techniques (i.e. differential thermal analysis, chromatographic analysis and X-ray diffraction) [63]. Carbonisations occurred by a stepwise process, postulated by the reaction sequence shown in Fig. 3.1. At about 185 ^{o}C, the development of a disordered structure in the pyrolysis of acenaphthylene coincided with the formation of polyacenaphthylene (I) as shown by the infrared and ultra-violet

studies. The presence of decacyclene (II) was shown by its characteristic X-ray powder pattern being present, superimposed on the scattering. Ultra-violet spectra showed the development of biacanaphthylidene structures (III) at temperatures below 340 °C. Examination of a plot of the average layer diameter of the molecular species present against the temperature showed two distinct steps: one at 340 °C and the other at 375 °C. Ruland [1965] postulated that the distinction was due to the formation of zethrene (IV), followed by its dimerisation to give the structure (V). The layer size increased continuously afterwards. It was then postulated to be due to the higher-order polymerisation of zethrene [63]. In the case of bifluorenyl, ultra-violet spectra showed an almost complete transition to bifluorenylidene (I) at temperatures below 400 °C. Between 400 and 500 °C there was a gradual increase in layer size, which then remained constant until 600 °C.

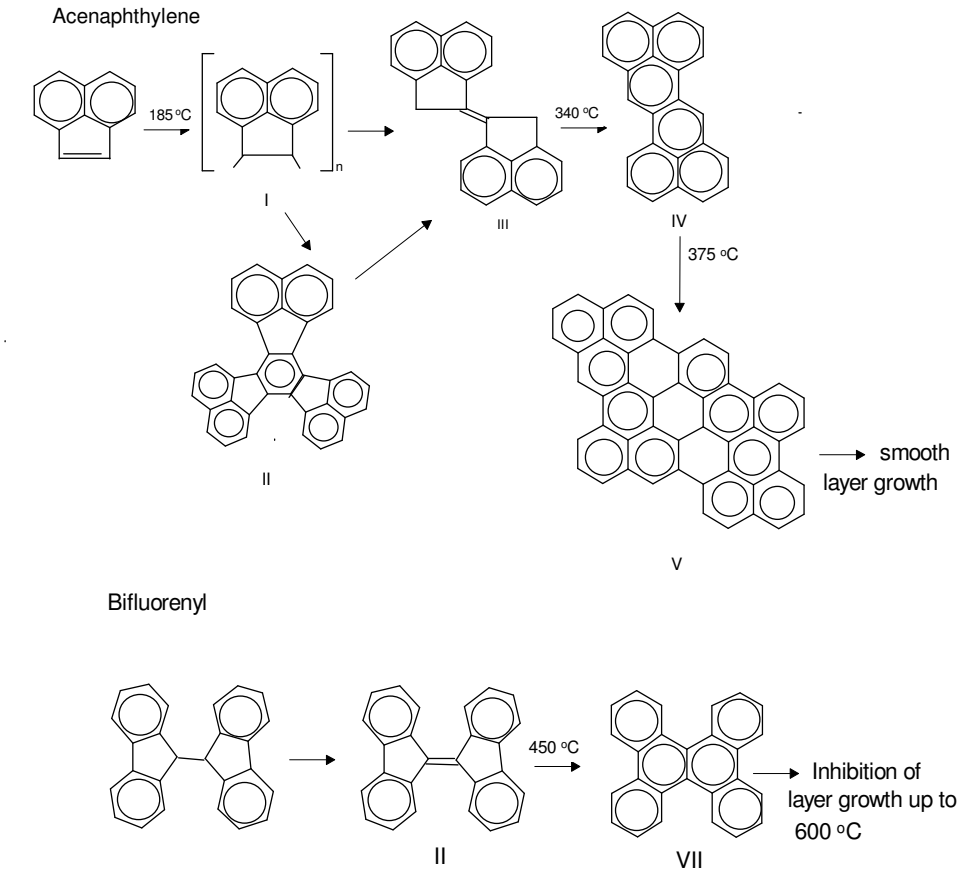

Figure 3.1: Initial stages of carbonisation [63]

The structural changes in the region of 400 – 500 ^{o}C indicated the formation of a planar molecule and this was postulated to be tetrabenzo-naphthalene. In contrast to zethrene, this molecule cannot build up aromatic layers without vacancies and this explains the fact that there is no growth in layer size after its formation. Research findings showed that the mechanism of carbonisation of organic compounds by electron spin resonance techniques is accompanied by the formation of large concentrations of free radicals (up to 3 x 20^{20}) unpaired electron per gram), making it possible to follow the carbonisation process by electron spin resonance [62, 64, 65]. However, this proved difficult due to the fact that only one unresolved line was observed for practically all chars and the identification of the radical giving rise to the electron spin resonance signal was not possible. A well-resolved hyperfine structure was obtained by carbonising in the inert liquid. This overcame the difficulty. However, later it was shown that metaquinquephenyl does not behave as an inert liquid. Carbonising in metaquinquephenyl was found to give rise to a great number of phenylated and/or polyphenylated compounds. By comparing the observed spectra with the computed spectra for certain free radicals, some of the radical intermediates in the carbonisation of aromatic species were identified. The perinaphthenyl radical in the carbonisation of acenaphthylene was thought to be an intermediate in the formation of zethrene.

Carbonisation of aromatic hydrocarbons is initiated by thermal C-C or C-H bond cleavage to yield reactive free radicals. These radicals can then undergo hydrogen abstraction, molecular rearrangements and growth to give condensed aromatic entities. The final stage of the carbonisation was thought to be the growth of these entities by dehydrogenation and side-chain elimination. A further study on the pyrolysis of acenaphthylene up to a temperature of 500 ^{o}C showed that decacyclene was the main product in the non-volatile residue [66]. This is inconsistent with the work of Ruland, which showed that decacyclene was an insignificant side-reaction product.

Warburton [67] reported that it was found that naphthalene undergoes self-condensation on heating to give, first, 1,1'-binaphthyl and, finally, the five aromatic ring system, perylene. Examination of the tars produced from the pyrolysis by mass spectrometry of the methylnaphthalenes at 475 ^{o}C showed the presence of dimers and other condensation products. Subsequent to that, it was reported that the coke formed from the pyrolysis of tetrabenzola [a, c, h, j] phenazine consisted primarily of the dimer, trimer and tetramer [67].

The mass spectrometry study of the liquid-phase pyrolysis on 20 aromatic compounds confirmed that the gas that evolved from thermally stable compounds (e.g. naphthalene, pyrene, chrysene) was primarily hydrogen, comparable to the methane and higher hydrocarbons from thermally reactive compounds (e.g. acenaphthylene, methylnaphthalene). Twice to 20 times as many molecular ions were detected in the mass spectra of these thermally reactive species compared with the residues from the pyrolysis of binary mixtures of these compounds, which did not show products having molecular weights higher than those of the pure compound [68, 69].

Examination of the spectra of the intramolecular and intermolecular vibrational frequencies for a series of polynuclear aromatic hydrocarbons heat-treated by neutron inelastic scattering revealed that the structural ordering of the resultant carbon depended upon both the skeletal structure and the molecular dynamics of both the original hydrocarbon and the reaction intermediates [70, 71]. The results suggested that graphitising carbons had temperature intervals for a major and stable species with a definite skeletal structure. The structure so formed persisted and finally fused together to form graphitic layers (e.g. acenaphthylene, bifluorenyl, etc.). Conversely, compounds which had large-amplitude skeletal or intramolecular vibrations, or which formed strained non-planar intermediates, did not form graphitising carbons (e.g. p. terphenyl) [71].

Evans and Marsh [72] provided some insight into the reaction sequence that takes place in the first and second stages of carbonisation. A high-resolution mass spectrometer was used to identify the products formed in the pyrolysis of acenaphthylene, anthracene, 9,9'-bifluorylidene, chrysene, phenanthrene, pyrene and mixtures of these. The condensation reactions to mass numbers in excess of 700 were followed [72].

Evans and Marsh found that the reactions taking place upon pyrolysis were predominantly dehydrogenative dimerisations, trimerisations, etc., which produced large flat sheets of condensed aromatic molecules. Little evidence of co-condensation of components was found when mixtures of two components were heated together; condensations appeared to be between identical molecules. Further interesting evidence from this study was that, in an attempt to reverse the carbonisation process by hydrogenating the solid cokes using atomic hydrogen, no new species were found. This suggested that the molecules going to make up the coke were simply condensation products of the type identified in the first and second stages of the carbonisation [72].

3.1.2 The mesophase stage

The phase-transition state similar to nematic liquid crystal, which is formed when coal of a particular rank is heated to a temperature of 400 - 500 ^{o}C, is called the 'mesophase'. Associated with this process is swelling from gases trapped within the plasticised macerals of the heated coal particle, coalescence of spherical bodies and consumption of the isotropic parent liquor. The softening and expansion of the coal particle is enhanced by the expansion of the trapped gas generated within the particle (Fig. 3. 2) [14, 73]. The result is the formation of an anisotropic mosaic coke structure. This intermediate stage was recognised by Brooks and Tailor as spherical bodies in the plastic carbonaceous material [74, 75]. The fluidity of the plasticised mass is thought to facilitate the suitable mobility of the aromatic molecules in the system. The aromatic molecules rearrange

themselves to create an intermediate anisotropic nematic liquid-crystal phase [76, 77, 78, 79].

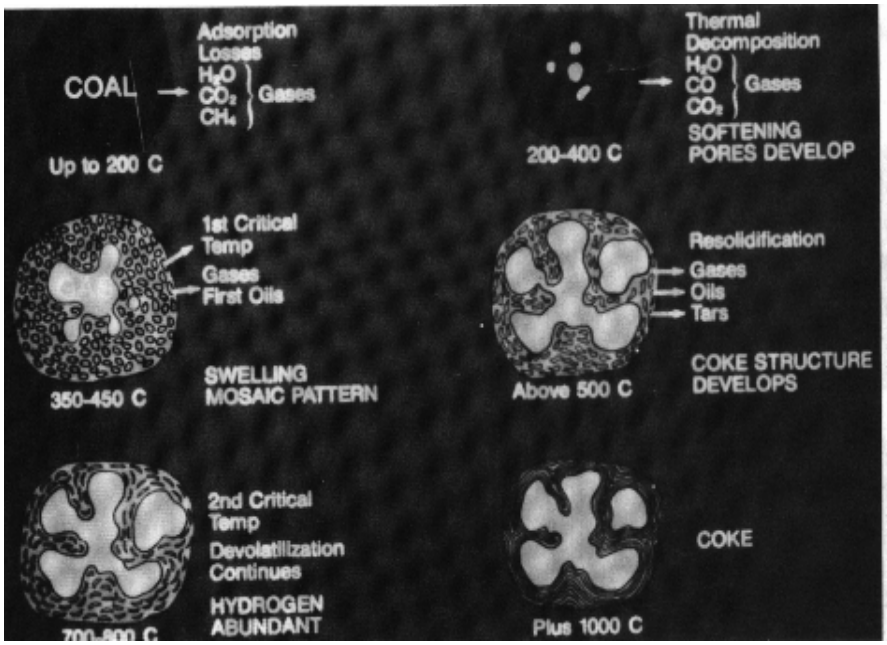

Figure 3.2: The transformation process during coking of a single particle of coal [14, 76]

Coalescence of the spherical bodies into a mesophase during pyrolysis of the coal has been extensively studied [80]. At a temperature of 475 ^{o}C, fine points of light were detected in the sample at the limit of the optical resolution. With a further increase in temperature to 480 ^{o}C (on Wongowilli seam vitrinite), these points grew until they resolved as spheres in the isotropic liquid vitrinite. When the number of spheres occupied about half the volume, they started to perturb each other's growth and their shape became progressively less uniform due to their coalescence. So long as the isotropic matrix persisted, there was continuous initiation of spheres and these existed in all sizes in the matrix. The final disappearance of the isotropic phase coincided with the solidification of the material to give semi-coke at 490 ^{o}C. Conclusively, the stages in the transition from the isotropic plastic vitrinite to the anisotropic semi-coke occurred over the

narrow temperature range of 10 – 15 ^{o}C [80]. Pyrolysis in pitches took place over a narrow temperature range of 480 – 500 ^{o}C [81].

The behaviour of these spheres under singly and doubly polarised light suggested that the spheres must have had the structure with equatorial stacking of layers perpendicular to the surface (Fig. 3.3). Despite the optical evidence to confirm this structure (using the electron diffraction technique), it was thought to be inherently improbable and an alternate structure was proposed in which the layers were flat and stacked on top of each other, and were parallel to the optical observations. The structure was thought to have inherent stresses due to shrinkage [80, 82, 83].

Initiation of spheres occurred in a variety of pitches, bitumens and single compounds, such as polyvinyl chloride and naphthacene, all of which produced graphitising carbons. However, compounds such as dibenzanthrone appeared to form the mesophase directly from the crystalline material without spheres being formed. Dibenzanthrone has been classed as a graphitising compound [59]. However, on the basis of X-ray diffraction it was classified as a non-graphitising carbon [59]. If the pitch-like material was stirred before cooling, a more complex structure arose in which the mesophase and isotropic phase became intimately mixed (as shown under a polarised light microscope). However, each retained its own identity. The mesophase, as well as the pitch, each behaved as a liquid. These observations led Brooks and Taylor to conclude that the spheres had the properties of nematic liquid crystals [82].

Carbonised pitch ($C_{100}H_{53}O$) showed a slightly different analysis of the spheres formed within it ($C_{100}H_{49}O_{1.4}$). More extensive condensation was observed in the molecules making up the spheres than in the original pitch. The carbonised pitch contained 27 % of spheres and the molecular species making up these spheres were found to have a molecular weight (as measured by a vapour-pressure osmometer) of about 1 626 compared with 415 in the pitch. The two important

factors controlling the rate of growth of the spheres were found to be temperature and time. The shape of these spheres was easily distorted by the presence of fine solid particles impeding symmetrical growth during coalescence. The edges were sharp and fluid at a particular temperature. The ultra-thin section showed the characteristic electron diffraction pattern, typical of parallel lamellae (Fig. 3.3). The position of the arc of the lamellae corresponded to an interlamellar spacing of 3.47 Å ± 0.01 [82]. The lower the temperatures of carbonisation, the fewer and larger were the spheres formed. Higher temperatures and prolonged heating led to a complete conversion into the mesophase. The higher the temperature, the shorter was the time required for complete conversion [82].

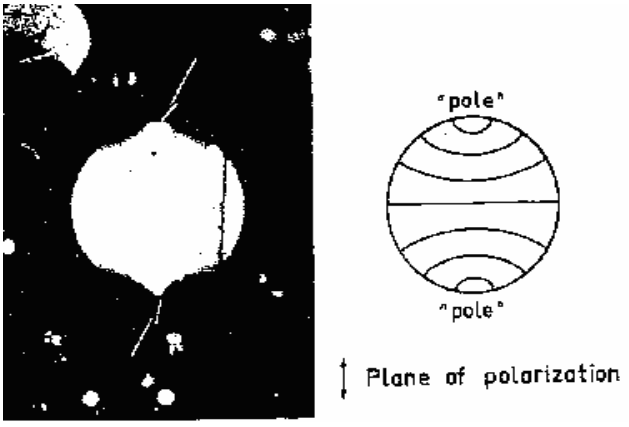

Figure 3.3: Development of a mesophase sphere in the transformation to a coke [80, 82, 83]

Proton nuclear magnetic resonance spectroscopy (NMR) in polynuclear aromatic hydrocarbons containing oxygen and nitrogen showed that 90 % of the protons observed were attached to aromatic rings, and that the spheres formed were soluble in pyridine and toluene. The components of the carbonaceous material from which spheres were formed consisted partly of two or more smaller rings joined in a non-planar fashion, presumably by diaryl-type linkages or methylene bridges or dihydroaromatic structures. The calculated potential ionisation energy of the reactive hydrocarbons from para position in the ultra-violet visible spectra

was less than 7.1 eV (p-band at about 387 m/u). Ultra-violet analysis of partly carbonised coke in benzene-pyridine showed absorption of about 4.2 eV. The results suggested that carbonisation forms more reactive hydrocarbons and that these decomposed, via a radical mechanism involving the loss of hydrogen, to form larger, more complex planar entities, and ordered lamellae of the mesophase [82].

Mesophase spheres are initially formed in the region adjacent to insoluble particles, also formed during carbonisation. Instead of the particles being incorporated into the spheres, they are rather aggregated around the surface of the sphere causing it to have irregular margins. The use of finely divided graphite on the toluene-soluble fraction of the carbonaceous material was found to induce nucleation successfully on carbonisation. Pronounced orientation of the mesophase spheres on the graphite surface was observed. Growth of the mesophase spheres was reported to be dependent on the rate of carbonisation. The lower the rate of carbonisation, the fewer and larger was the spheres formed. It was shown that at temperatures of 400 ^{o}C and above, for an increased time of carbonisation, the number of spheres remained constant. Prolonged heating at high temperatures above 400 ^{o}C was reported to result in the complete conversion of carbonaceous material to the mesophase. Stirring and the presence of fine particles are also factors proved to accelerate slightly the formation of mesophase spheres [82].

In a study of the relationship between the development of the mesophase spheres and residence time, within the temperature range of 400 – 450 ^{o}C for various pitches, it was shown that the first hour at a specific temperature corresponded to the nucleation region [84]. From one to 40 h was the growth region and longer times produced little change. The activation energy for the growth process was estimated to be 35 – 45 kcal per mole (146.44 - 88.28 kJ mol^{-1}); this is equated with the rearrangement of C–C bonds and with the vaporisation of the low-molecular-weight material. In further studies in which

anthracene was heated under pressure of 2.5 kilobars (250 MNm^{-2}) and at temperatures of about 550 ^{o}C the mesophase spheres were formed. The effect of pressure prevented the coalescence of the spheres by enhancing the viscosity of both the isotropic liquid matrix and the liquid crystal structure [85].

3.2 Structure of solid carbon

Solid carbon may be formed either from a liquid crystal phase, by deposition from the vapour or gaseous phase, by charring of a non-fusing solid or by charring of a fusing solid. Further heating of the resultant solid causes the volatilisation of the remaining non-carbon elements and some ordering of the carbon atoms. This section describes the determination of the structure. First, the turbostratic model will be described, followed by the reasons why this was considered inadequate and finally the proposed modified structure is given.

3.2.1 The turbostratic model

The scattering pattern of a carbon black in Fourier integral analysis revealed radical distribution of the carbon atoms around each other. This suggested the presence of graphite-like layers. The layers were arranged in parallel and equidistant from each other but randomly in translation parallel to the layer and randomly with respect to rotation about the normal to the layer. The term “turbostratic” (i.e. not ordered layers) for this type of structure was then suggested [86]. The size of the two-dimensional layer (L_a) was related to the breadth of the two-dimensional reflection at half-maximum intensity (β) by equation (3.2.1):

$$L_a = \frac{1.84\,\lambda}{\beta \cos\theta} \qquad (3.2.1)$$

The value of the constant was later found (by a more rigorous technique) to be 1.77. From small-angle scattering of X-rays by carbon blacks, it was concluded that carbon blacks consisted of clusters of a few hundred angstroms in size, within which the parallel layers were arranged as shown in Fig. 3.4. Heat treatment increased the size of the parallel layer groups, without markedly increasing the three-dimensional ordering, until a temperature was reached at which the carbon black changed discontinuously to a more crystalline graphite structure. The thinking was that graphitisation occurred when layers were given sufficient thermal energy to rotate into the graphite configuration.

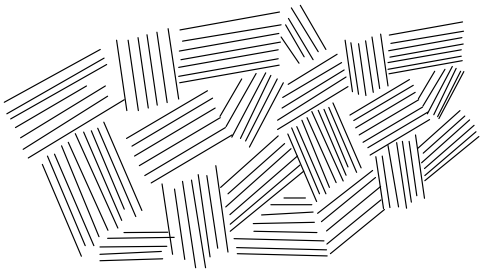

Figure. 3.4: Schematic representation of carbon black cluster [86]

An X-ray diffraction study on carbon from polyvinylidene chloride carbonised to 1 000 ^{o}C showed that not all carbons were in the form of graphite-layers: only about two-thirds of carbon was in the form of graphite-like layers, the rest of the carbon atoms were in a disorganised state. The graphite-like layers, although perfect, were very small (15– 20 Å). About 65 % of the carbon was calculated to be highly perfect and planar graphite-like layers of diameter 16 ± 1 Å and 35 % of the carbon was in a highly disordered form. Moreover, about 55 % of the graphite-like layers were grouped in pairs of parallel layers with an interplanar spacing of 3.7 Å and 45 % of the layers showed no mutual orientation [76]. The structure determined was specific and believed to be not necessarily representative of all carbons. An extended study, to include other carbons, revealed that for carbons containing, on average, fewer than five orientated layers, the interplanar spacing changed very markedly. For two orientated layers,

the d value was 3.7 Å, for two to three layers the d-value was 3.6 Å and for four to five layers, the d value was 3.44 – 3.445 Å. For more than five orientated layers, the change was small. The conclusion reached was that all carbons that show undeformed (hk) bands have an interplanar spacing of greater than 3.44 Å [87].

The X-ray diffraction study was extended to include carbons that graphitise on heating to sufficiently high temperature. This showed a gradual change to the ordered structure of graphite. Although some non-graphitic carbons showed a continuous and homogeneous evolution (to temperatures between 1 700 and 3 000 ^{o}C from a non-graphitic to a graphitic structure), other non-graphitic carbons that were termed “non-graphitising carbons” showed no trace of homogeneous development of a graphite structure, even after heating to 3 000 ^{o}C. The contribution from non-organised carbon was neglected in graphitic carbons because in all cases, where measurable graphitisation occurred, the layer diameter was in excess of 80 Å and the proportion of non-organised carbon was negligible in carbons where the layer diameter was greater than 25 Å [87].

It was found that if a series of graphitic carbons were arranged in order of increasing degree of graphitisation, i.e. increasing development of (hkl) lines, then the other parameters would be in the same sequence. These parameters included the diameter of the graphitic layers, the average number of layers arranged three-dimensionally and the interlayer spacing (d). The decrease in interlayer spacing that accompanies graphitisation had been previously reported [88]. Further research showed that for non-graphitic graphitising carbons, i.e. those capable of forming graphite at high temperatures but in which the graphite structure had not yet developed, the interlayer spacing was virtually constant and equal to 3.44 Å, whereas in a single-crystal graphite the d-spacing was 3.354 Å.

However, it was believed that the d-spacing of a graphitic carbon changed continuously from 3.44 Å to 3.354 Å. The widths of (002) and (004) reflections in

graphitic carbons were found to be different; this meant that the d-spacing was not rigorously constant but a mean value. In this case it was concluded that graphitic carbons contained a mixture of orientated and disorientated layers which were intimately mixed, forming a single phase, otherwise the (001) bands would have been resolved into doublets [87].

The graphite model showed a random distribution of orientated and disorientated layers. The term 'p' was used as a measure of the degree of graphitisation and was defined as the probability that a random disorientation had occurred between any two given neighbouring layers. However, the d-spacing was 3.354 Å at each orientation, and 3.44 Å at each disorientation. There was a random distribution of orientated and disorientated layers, and a linear relationship between them could be explained if there were layers separated by a distance of less than the 3.44 Å for a disorientated layer but greater than 3.354 Å for an orientated layer. The spacing, a, is 3.354 Å and corresponds to the spacing between orientated layers, b is the normal disorientation spacing of 3.44 Å, c is an intermediate value caused by having a group of orientated layers on one side of it and d is another intermediate value caused by having groups of orientated layers on either side of it [87].

$$d = 3.44 - 0.086\left(1 - p^2\right) \qquad (3.2.2)$$

Using a simplified version of this model ($c = d = 3.399\text{Å}$), a relationship (equation 3.2.2) showed an agreement with the experimental results over the whole range of graphitic carbons. The non-graphitic carbon, even after heating to 3 000 ^{o}C, was found to have no layer diameter of more than about 70 Å and the number of layers per parallel group was no more than 12. Graphitising carbons with a layer diameter of about 70 Å, produced by heating to only 1 720 ^{o}C, had about 30 parallel layers. This difference in the number of layers per stack was considered to be a method of distinguishing between the graphitising and non-graphitising carbons even at temperatures as low 1 000 ^{o}C, where graphitising carbons had

approximately four layers per stack whereas non-graphitising carbons had 2 to 2.5. Density measurements on the graphitising and non-graphitising carbons showed a sharp divergence, graphitising carbons having a density of 1.99 - 2.25 g cm^{-3}. This meant that the non-graphitising carbons must have a more open type of structure compared with the graphitising carbons (Fig. 3.5) [86].

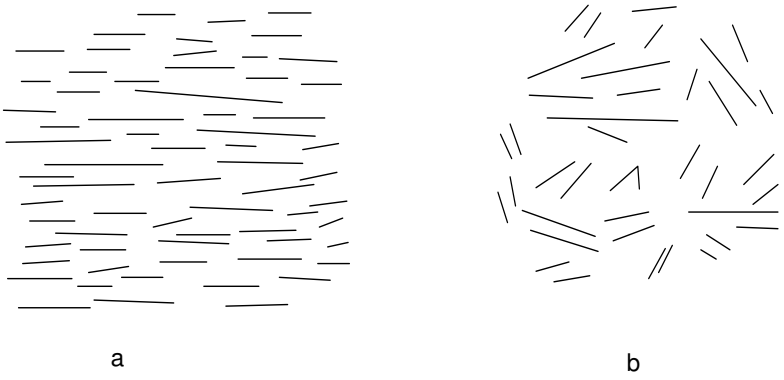

Figure 3.5: The proposed models for the structure of (a) graphitising carbon and (b) non-graphitising carbon [86]

Graphitising carbon shows the orientation of all the groups of parallel layer planes within a few degrees of each other, whereas the groups of parallel layers planes in non-graphitising carbon are orientated randomly and heavily crossed-linked into a rigid structure. Further study on the turbostratic model initially proposed by Franklin resulted in a relationship (equation 3.2.3) [89]:

$$d = 3.44 - 0.86(1-p) - 0.064\,p(1-p) \qquad (3.2.3)$$

The equation gives a better agreement for carbons with a low degree of graphitisation. It accommodates reduced spacing for the disorientations that were next to an orientated group with increasing graphitisation. However, allowance would have to be made for a reduced spacing for those disorientations that were next but one to an orientated group, a factor Franklin ignored.

3.2.2 Determination of crystallite sizes

The approximations made in deriving the equation relating L_a to the breadth of a (hk) reflection are such that the values obtained become progressively less reliable as the size of the layer plane decreases [76]. Attempts to develop a new technique for determining the layer plane size for carbon with very small layer planes has been done [90]. X-ray diffraction scattering pattern for randomly orientated, perfect aromatic molecules was calculated from the radical distribution function for various classes of molecules and the molecules in each class being approximately to the same size, ranging from 5.8 – 30 Å [90].

A description of a technique whereby a linear combination of these theoretical curves fits the observed curve by the method of least squares refinement has been documented [67]. The layer plane size distribution and the proportion of disorganised carbon were determined. Using this technique and the Hirsch method for calculating the distribution of numbers of stacks containing 2, 3, 4… orientated layers, a picture of the structure of four British coals and their carbonisation products was formulated and reported [65]. Up to 500 ^{o}C, the main process is one of the volatilisation of the disordered material. Between 500 ^{o}C and 600 ^{o}C, growth was started by the coalescence of neighbouring layers because of a wider distribution of molecular sizes. The stacking in this region, however, deteriorated due to the realignment of the molecules necessary for coalescence. The layer growth was found to be approximately linear up to 1 000 ^{o}C, although the layers produced were imperfect, probably bent coalescence junctions. Above 700 ^{o}C, the stacking improved by gradual realignment. The rate of growth was found to be greater for anthracites than for lower-rank coals, probably as a result of layers already being in reasonably good alignment and because of their greater initial size [67].

The method has been the subject of much criticism. An attempt to use Diamond's method for determining the distribution of layer sizes gave a negative weight

fraction for the 5.8 Å size group in certain anthracite samples [91]. The corrections for Compton (incoherent) scattering and the scattering caused by the presence of non-carbon elements (ignored by Diamond) were found to be most important and could not be neglected. The method was applied to a number of liquid hydrocarbon specimens (which represents a reasonable test). The results showed that amongst the four non-aromatic compounds examined, only one, cyclohexane, was found to be predominantly amorphous (i.e. non-planar), while of the 17 aromatic structures examined, only two were found to have appreciable amorphous (i.e. non-aromatic) content [92]. The method was concluded to be inaccurate and, with these inaccuracies, shown to be inconsistent. The main criticism of Diamond's method was that each single layer scattered independently and no allowances were made for layer-layer orientation. Further research on Diamond's work concluded the case of parallel layer groups containing several layers, and a rigorous correction for Compton scattering was made. This method led to the theoretical diffraction patterns, which gave a better approximation to the structure of carbon containing small layer planes. Various models for calculating L_a for turbostratic carbons showed that the Warren-Bodenstein approach was the most satisfactory. It was concluded that L_a calculated from a (10) reflection could give a higher result, by a factor of 1.09, than from a (11) reflection [93].

3.2.3 Tetrahedral carbon atoms in non-graphitic carbons

The turbostratic model of carbon is based on the fact that the atoms give rise to the (hk) and (002) reflections observed in the X-ray diffraction pattern, where all are arranged in perfect graphite-like layers. However, the hardness, density and non-graphitisability of some carbons did not appear to be entirely compatible with a structure containing only graphite-like layers. This basic assumption of perfect graphite-like layers was challenged, as was whether tetrahedrally bonded carbon atoms could explain the anomalies [94]. The X-ray diffraction curves for the 26-atom molecule arranged in a graphite-like layer, a cubic diamond-like lattice and

a hexagonal diamond lattice were then calculated. All the structures gave rise to reflections in the same region as the (hk) reflections of graphite. It was then concluded that although there was no proof of the existence of the tetrahedrally bonded carbons in non-graphitic carbons, a claim that the evidence showed that they were non-existent was not valid, and it was felt that some of the anomalies in certain carbons might be explained by postulating a model in which tetrahedrally bonded carbon atoms were present [94, 95].

3.2.4 The influence of oxygen on carbonisation

Carbonisation of an aromatic hydrocarbon in the presence of oxygen was found to lead to the formation of a quinone intermediate. Further studies showed that heat treatment of an aromatic quinone at 3 000 ^{o}C led to a carbon with higher interplanar spacing than the 3 000 ^{o}C corresponding hydrocarbon. This effect was thought to be due to the fact that carbonisation of the quinone resulted in the degradation of the aromatic ring system through the elimination of carbon dioxide. This degradation led in general to non-planar free radicals, which polymerised to give a cross-linked disordered carbon, although it was found that in certain cases a rearrangement to give planar aromatic structures was possible [63]. Fitzer *et al.* [66] extensively examined various additives that influence the carbonisation process. Of the various materials, oxygen has been most widely studied. Severe oxidation is believed to reduce drastically the graphitisation of pitch. Oxidation has also been found to inhibit mesophase development [53, 61, 96]. X-ray diffraction analysis of oxygen-containing aromatics showed that oxygen substitution could result in both well and poorly ordered graphite [63]. Mild oxidation has been shown to reduce dehydrogenative polymerisation without necessarily leading to a less graphitic final structure [96]. Lewis and Singer used electron spin resonance to study the air oxidation of aromatic hydrocarbons. Aryloxy radicals were identified as intermediates. The formation of quinines that lost carbon monoxide (CO) on pyrolysis to give non-planar radicals led to a dramatic decrease in the final graphitisability of the starting material (Fig. 3.6).

The results of the electron spin resonance study suggested that oxygen had inhibited the formation of graphitisable carbon [14, 20, 61].

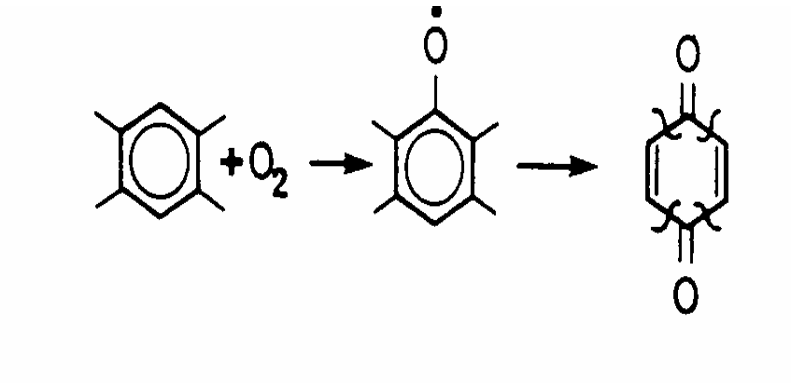

Figure 3.6: Reaction of oxygen with aromatic hydrocarbons during carbonisation [14, 20,57]

The bond cleavage in the absence of oxygen is believed to lead to molecular rearrangement, thermal polymerisation and aromatic condensation to form graphitic carbons. Although these processes are believed to occur in parallel during carbonisation, they can be considered separately from the mechanistic viewpoint [20,59]. Extensive work has been reported in the literature on the effect of oxygen on the growth of the mesophase spheres. Exposure of coals and pitches to oxygen showed that, in the presence of oxygen content of greater than 7 %, mesophase spheres were formed in the liquid phase. With oxygen content of 5 %, small isolated spheres were formed and more extensive growth of spheres only occurred in those coals that had oxygen content of less than 5 % [97]. The results suggested that there is a minimum amount of oxygen that inhibits the formation of the mesophase spheres.

The exposure of coal to oxygen and heat (~170 ^{o}C) was presumed to result in various types of microcracks or darker microfissure structures, an increase in the reflectance of vitrinite with temperature of oxidation and the development of oxidation rims (bright edges) around the grain. Such highly oxidised coals are reported to be difficult to burn effectively in thermal power stations.

Photomicrographs (Fig. 3.7) showed the typical oxidation rims formed by the heating of crushed samples (< 3 mm) at 250 °C. In addition to oxidation, microfissures are reported to be associated with the quick release, in substantial quantities, of gas in the final stage of carbonisation. Occasionally, vitrinite is surrounded by darker edges (or rims) due to the formation of humic acid (soluble in KOH). Oxidation rims are favoured by coal oxidised at temperatures above 200 °C [14].

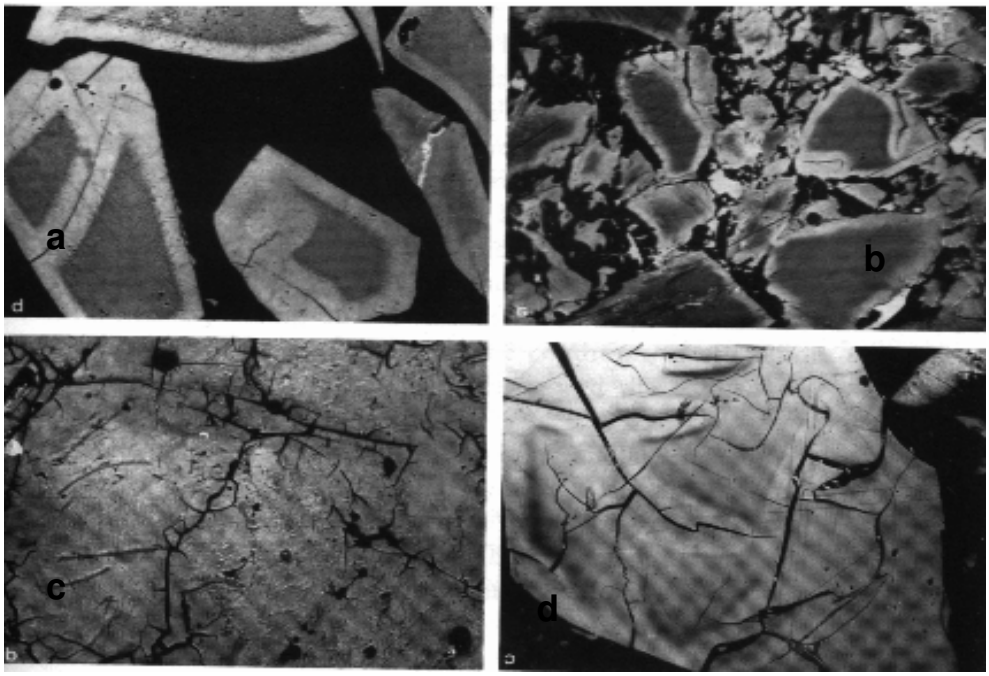

Figure 3.7: Photomicrographs of the polished surface of oxidised coal carbonised at 300 °C (oil immersion) [14]
(a) Oxidation rims of coal heated at 300 °C
(b) Oxidation rims of bituminous coal after heating at 250 °C for 120 min
(c) Oxidation rims of coal heated at 300 °C after 300 min
(d) Strongly weathered coking coal with fine pores, desiccation cracks, dark oxidation rims and black holes.

3.2.5 The influence of additives on carbonisation

The thermal reactions of carbonisation can be altered considerably through the use of certain additives. These are chemical substances that influence the thermoplastic properties of coal. Their effect on coal structure takes place via active centres of the coal macromolecules (functional groups, labile hydrogen) and influences the condensation reactions at pre-coking temperatures with the evolution of free radicals at increasing carbonisation temperatures. This effect depends on the nature of the additive used, the amount added and also the structure of the parent coal [95].

3.2.6 The influence of sulphur on carbonisation

Little is known about the effect of sulphide on the carbonisation of coal. However, elemental sulphur has been used extensively as an additive. Sulphur could increase the yield of carbon obtained from acenaphthylene. High sulphur dosage in the starting carbonaceous material is non-graphitising. The reverse was found to be true for lower levels of sulphur [67, 98, and 99]. Sulphur-containing radicals were proposed as intermediates in some reactions. When it was incorporated (as sulphur heterocyclic compounds) into strained ring systems, it was possible to eliminate sulphur readily in the early stages of carbonisation [100, 101]. The reaction of sulphur with aromatic hydrocarbons has been reported to give sulphur-containing polymers, which were stable at high temperatures [102].

Elemental sulphur has also been used extensively as a dehydrogenating reagent in the synthesis of polycyclic aromatic hydrocarbons and their derivatives [103]. At temperatures above 200 ^{o}C, sulphur extracts hydrogen from aromatic compounds [17]. Further reaction of sulphur with aromatic compounds gave Ar–S-Ar-type compounds [104, 105]. Subsequently, molecular condensation of aromatics with or without the incorporation of sulphur significantly increased their softening points and carbon yields. Shevkoplyas showed that on carbonisation,

thioether C-S bonds are broken to release active fragments that could participate in radical polymerisation, addition and substitution reactions [106].

3.2.7 The carbon solid and its influence on carbonisation

The structure of carbon black (Fig. 3.8) has larger layers. Ergun made a careful analysis of the radical distribution functions of a carbon black [107]. The analysis indicated the presence of extensive but faulty stacking, rather than short stacks of small layers. However, the most easily appreciable evidence for the existence of extensive but defective layers in a graphitisable carbon black comes from the electron micrographs, which showed visible orientation of the atomic layers. The graphitic layers visible in a carbon layer were significantly larger than those that a conventional X-ray diffraction analysis would have shown. The lower values of X-ray diffraction analysis were considered to be attributable to layer plane bending due to non-basal edge dislocations [107].

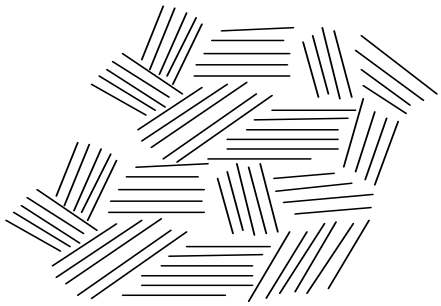

Figure 3.8: The line diagram of carbon black [107]

Carbon black is widely used in polymers as a filler of free space made by the grains of conductive materials in the rubber industry (90 % of world carbon black consumption), and as a black pigment. It is known to provide an enhanced ultra-violet stability to the polymers. Its performance property is explained by its chemical structure and physical properties. Its end-use depends on its particle

size distribution, the morphology of the particles and aggregates, its specific surface area, its elementary grain microtexture, its surface chemical bonds, etc [108]. The most common constituents of carbon black are a polyaromatic structure containing hydroxyl, carboxyl and quinine groups, which are prone to absorb ultra-violet light, and smaller particles (1-30 nm) with an ordered microstructure and a smooth surface [109].

There are many reports about the formation of carbonaceous mesophase spheres and the influence of inert solids [110 - 116]. Mesophase nucleation is initiated homogeneously because the chemical composition of the precursor pitch and the dynamic motion in the fluid are related to the nucleation of the mesophase spheres [110, 111]. Brooks and Tailor [72, 78] found that primary quinoline-insoluble and carbon blacks in coal tar pitch, gathered on the surface of the mesophase spheres, tend to produce a larger number of smaller spheres by limiting growth and coalescence [117, 118, 119]. Further work showed that there was no significant effect on the nucleation or the rate of mesophase formation. However, Kuo *et al.* noticed the difference in the size and structure of primary quinoline insoluble and carbon black [120] The primary quinoline is distinct from carbon black because it has a broader particle size distribution and a different shape, whereas carbon black forms chain aggregates that are well defined by transmission electron microscopy. There was no indication of carbon black behaving as nucleation centres for the mesophase formation [121].

It has been reported that the presence of carbon black in carbonisation systems delays the appearance of liquid crystals and causes to some degree the supersaturation of mesogens so that they do not precipitate [120]. Gentziz *et al.* studied the effect of carbon additives on the mesophase induction period of Athabasca bitumen [121]. Without carbon additives, the mesophase occurred after 61 to 67 min at reaction temperatures of 450 ^{o}C to 440 ^{o}C respectively. With carbon additives (ca. 5 wt %), the mesophase formation time was shortened to almost 45 – 50 min. However, the coke was reported to have a surface area of

1.65 m^2/g, with enhanced bitumen fluidity and a large–textured mesophase [121]. Such supersaturation is thought to lead to a large number of smaller sized spheres. The interaction between carbon black and the mesophase is believed to take place in the early stage of carbonisation.

The surface functionality of carbon black is thought to advance its chemical interaction with the pitch [122]. Carbon black enhances mesophase pitch formation by increasing the number of spheres through restricting their coalescence [123]. Korai *et al.* showed that carbon black enhances the nucleation and inhibits the growth and coalescence of the mesophase spheres [124, 125 and 126]. Kanno *et al*. showed that a 5 % carbon black addition is sufficient to suppress the swelling of mesophase pitch by initiating pyrolysis at lower temperatures, thus avoiding the intense evolution that leads to severe swelling and to an increase in the size of the optical units [127].

Pyrolysis of coal-tar pitch showed that adding 10 % of various polymers increases the kinetics of conversion and affects the morphology of the mesophase. The result is an accelerated growth of the mesophase and an increase in the proportion of areas of isotropic appearance in the optical texture [128]. In a similar study in which quinoline-insoluble material (inert material) was added to coal-tar pitch, it was found that the inert material tended to concentrate on the surface of the mesophase spheres. This was reported to inhibit the growth and coalescence of the spheres, leading to the deterioration of the coke's optical texture [74, 116 and 129]. It was established by Jakab and Blazso that carbon black has an influence on chain cleavage and on the H-transfer reaction in polypropylene [117]. It participated in the termination of the chain reactions, resulting in a reduced yield of the oligomers from vinyl polymer. Its involvement in the H-transfer reaction was confirmed by increased yield of the hydrogenated product [130].

The interaction of carbon black with pitch is temperature-dependent (< 425 ^{o}C). However, hydrogenation, polymerisation and an increase in carbon yield did not affect the pitch fluidity. Consequently, the porosity of the coke was observed at an initial stage, with the formation of a smaller mosaic texture [131]. When 10 % of carbon black was dispersed in pitch, chain-like aggregates that possessed a 3D-expandable cage structure were formed. The structure hindered the growth and stacking of mesophase molecules, thus reducing the size of the optical units to provide a fine-grained mosaic texture [122].

3.3 Chemistry of carbonisation

Carbonisation is considered to be a process in which a small aromatic structure is polymerised to an aromatic polymer, which ultimately achieves the three-dimensional order of graphite. Aromatics are the key building blocks for carbon, so that non-aromatic structures are first aromatised before undergoing the carbonisation process. For example, the aliphatic polymer polyvinyl chloride thermally converts to a pitch containing polycyclic aromatic structures, prior to the formation of carbon [131, 132]. The overall process of carbonisation is exceedingly complex. However, the individual processes that represent some of the major reactions involved in the pyrolysis of aromatic hydrocarbons can be considered: C-H, C-C bond cleavage to form reactive free radicals, molecular rearrangement, thermal polymerisation, aromatic condensation and elimination of side-chains.

Although all theses processes can occur in parallel during carbonisation, they can be considered separately from a mechanistic viewpoint. The initial thermal reaction in the carbonisation of an aromatic hydrocarbon is only poorly understood, but it is believed to involve the formation of free radicals. There are two types of radicals that can be formed by bond cleavage in the aromatic molecule. The first is a σ-radical produced by breaking an aromatic molecule. This reaction is a high-energy process since the bond dissociation energy is of

the order of 100 kcal/mole [133]. The σ-radical intermediate is very unstable and the free electron is localised. For example, the naphthyl radical has been detected by electron spin resonance only when frozen in a solid matrix at 77 kcal/mole. The second type of radical is an aromatic π-radical, which is considerably more stable. Much less energy (77 kcal/mole) is needed to break the methyl C-H bond in toluene. The unpaired electron is resonance-stabilised and simple π-radicals, such as the benzyl radicals, can be detected by electron spin resonance at room temperature [133, 134].

Stein *et al.* used principles of thermochemical analysis to predict the initial reaction pathways in the pyrolysis of polynuclear aromatic hydrocarbons [135, 136]. The π-radical (I) could be generated by a small amount of the unstable anthryl σ-radical. Theoretical studies such as these, coupled with recent experimental breakthroughs in observing unstable radicals, could greatly clarify the initial reactions of carbonisation [136].

Once formed, the reacting intermediate can undergo direct polymerisation as in the formation of naphthalene polymer from naphthalene. These initial polymerisation reactions involve the loss of hydrogen, which can often be accomplished through internal hydrogen transfer. Hydrogen transfer in pyrolysis is important because major condensable volatile materials (identified during the pyrolysis of several polynuclear aromatic hydrocarbons) are produced. These products all consist of hydrogenated derivatives of the original compound, with hydrogen added at the most reactive position in the molecule [136].

An important step in the early stages of carbonisation is the thermal rearrangement. It is this reaction that often makes it difficult to relate the starting structure to the subsequent course of graphitisation. Research on the polymerisation of acenaphthylene and bifluorene showed that an unstable five-membered ring is transformed to a stable six-membered ring system without the loss of carbon atoms. It is believed that either the starting molecule or a

rearranged entity serves as the building block in carbonisation. One of the factors that make carbonisation so complex is believed to be numerous polymerisation sites in an aromatic molecule [137, 138]. In a simple dimerisation of anthracene, 11 reaction products are possible and, as the reaction proceeds, the number of isomeric structures increases rapidly.

The site in the aromatic ring at which polymerisation predominantly occurs can be predicted. Various reactivity parameters are used, including free valences, unpaired spin densities, localisation energies, and thermochemical kinetic analysis [52, 61, 63]. Steric effects are, however, important in the polymerisation process and can override reactivity factors. The polymerisation process of aromatic hydrocarbons occurs in two stages, viz. the condensed or non-condensed polymers. In naphthalene, the loss of two hydrogen atoms between two reacting molecules leads to polymers in which the units are linked by single bonds. An additional loss of two hydrogen atoms produces a fully condensed polymer (Fig. 3.9). Although the non-condensed and condensed polymers have virtually the same molecular weights, they vary considerably in structure and properties. The non-condensed polymers are non-planar and their reactivities and ionisation potentials change very slowly with increasing polymerisation. The condensed polymers are fully planar and show marked changes in reactivity and ionisation potential with increasing size. The relative role of these two processes is thought to be critical in carbonisation [139].

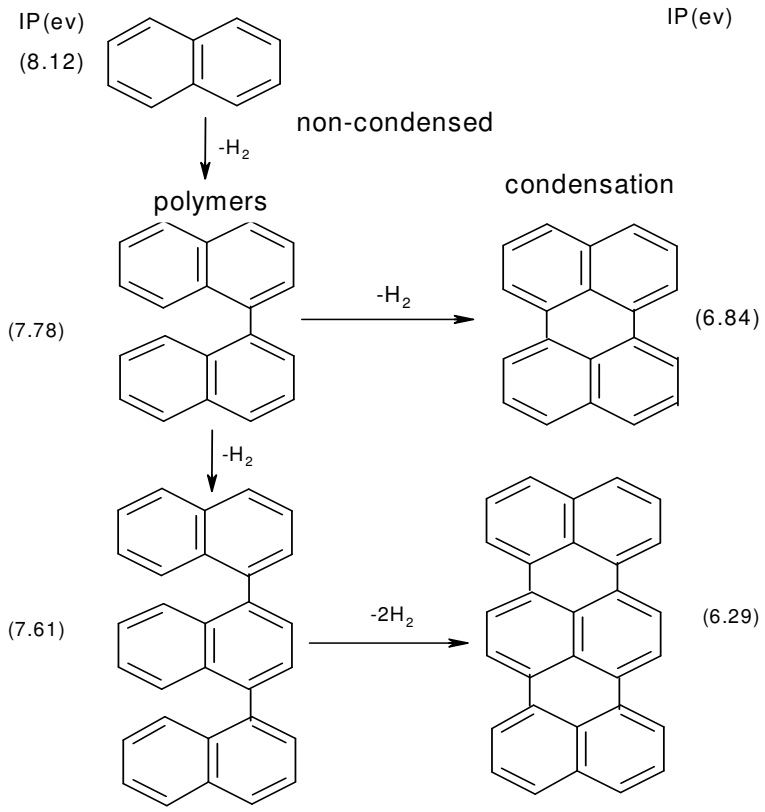

Figure 3.9: Polymerisation-condensation process in carbonisation [139]

Thermal polymerisation pathways were determined for a number of aromatic hydrocarbons. In the pyrolysis of anthracene, a number of initial non-condensed products were identified [133, 140]. However, only certain of these structures, which have the right steric conformation to undergo an additional dehydrogenation reaction to give a fully condensed molecule containing the most reactive 9-position in the anthracene ring, do achieve this result (Fig. 3.10).

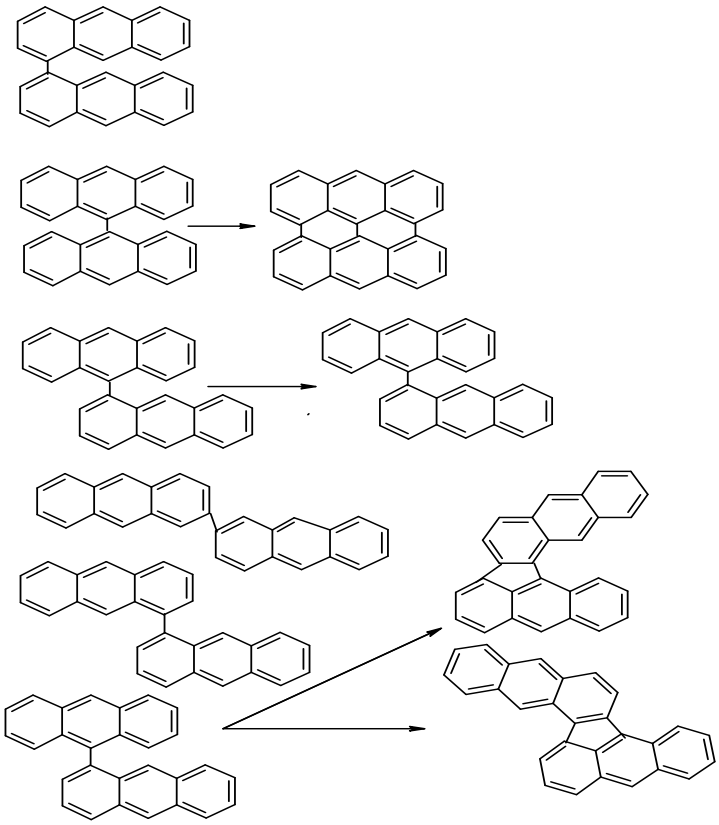

Figure 3.10: Reaction products from the pyrolysis of anthracene [133]

Research data from the pyrolysis of naphthalene showed that polymerisation at the most reactive 1-position leads to naphthalene polymers which can form fully condensed polymers composed of only six-member rings, while polymerisation utilising the less reactive 2-position can inhibit condensation (Fig. 3.11).

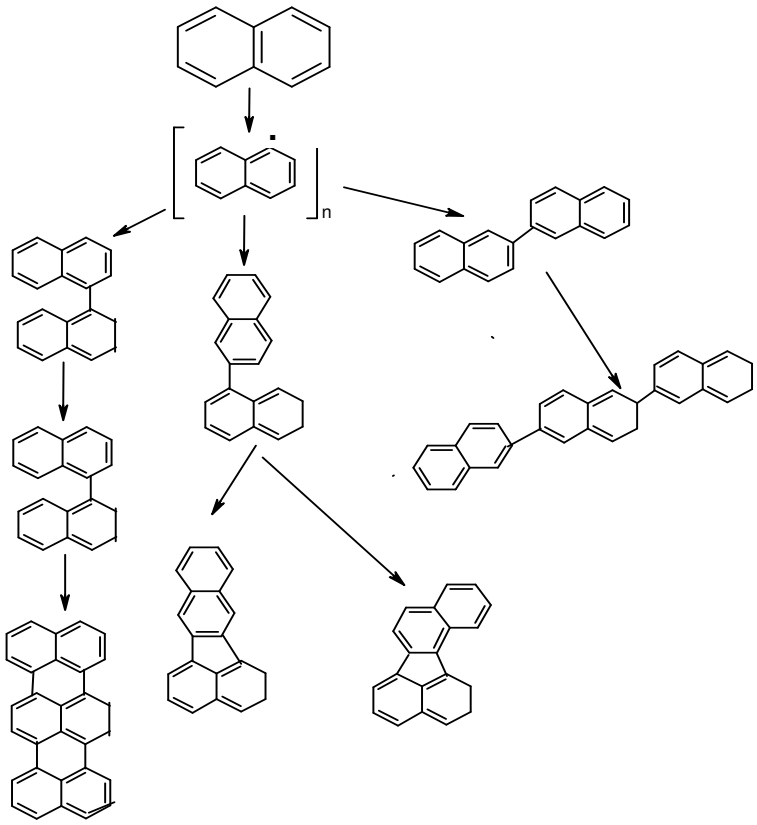

Figure 3.11: Reaction products from the pyrolysis of naphthalene [133, 141]

Lewis and Singer [142] used the reaction scheme in Fig. 3.12 to show how alternate radicals are involved in the polymerisation-condensation process in carbonisation. In naphthalene, a non-condensation polymer (111) is formed by rapid polymerisation. This polymer contains three non-condensed naphthalene units and a total of 30 carbon atoms. The loss of a single hydrogen atom from the polymer leads to a free radical (1V), which contains 30 carbon atoms with a single sp^3 tetrahedral carbon. The total aromatic π-system contains 29 carbon atoms and the unpaired electron is stabilised by resonance delocalisation. The loss of an additional hydrogen atom would create a fully condensed molecule, but would not result in a substantial increase in resonance stabilisation. A further complication of the carbonisation process is that the eventual polymerisation to carbon occurs in two dimensions [142].

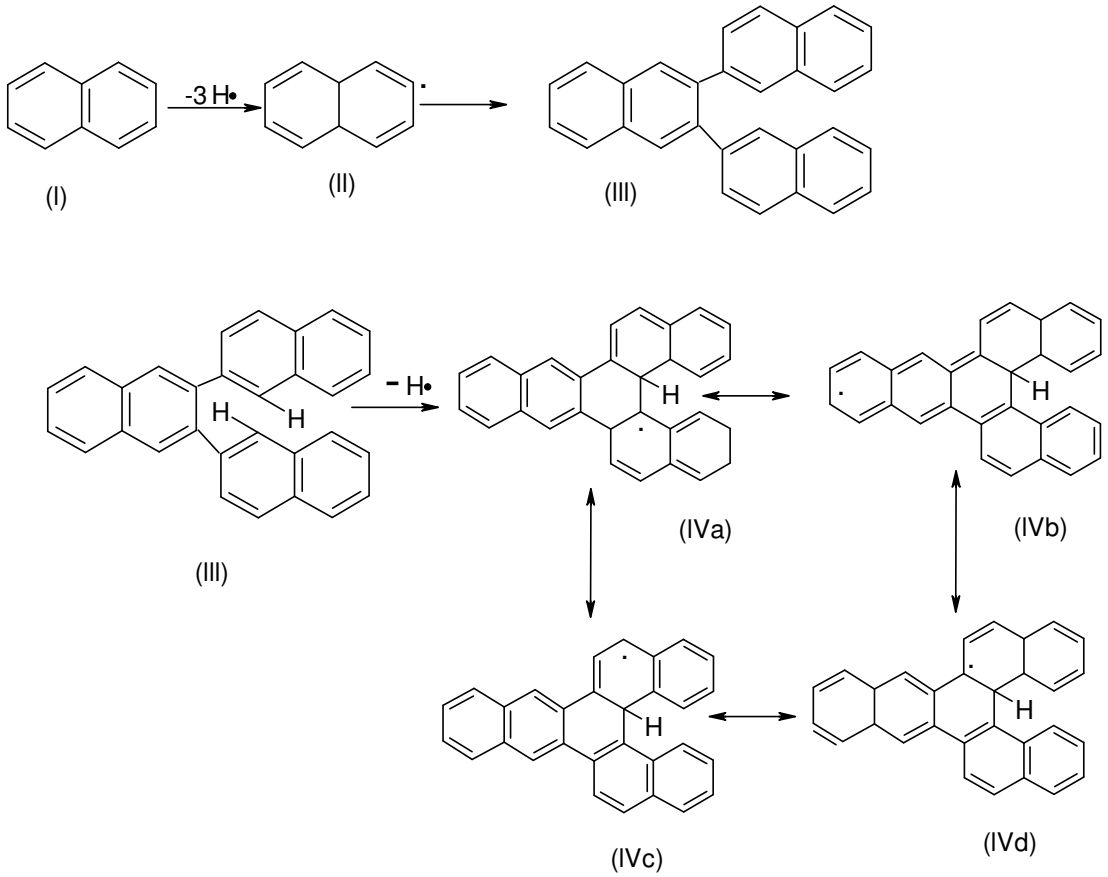

Figure 3.12: Formation of stable odd-alternate free radical structures during carbonisation [142]

The key to this process is how well the aromatic building blocks polymerise to develop a perfect graphitic network. Fig. 3.13 shows how the molecule zethrene, identified from the pyrolysis of zenaphthylene [63, 143] has the perfect shape and reactivity to polymerise in two dimensions to a planar graphite-like structure without vacancies.

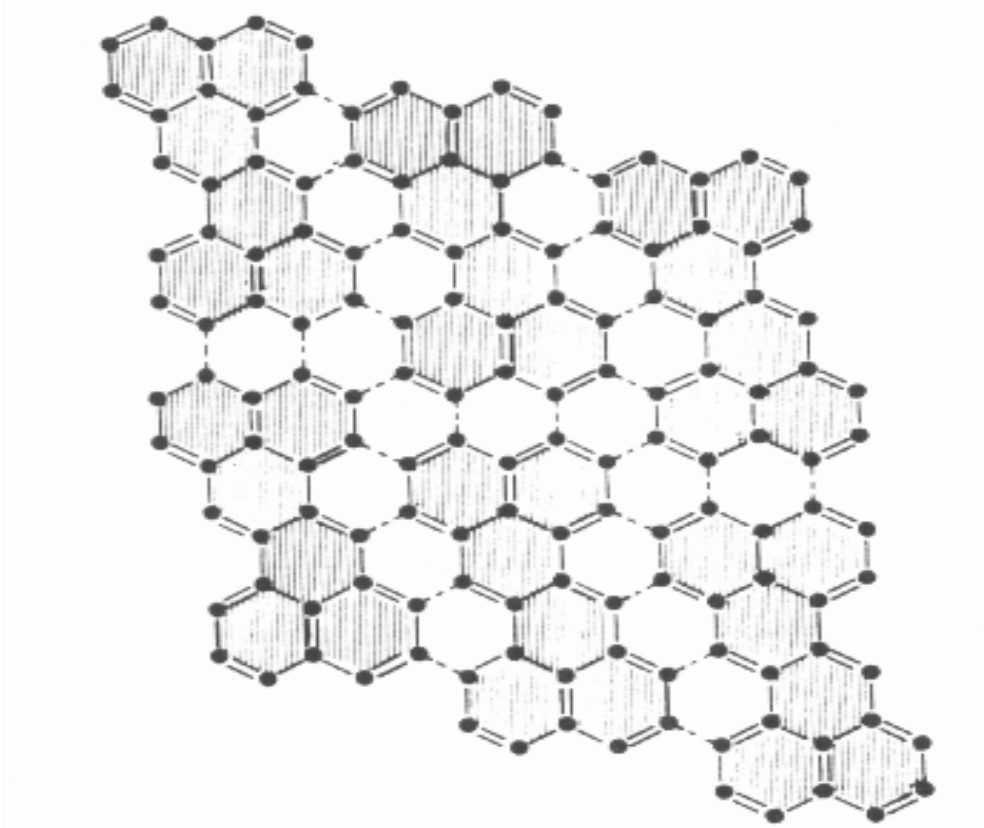

Figure 3.13: Two-dimensional polymerisation scheme for zethrene [63]

In contrast, poorly graphitising compounds such as tetrabenzonaphthalene, which has a non-planar structure, cannot polymerise without creating vacancies.

It can be concluded that carbonisation involves a stepwise molecular rearrangement in which intermediates formed through radical formation condense into solid coke on further heat treatment. The intermediates formed are radicals generated by homolytic cleavage of bonds and condense into solid graphitising or non-graphitising carbon. The intermediate stage formed during carbonisation is called 'mesophase'. This is a liquid phase, which is rich in aromatic radical produced around 400-500 ^{o}C as coal of particular rank soften

and swells from trapped gas and produce an anisotropic mosaic coke texture. This liquid phase is formed from spheres, which grow and coalesce into isotropic phase that solidifies to give a solid coke. Further heat-treatment of the coke produce graphite whose quality is measured by the d-spacing of orientated layers and calculated to be 3.354 Å. The mesophase is inhibited by the presence of oxygen. The aromatic compounds are oxidised by the oxygen into quinines intermediates that loose carbon dioxide to form non-planar radicals with subsequent decrease in the degree of graphitisation. Carbon additives inhibit formation of the mesophase by suppressing release of volatiles during carbonisation. Reaction of sulphur with aromatics compounds occurs during carbonisation and form sulphur containing polymer, which through sulphur radicals form S-Ar-type polymers. Molecular condensation of aromatics with sulphur is known to increase the softening points and carbon yields of the cokes.

CHAPTER 4

GRAPHITE

The graphitisation process is essentially an ordering of the carbon atoms within the carbon matrix towards the perfect structure of hexagonal graphite in a heat-treated carbon. The quality of the graphite depends on the purity and quality of the starting material, and its specific properties depend on its end use. The transition to graphite is not only temperature-dependent or time-dependent, it is a factor of the additives used in the starting material. However, the kinetics of the graphitisation process do not form part of this discussion. Graphite is not composed entirely of carbon but also contains heteroatoms such as H, N and O, etc. The effect of these heteroatoms on graphitisation will therefore also be examined. Understanding the effect of additives in modifying the graphite's properties and in lowering the temperature required to bring about a certain degree of graphitisation or to promote a more graphitic structure are important objectives of this chapter.

4.1 Crystalline forms of carbon

The two known crystalline forms of carbon are diamond and graphite. Diamond is a metastable crystalline form of carbon, with a face-centred cubic lattice of side 3.5667 Å and can be converted to graphite by heating. The carbon atoms are bonded tetrahedrally to four other carbon atoms. To convert graphites to diamond requires both elevated temperatures and pressures. The structure of graphite as reported by Warburton was first proposed by Hull (1917) and confirmed by Bernal (l924) [67]. The structure has a hexagonal unit cell of dimensions $L_a = 2.4615$ Å and $L_c = 6.708$ Å, and an interlayer spacing (d_{002}) of 3.354 Å. The atoms are hexagonally arranged in layers, with the interatomic

distance being 1.42 Å [144]. The layers are arranged in a regular starting sequence ABABAB (see Fig. 4.1).

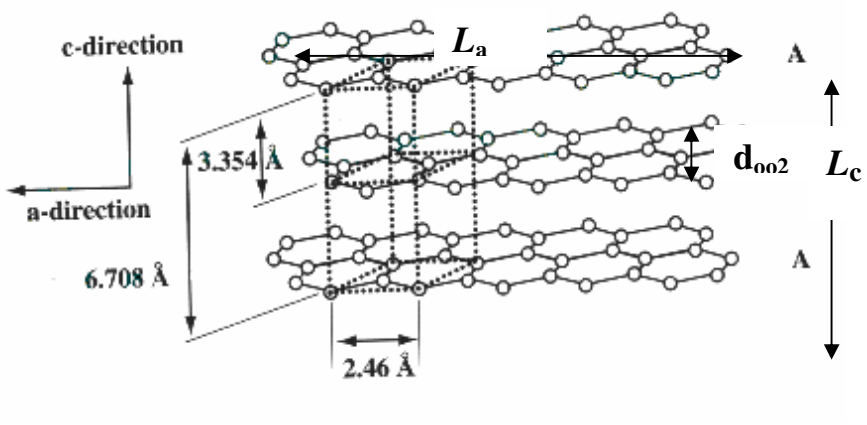

Figure 4.1: The structure of graphite [140]

The structure of graphite does *not* show certain faint lines in the X-ray diffraction powder photographs of both natural and artificial graphites as was thought earlier from electron diffraction photographs of graphite [145, 146]. Instead, the lines found were due to the presence of a rhombohedral structure (about 14 %) in which the layers were stacked ABCABC (Fig. 4.2b) [67].

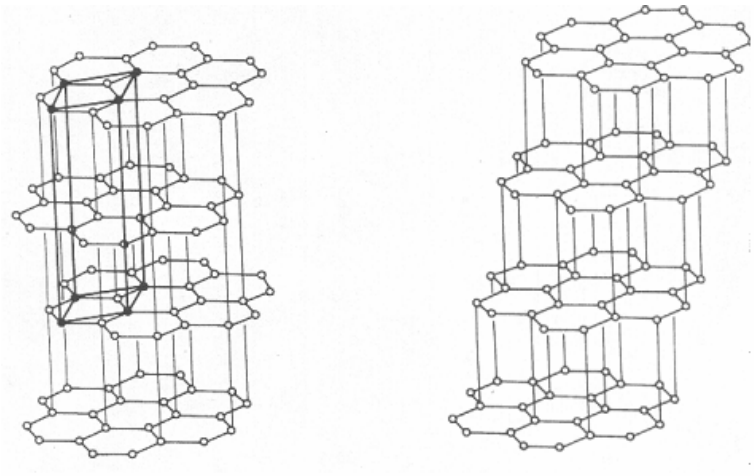

Hexagonal (a) Rhombohedral (b)

Figure 4.2: Lattice structure of hexagonal (with unit cell) and Rhombohedral structures in graphite [67].

It was further proposed that the rhombohedral form comprised up to 30 % of natural graphite and that it could be converted to the hexagonal form (Fig. 4.2a) by heating to 2 000 ~ 3 000 ^{o}C. Because the rhombohedral form has never been isolated, doubt has arisen as to whether it is a separate crystalline form or simply a stacking fault in the hexagonal ABABAB sequence, producing ABCABC sequences. The enthalpy change in going from rhombohedral to hexagonal graphite was reported to be - 0.l44 ± 0.041 kcal per g-atom (- 602.496 ± 171.544 J per g-atom), thus confirming that hexagonal graphite is the most stable phase [147].

4.2 The graphitisation process

Graphitisation as reported by Warburton in the work of Houska and Warren (1954) was based on an incorrect structural model. Small layers in carbon black were thought to grow (either by migration of individual atoms from one layer to another, or by joining of layers) to reach a size (L_a = 100 Å) that was energetically favourable for pairs of nearest neighbours to rotate and take on the graphite relationship [148]. However, the model has been superseded by one in which large layers are already present, the graphitisation process being the thermal annealing out of the defects at low temperature.

Despite the lack of a satisfactory model for pre-graphite carbon, there was enough evidence that such carbons contain extensive areas of graphite-like material. The mesophase studies of Brooks and Taylor [74] demonstrated how this came about. These extensive graphite-like layers are imperfect, although the nature of the imperfection is open to discussion. Whatever their nature, the removal of these imperfections by heating to elevated temperature is responsible for bringing about the formation of a graphitic carbon.

Graphitisation is entirely different from the process just described. Firstly, it takes place in hard carbons and secondly, it involves only a small percentage of the carbon atoms present [149]. Many non-graphitising carbons when heated to temperatures between 2 000 and 3 000 ^{o}C were found to contain a small proportion of graphitic carbon. This was detectable from the diffuse (002) band superimposed upon it, either one (2-phase graphitisation) or two (3-phase graphitisation) sharp lines [150]. The conclusion drawn was that these graphitic components were caused by the high internal stresses set up during thermal treatment. It was thought that a localised crystallisation, under high pressure, had taken place in the interior of the solid. This formation of graphitic carbon would relieve the stress in the remaining cross-linked structure and when the tension in the non-graphitic structure had been reduced sufficiently, the formation of graphitic carbon ceased. Franklin's rigid classification into graphitising and non–graphitising carbons [149] is no longer valid and two–phase graphitisation could take place in what was termed 'non-graphitising carbons' (e.g. epoxide resins, phenol–formaldehyde resins, intermediate carbons (3,5-xylenol/formaldehyde) and in 'graphitising' carbons (polyvinyl acetate, Ford's pitch) [151]. The temperatures at which the graphitic components first appeared were, however, very different. The components appeared in the graphitising carbons at less than 1 000 ^{o}C, at between 1 000 and 2 000 ^{o}C for the intermediate carbons, but not until 2 000-2 600 ^{o}C for the non-graphitising carbons. The non-graphitic component was thought to be due to non-organised carbon. The latter view is somewhat surprising as it is reported that non-organised carbon is present in all the graphitising carbons examined, even at 2 600 ^{o}C.

4.3 The effect of heteroatoms and/or additives

The incorporation of elements such as boron, nitrogen, oxygen and sulphur into the layer planes of a pre-graphitic carbon is analogous to their existence in heterocyclic ring compounds. It has been reported that 1 - 2 atoms of boron could be stably incorporated into the graphite. Carbon prepared at 1 000 ^{o}C or

below may contain up to several per cent by weight of heteroatoms [152]. The majority of heteroatoms are, however, removed by heating to temperatures in excess of 1 500 ^{o}C. It was found that the hydrogen content of the various cokes studied was less than 0.1 ppm at 1 500 ^{o}C, but 40 - 50 ppm of hydrogen persisted in commercial-grade nuclear graphite which had been heated to about 2 700 ^{o}C . About 200 ppm of sulphur in commercial graphite is retained up to temperatures much higher than 2 000 ^{o}C [152].

Small amounts of oxygen in the atmosphere of a baking furnace were found to increase the yield of coke from the binder and thus increase the strength of the artefact [153]. The oxygen acted presumably by forming cross-linkages.

Dehydrochlorination of polyvinyl chloride in the presence of air, at temperatures below 250 ^{o}C, formed non–graphitising carbon, whereas heating in an inert atmosphere produced graphitising carbon [154]. The exposure to air was thought to produce extensive cross-linkages, which inhibited the fusion that may otherwise have occurred in the later stages of carbonisation. It has been noted that for many carbons (e.g. polyvinyl chloride, sucrose and a variety of industrial cokes), the temperature at which the concentration of heteroatoms dropped to less than 0,1 % was close to that at which the three–dimensional ordering commenced [154].

It has been reported that treatment of fibres prepared from molten polyvinyl chloride in ozone and oxygen resulted in an infusible and completely insoluble product (in all solvents) [155, 156]. It was concluded this was due to the formation of cross-linkages between the aromatic planes. Kipling *et al*. [54, 154] found that the progressive addition, prior to carbonisation, of sulphur to polyvinyl chloride led to reduced graphitisability. The addition of 9 % sulphur was thought to be sufficient to change a polyvinyl chloride carbon, heat-treated at 2 700 ^{o}C, from graphitic to non-graphitic carbon. Microscopic examination showed that in

the intermediate range of sulphur addition (5% S), there was a two–phase structure – one phase graphitic, the other non-graphitic.

The conclusion reached was that sulphur acted by forming cross-linkages and promoting dehydrogenation. It is interesting to compare the results of Kipling *et al.* [54, 154] with those of Ihnatowicz *et al.* [95] who studied the effect of oxygen content on the formation of the mesophase spheres. These results showed that for an oxygen content of greater than 7 %, no spheres were formed; from 5 - 7 % oxygen, only small isolated spheres were formed; and only those carbons that originally contained less than 5 % oxygen showed extensive formation of spheres. It would appear from this work that there is a minimum amount of oxygen or sulphur tolerated: up to 7 % oxygen and 9 % sulphur [157].

However, Gillot *et al.* found that removing the sulphur (by heating with hydrogen) from a petroleum coke, at a temperature lower than that at which it would normally be removed, led to the formation of a small fraction of graphitic carbon (d = 3,36 Å, L approx. 500 Å) [158]. A linear relationship was found to exist between the square root of the concentration of heteroatoms and the graphitisability of carbons derived from Catarex pitch, although the addition of sulphur (up to 16.7 % in the case of acenaphthylene) to diphenylamine and acenaphthylene, prior to carbonisation, did not produce any change in their graphitisability [159, 160].

4.4 Catalytic graphitisation

Since the graphitisation process is essentially an ordering of carbon atoms within the carbon matrix towards the perfect structure of hexagonal graphite, heat treatment to temperatures around 3 000 ^{o}C can produce these changes, with the vibrational energy of the lattice being increased sufficiently to promote the atomic displacements. Heat treatment, however, is not the only experimental parameter available to bring about changes. The addition of certain inorganic and organic

additives can improve the graphitisation process. The overall effect is to lower the temperature required to bring about a certain degree of graphitisation or to promote a more graphitic structure at a fixed heat-treatment temperature.

4.4.1 Mechanisms of catalytic graphitisation

The mechanism of catalytic graphitisation varies from system to system, and depends upon the additive and the nature of the carbon (hard or soft). Several distinguishable mechanisms in which the inorganic additives promote graphitisation have been reported. The more familiar mechanism involves growing crystals of graphite from melts of either metal or metal carbide. These crystals dissolve the carbon into amorphous carbon and reprecipitate it as graphite either when it is cooled or as a natural consequence of supersaturation. The driving force of the reaction is a favourable change in free energy in going from the disordered amorphous carbon to a highly ordered graphitic carbon. The production of Kish in the steel-making industry is a common example of this mechanism [161, 162].

In the other mechanism, elements such as aluminium, iron, silicon, etc. are thought to combine with carbon to form carbides. These carbides show appreciable thermal stability, as opposed to cobalt and nickel whose carbides decompose below 400 ^{o}C. The thermally stable metal carbides decompose around 1 500 ^{o}C or higher, and the carbide lattice leaves behind a graphitic lattice. Externally, these graphite crystals are pseudomorphs of the original carbide crystal and result from the vaporisation of the metal. A simple physical picture explaining this phenomenon may be that because these carbides are usually interstitial carbides, they contain close-packed layers of meta-atoms, between which lie the carbon atoms arranged in hexagons. When the metal leaves the lattice, the carbon atoms are left approximately in layers and within these layers they are arranged hexagonally. It is therefore easy to conceive a rearrangement to give the layered graphite structure [67].

4.4.2 The effect of additives on catalytic graphitisation

The incorporation of small amounts of non-volatile metallic oxides of aluminium, iron, magnesium, titanium or vanadium with pitch and binder is believed to catalyse the transition of the carbon to graphite [163]. Highly pure graphite was produced by the addition of aluminium carbide (Al_4C_3) and subsequently heating to 1100 ^oC in a stream of chlorine [164]. The carbide decomposed to graphite and acted as a nucleus for further graphitisation, and the metal was removed as volatile chloride. The temperature of 1 100 ^oC was lower than the decomposition temperature of the carbides (SiC, Fe_3C). Further heating to 2 000 ^oC for 2 h completed the graphitisation. The addition of Al_4C_3 led to an increase in the crystallite dimension L_c with a subsequent increase in the density of the graphite and an improvement in its neutron radiation stability.

In a heated series of metal compounds mixed with hard carbons at temperatures between 1 400 and 2 300 ^oC, X-ray diffraction techniques revealed aluminium to be an effective catalyst at 1 500 ^oC. An extra diffraction line was found and appeared to be due to an intermediate between the metal being considered and carbon. The decomposition of the intermediate is thought to have enhanced graphitisation [67].

The iron-carbon system in graphitisation has been well studied. Studies have focused primarily on the mechanism associated with carbon dissolving in molten iron and precipitation of the graphite. The intermediate carbide is formed. A large single crystal of graphite was grown by saturating solutions of iron (or nickel) with a low supersaturation of carbon, and then slowly cooling in steady-state thermal current [165]. However, the technique was later modified by dissolving the carbon in molten iron and evaporating the iron at an elevated temperature. The iron enclosed in the graphite was evaporated at temperatures of 3000 – 3200 ^oC for an hour, resulting in the formation of graphite crystals from the central volume occupied previously by the evaporated iron [165].

The role of iron in the graphitisation of petroleum coke and of non-graphitising carbon from sucrose on heat treatment from 1 800 – 2 400 ^{o}C was studied. The results were postulated to follow the mechanism in which the iron combines with carbon to form cementite, which then decomposes into graphite. In the process, the iron diffused through the grains of the coke and altered the structure within the grains to promote graphitisation within the non-graphitising carbon [166].

Heating a hard carbon in the presence of iron transformed it into a mixture of graphite and graphitisable carbon. Observation of the external surfaces of the coke grains showed that they were not changed by the iron, although they appeared earlier – at 1 600 ^{o}C instead of 2 200 ^{o}C. The effect was observed within the grains of the coke: iron carbide or cementite appeared to have been formed within the boundaries of the domains constituting hard carbon. These domains became free to orientate themselves on the surface of the droplets of the iron carbide, with their carbon layers parallel to the surface. The droplets coalesced into graphitisable carbon. This means that graphite was produced by dissolution of iron to form Fe_3C and that carbon was precipitated as graphite [167].

Heat treatment of iron or iron compounds with amorphous carbon led to the formation of the carbide, cementite (Fe_3C), which decomposed on further heating to give graphite [168]. Dispersion of cementite in amorphous carbon at 110 ^{o}C over a stream of chlorine was found to decompose the carbide into graphite, which then nucleated the graphitisation at 2 000 ^{o}C for 2 h [164]. The formation of cementite as intermediate carbide was further reported to yield even better graphite when used in conjunction with silicon as ferrosilicon [169]. Improved graphite density and neutron stability was achieved on addition of ferric oxide and led to an increase in the crystallite size parameter L_c [170]. Incorporation of small amounts of iron oxide with pitch and coke was reported to enhance the transition from amorphous carbon to graphite [67, 159].

It can be concluded that iron or an iron compound catalysed the conversion of hard carbon into a graphitisable carbon by firstly dissolving the hard carbon to form an intermediate phase, cementite Fe_3C, which separated on further heating into graphite formed in the spaces left by the evaporated iron.

4.4.3 The effect of side-chains on graphitisation

Graphitisation of a series of carbazole derivatives substituted at the ring position by one or more methyl, ethyl or butyl group(s) revealed that these carbons become more graphitic with increased alkyl substitution and with increased chain size of the alkyl group [166]. Carbazoles normally form non-graphitisable carbons due to the radicals formed during carbonisation being non-planar and forming a three-dimensional cross-linked carbon. It was then postulated that the enhancement of graphitisation by alkyl substitution was most likely due to planar aromatic free radicals being formed by thermal cleavage of the alkyl group. A competing reaction by which carbazoles carbonised in the normal way occurred. Such competing reactions were thought to be responsible for the resulting multi-phase carbons. The extent of planar free radical formation was thought to be dependent on the number of alkyl groups per molecule and the case of formation of the radical [171].

In conclusion, it would appear that the inclusion of heteroatoms into the carbon precursor leads to a less graphitic product and this is exactly what would be predicted from the modern ideas on pre-graphitic carbons. The inclusion of a heteroatom must lead to the formation of a point defect, and the removal of defects of one sort or another is the very essence of what is now understood by the graphitisation process. An exception to the general rule, whereby carbonising in oxygen leads to a less graphitic product, has, however, been reported. A more graphitic carbon was derived from a poly-2-h-dimethylphenylene oxide which had been cross-linked, by pre-oxidation, before pyrolysis [172]. It was shown that

after such a carbon had been heated to 2 900 ^{o}C, the d-spacing was 3.36 Å compared with 3.38 Å for the non-oxidised polymer, despite the fact that the polymer was known to exhibit melting during the first stage of pyrolysis. The reason for this anomaly is that the ether bridge in the un-oxidised polymer is ruptured at 370 ^{o}C, producing a rigid system of benzene rings separated by a conjugated system of one single and one double bond.

Condensation of this polymer occurred at 400 ^{o}C to produce an aromatic system that was incapable of building up into an extended aromatic layer without the inclusion of vacancies. The ether bridges in the oxidised polymer, on the other hand, rupture at temperatures ranging from 300 – 500 ^{o}C and continuous rearrangement of the intermediates created an aromatic system that was capable of producing an extended aromatic layer [172].

The above studies all relate to heteroatoms incorporated during carbonisation, either by exposure to air or by addition prior to carbonisation. Further study of carbonisation on aromatic hydrocarbons with heteroatoms revealed that not all of these molecular species form non-graphitising carbons. It appeared that if a compound forms an intermediate, with the elimination a heteroatom, the intermediate condenses to form an extended aromatic molecule, resulting in good graphitisability. Heterocyclic compounds containing sulphur and nitrogen could produce quality graphite [173].

Oxygen, sulphur or nitrogen, when present in the precursor, remains entrapped in the carbon skeleton to 2 000 – 2 200 ^{o}C. The presence of these elements may result in the degradation of the aromatic ring system through the elimination of carbon dioxide. This degradation generally led to non-planar free radicals, which polymerised to give mostly a cross-linked disordered carbon. The enhancement of graphitisation by alkyl substitution was shown to be due to planar aromatic free radicals being formed by thermal cleavage of the alkyl group. The extent of planar free radical formation was dependent on the number of alkyl groups per

molecule and the manner of formation of the radical. Aromatic systems promote mesophase formation by virtue of their planarity and low reactivity [173, 174].

4.5 Properties of graphite important to the nuclear industry

This sub-section focuses on those applications of graphitisable carbon relevant to the nuclear industry. Its commercial use in aluminium as graphite electrodes, in steel as coke (as a reducing agent), as carbon mesophase powder for providing structural stability, as a lubricant and in aerospace as coke, though important, will not be discussed in this sub-section. The properties of graphite required for the reactor reflector in nuclear energy industry will be discussed.

Gilsonite material has been used in the United Kingdom and elsewhere as a starting material for the moderator graphite since it produces graphite with near-isotropic bulk properties. The coefficients of thermal expansion for an extruded Gilsonite pitch graphite are parallel and perpendicular to the extrusion direction, being 4.0 and 4.5 x 10^{-6} $^{o}C^{-1}$ respectively, whereas for an extruded petroleum coke graphite they are 1.3 and 3.2 x 10^{-6} $^{o}C^{-1}$ respectively [10]. Graphite forms a major component of the fuel, which is composed of particles of UO_2 kernels successively coated with pyrolytic carbon, silicon carbide and pyrolytic carbon. Graphites subjected to a high dosage of neutron irradiation (>5 x 10^{21}n/cm$^{2)}$ at 300 – 1 500 ^{o}C showed pores and cracks at the boundaries between the filler the particles, causing them to disintegrate. The effect was observed to be less marked for graphite with near-isotropic bulk properties than for conventional anisotropic graphites, when compared at the same neutron dosage and temperatures [11, 12].

A highly anisotropic coke leads to graphite with properties such as high magnetic susceptibility, high electrical conductivity and a high coefficient of thermal expansion. The strength of graphite at high temperature and its behaviour with respect to the products of nuclear fission/fusion make the material suitable as a

nuclear moderator and reflector, and as a material for construction and for thermal columns in various reactors [175]. Advanced gas-cooled reactors, high-temperature gas-cooled reactors, molten salt breeder reactors and liquid-fuelled reactors all use graphite moderators. Graphite suitable for nuclear reactors must have uniform coefficients of thermal expansion across and along the plane (a-axis and c-axis plane of the crystallite) so as to prevent the reactor block from swelling (see Table 4.1). (Isotropy of the graphite with low boron content is preferred as it confers the required properties on the graphite.)

Table 4.1: Properties of nuclear graphites [176]

Property	**Anisotropic graphite**	**Isotropic graphite**
Density (g/cm^3)	1.71	1.86
Resistance (μΩ·cm)	735	1 000
Tensile strength (kPa^c)	9.93	46.172
Coefficient of thermal expansion (10^{-6}/ ^{o}C)		
With grain	2.2	5.3
Against grain	2.8	5.3
Anisotropy ratio	1.73	1.0
Total ash (ppm)	740	400
Boron content (ppm)	0.4	0.3

The properties of two types of graphite used as moderators or reflectors in nuclear reactors are listed in Table 4.1. The data for the coefficient of thermal expansion indicate that anisotropic graphite shows unequal coefficients of thermal expansion in the a-axis and c-axis of the crystallite graphite and it is therefore not preferred for nuclear reactors [176].

With exposure to high-temperature radiation over a long time, graphite undergoes dimensional changes in length and volume. Fig. 4.3a shows the length change in isotropic nuclear graphite during irradiation at various temperatures of relatively high fluxes, while Fig. 4.3b shows the volume changes in conventional nuclear graphite during irradiation at various temperatures of relatively high fluxes.

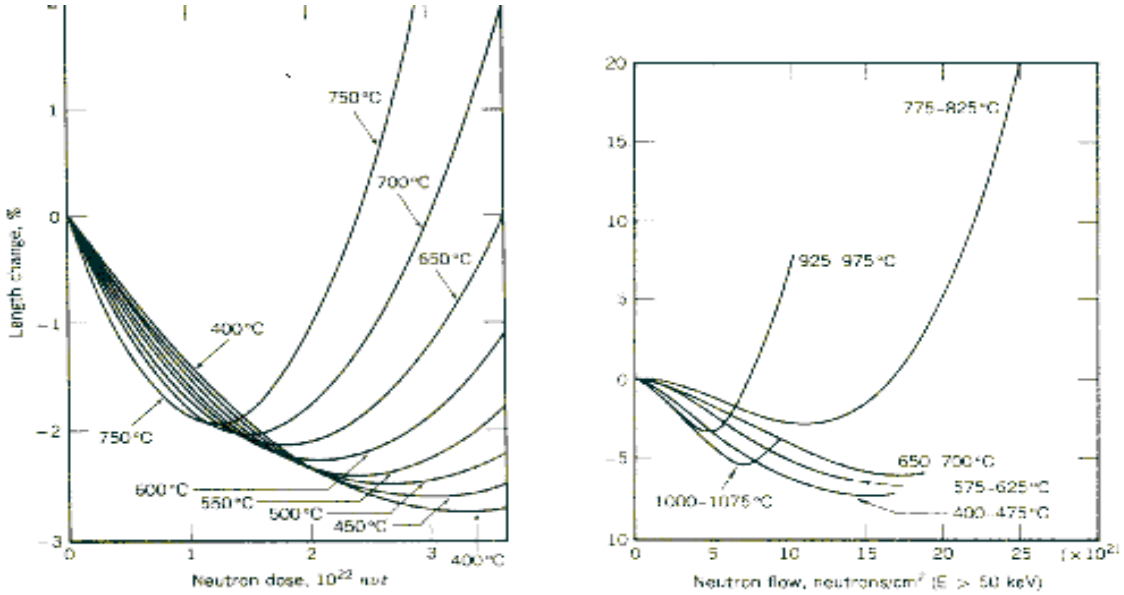

a **b**

Figure 4.3: Radiation-induced dimensional changes in isotropic graphite
(a) At various temperatures (nvt = neutron density) x velocity x time.
(b) Volume change in anisotropic graphite during General Electric Test Reactor irradiation [176].

The graphites initially contract on exposure to fast-moving neutron doses, but the rate of contraction decreases with exposure until the graphites reach a minimum volume. Further increases in neutron doses cause volume expansion, with the rate of expansion increasing very fast at a neutron dose above 3 x 10^{22} neutron/cm^2 (> 50 keV) [176].

A good moderator material must not react with neutrons, because if they are captured in the moderator, they cannot sustain the fission process. Moreover, the neutrons should slow down over short distances and there should be few collisions in the moderator. Ideally, moderators should be inexpensive and should be compatible with the reactor's structural design. A good moderator should efficiently energise fast neutrons through the process of elastic collisions. The maximum energy loss per collision occurs when the target nucleus has unit mass, and tends to zero for heavy target elements. A low atomic number is a prime requirement for a good moderator. The slow-down power should be large compared with the tendency to capture neutrons (capture cross-section), which should be small [176].

Graphite is used in nuclear reactors because of its availability, its good moderating properties and its low neutron capture cross-section of $0.0032 \pm 0.002 \times 10^{-24}$ cm^2. The latter is a factor of the purity of reactor-grade graphite, which depends on the raw material selected and on its subsequent processing and purification. The degree of purity required is determined by the reactor design. Taking into account the density of reactor-grade graphite (bulk density of 1.71 g/cm^3), the bulk neutron adsorption coefficient is 0.0003/cm. This suggests that a slow neutron may travel 32 m in the graphite without capture. The unique properties of such graphite are its mechanical strength and excellent machinability [177]. Furthermore, the thermal stability, resistance to corrosion and high thermal conductivity of graphite makes it a most suitable moderator material for consideration in advanced design, high-temperature and atomic energy-efficient nuclear reactors [177, 178].

CHAPTER 5

GRAPHITE CHARACTERISATION METHOD

Structural analysis of the graphitisable carbon produced requires instruments whose precision is necessary for reliable, accurate and reproducible results. It is important to understand the techniques used for obtaining the optical texture of the coke and the graphite, and to understand the industrial relevance of these techniques. This chapter therefore provides information on the instrumentation and operational techniques used in assessing the quality of the coke and graphite produced as discussed in the experimental section (Chapter 6).

5.1 Determination of the optical texture of the coke

The polished block of a carbon sample mounted in resin is observed using the polarised light of an optical microscope (Fig. 5.1) and an analyser at 90 °C (cross-polar). Isotropic materials such as resin appear black, whereas crystalline media reflect the light when the molecular orientation of the surface of the section is not parallel to a symmetry fold, and domains with molecules lying flat disappear (Fig. 5.2a).

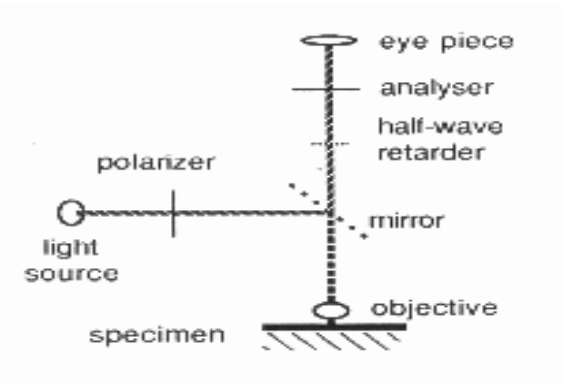

Figure 5.1: General outline of the optical microscope [178]

In other domains, disappearance occurs when molecules are parallel to either the polariser or analyser; black lines or contours are seen. The introduction of the λ-plate causes the retardation to introduce interference colours, which change with the orientation of the layers (Fig. 5.2b) [179].

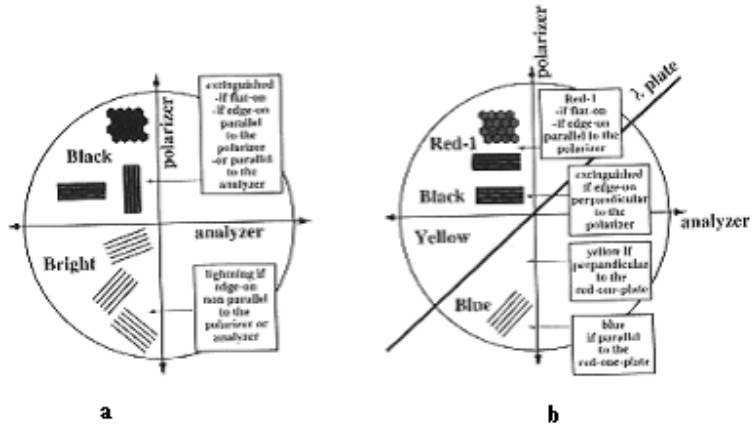

Figure 5.2: (a) Extinction and reflection under cross-polars and (b) Interference colours with the addition of a λ- plate [179]

The technique for measuring the optical anisotropy of the coke is to use a reflected polarised microscope equipped with a rotating analyser. It maps out gradients in artefacts. The reflectance of the coal macerals is used as a measure of the percentage of optical anisotropy and is a proportion of the direct light that is reflected from the polished surface under specific conditions of light exposure [179]. Vitrinite in coal develops anisotropy and thus show bi-reflectance. By measuring the true maximum and minimum reflectance, the anisotropy can be calculated by the difference R_{max} - R_{min} [179].

Consider an example illustrated with polarised optical microscopy (Fig. 5.3). The microscope is equipped with an NS polariser and a WE rotating analyser. In this example, a thick-coated fibre (~2 μm) is used. In the WE position, the rotating analyser indicates Ae = 0^{o} and the two polar hairs are said to be 'crossed' (a Maltese cross is observed).

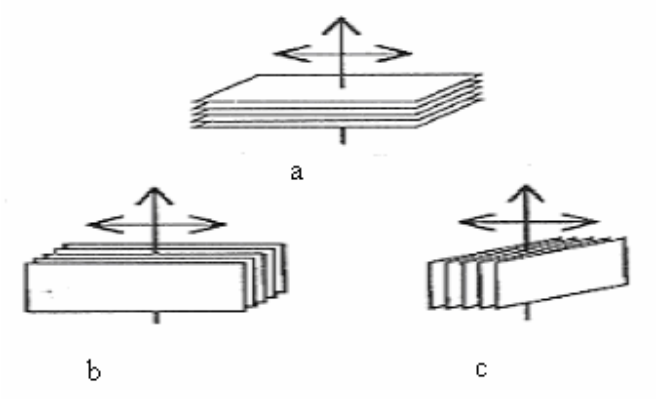

Figure 5.3: Retardation parallel plates used to observe interference colours [179]
(a) Basal plane interaction near maximum
(b) Maximum interaction with polarisation parallel to the planes
(c) Minimum interaction with polarisation perpendicular to the planes.

The measurement is made on the bisector of the first quadrant (white arrow) (Figure 5.4). The analyser is rotated clockwise so that the N and E branches of the Maltese cross fuse together on the bisectors. The quadrant is extinguished, and then becomes bright again. At the position of complete darkness, the extinction Ae is read directly on the vernier micrometer of the analyser [179]. Ae (expressed as degrees) is related to the reflectance anisotropy ratio Ro/Re by the simple relation:

$$Ro / Re = tg^2 (45 + Ae) \qquad (5.1)$$

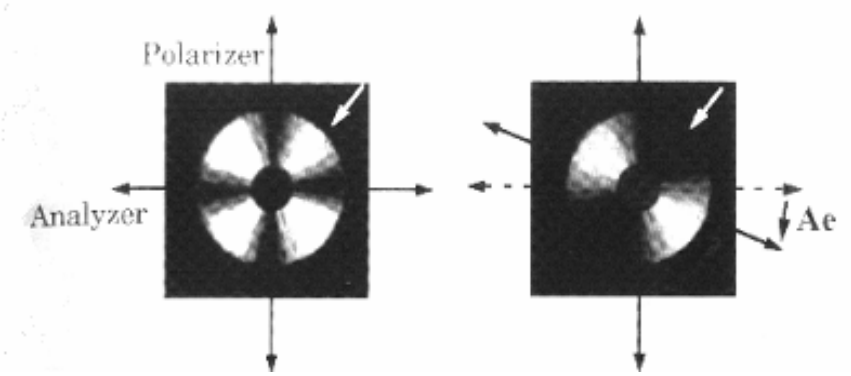

Figure 5.4: Polarised light optical microscopy showing extinction angles The extinction angle Ae is measured under cross-polarised light. The extinction is obtained in the first quadrant (white arrow) by rotating the analyser clockwise [179]

The crystallite arrangement in carbonaceous solids is observed after they have been heated to 1 000 ^{o}C. This crystallite arrangement starts over a narrow temperature range at 450 ^{o}C, coinciding with the development of the mesophase, which leads to the anisotropic structures found in coke. The shape and size of these anisotropic structures determine the behaviour of a particular coke. Unlike isotropic liquids, a crystal is characterised by a long-range order. Liquid crystals are droplets of spheres within the isotropic mass that coalesce into crystalline domains (molecular order). The molecular arrangement is envisaged as rod-shaped, with similarly sized molecules lying parallel to each other but with no stacking order. Classification of the coke is therefore based on the shape and size of the anisotropic structure, as follows [180]:

Isotropy	No optical activity, uniform, light purple colour on the surface
Anisotropy via mesophase	Dark purple, yellow and blue areas of varying shape and size
Fine-grained mosaic	Irregular shape, isochromatic areas (ISA), 0.5-1.5 µm long
Coarse-grained mosaic	ISA, 5.0 – 10 µm long
Coarse flow	Rectangular, flow-type structures, 30 -60 µm long, > 10 µm wide
Flow domains	Flow-type structures, > 60 µm long, > 10 µm wide
Domains	Isomeric structures, > 60 µm long
Basic anisotropy	Flat, featureless anisotropy associated with the parent unreacted (or slightly altered) vitrain from a high-rank coal

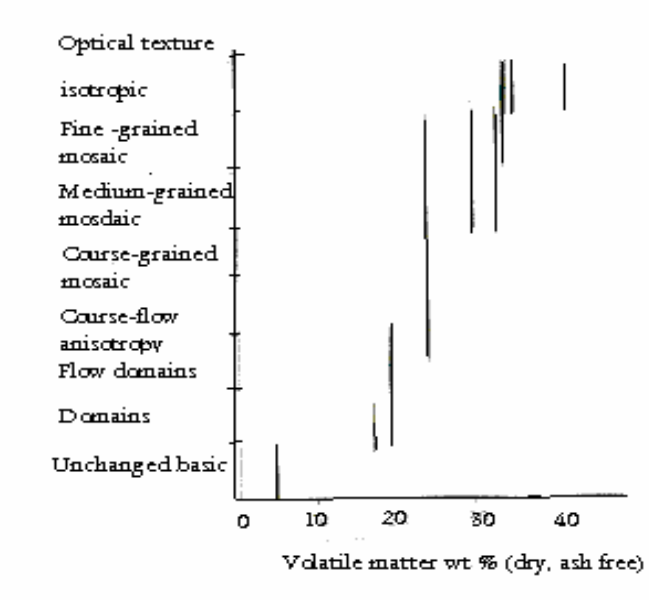

Figure 5.5: Variation of a coke's optical texture with the volatile matter content of the parent vitrains [180]

The size of the anisotropic structures in coke increases with increasing coal rank, which is a factor of the volatile matter released (Fig. 5.5) [180].

5.2 X-ray diffraction

The quantitative X-ray diffraction analysis of carbonaceous material was first conducted by Warren [93]. Today, structural parameters such as crystallite size and its distribution, L_a, L_c and d_{002}, P_n, are determined. The X-ray diffraction technique is sensitive to crystal defects, non-destructive and requires sample preparation. A high-resolution X-ray diffractometer is used with a 2.2 Kw Cu X-ray tube, the focus of which can be set to either a line or point source. For the point source, the beam is monochromised and collimated by the Ge 220 four-crystal monochromator to select the $CuK_\alpha 1$ wavelength λ (normally 0.1540511 nm) with a wavelength spread, $\Delta\lambda$, of 0.0000461 nm [181].

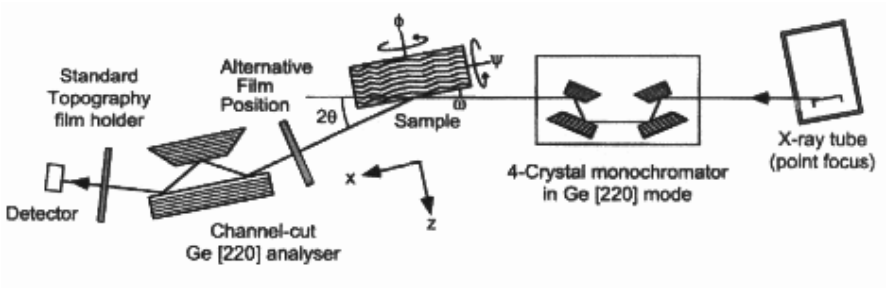

Figure 5.6: Schematic diagram of the X-ray diffraction system [181]

The incident beam is filtered by the Ge 220 monochromator. The beam reaches the sample at an angle of ω to the diffraction plane. ψ is the tilt angle of the sample and ϕ is the angle of rotation around the sample holder normally. The outcoming beam reaches the detector after having collided with the triple-axis crystal. A photographic film sensitive to X-rays can be placed before or after the triple-axis analyser crystal to produce X-ray topography images (Fig. 5.6). The

measured crystallite sizes, L_a and L_c, and the interlayer spacing, d_{002}, of the carbonised material can be obtained [181].

5.2.1 Measurement of interlayer spacing d_{002}

The interlayer spacing, d_{002}, is obtained by measuring the 2θ angle at the maximum of the 002 peak ($25^o > 2\theta < 26.6^o$ for a Cu anti-cathode). Accurate results are obtained by the addition of an internal standard (such as Si with Si_{111} at 340 pm) to a powder of the sample. The 2θ values at the maximum of the smoothed peak is used to calculate the mean d_{002}-spacing of the sample by means of the Bragg equation (5.1).

$$2d_{hkl} \sin(\theta_{hkl}) = n\lambda \qquad (5.1)$$

where θ_{hkl} is the scattering angle and d_{hkl} is the spacing between hkl planes.
The d spacing (pm and pm = 10^{-12} m) is related to the degree of graphitisation by the Maire and Meiring equation (5.2) [181]:

$$g = (3.44 - d_{(002)}) / 0.086 \qquad (5.2)$$

5.2.2 Measurement of crystallite size L_a and L_c

The coherent lengths, L_a and L_c, are estimated from the amount of peak broadening, β, using the Scherrer equation (5.3):

$$L = K\lambda / \beta\cos\theta \qquad (5.3)$$

Where L = the coherent length
λ = the wavelength
β = the width at half peak-height
θ = the Bragg angle of the line
K = the Scherrer reflection.

Measurement of the peak width, β_{002}, from the 002 or 001 reflection is used to determine the stack size, L_c.

5.3 Raman spectrophotometry

During the past few years, Raman spectroscopy has evolved as an effective technique for a rapid and non-destructive characterisation of carbonaceous materials and to follow the graphitisation process (Fig. 5.7). It relates to the frequency changes observed when a monochromatic light beam is scattered by the molecules contained in the sample. The frequency shifts observed for the scattered light are due to the interaction of the incident light with vibrating molecules [182].

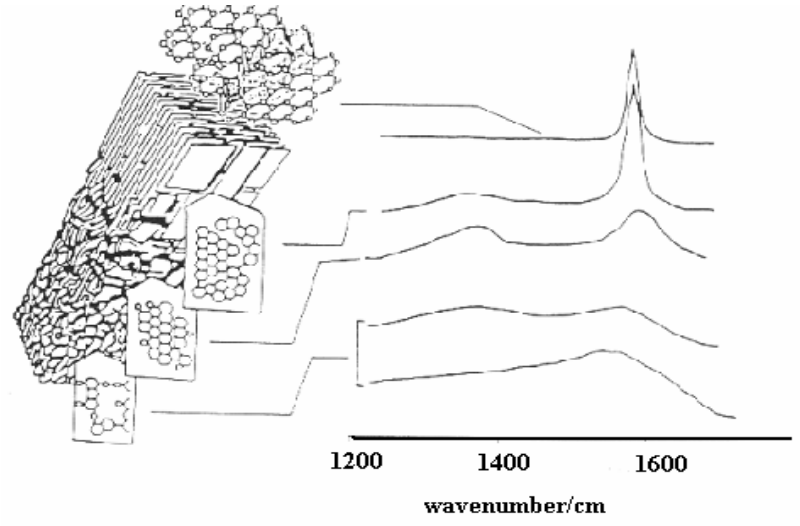

Figure 5.7: Evolution of Raman spectra from carbonaceous material to graphite [182]

5.3.1 Raman microscope

Raman microscopy is very appropriate for studying at the micrometre scale the chemical bonding, the phase composition and the crystalline state of solids, from

poorly organised to well-crystallised structures. This technique is based on the analysis of the spectral characteristics of the vibrational modes associated with the Raman shifts (wave number, bandwidth and intensity). The instrument used for this work is based on the latest fibre-bundle image compression (FIC) design, a technique that allows simultaneous collection of a spectral 3-D data cube in one read-out of a CCD detector. In this FIC-based instrument (Fig. 5.8), the light propagates from the sample to the spectrograph through an optical fibre bundle. At the collection end, the optical fibres are ordered in a square array where each fibre collects light from a unique spatial point in the sample. At the distal end of the bundle, the optical fibres are ordered in a linear stack, which serves as the entrance for an imaging spectrograph. The linear stack is attached to an imaging spectrograph and provides 80 Raman spectra per image frame, each with 900 wavelength channels.

The sample is imaged onto the fibre bundle by optically coupling the bundle to an Olympus BX-60 microscope. A x 20 microscope objective (Olympus IC-20) yields a single-frame field of view of 70 x 56 μm, with a spatial resolution of 7 μm per FIC image pixel. The sample is globally illuminated by a 500 mW diode laser (SDL-8630) operating at 785 nm, with a total power of view (or about 1 mW of excitation power per Raman spectrum). Besides the imaging capabilities of the instrument, the system can be used as a conventional Raman microscope where a single-frame field of view gives one average spectrum (single-frame exposure), corresponding to the sum of all 80 Raman spectra in a single-image frame [183, 184].

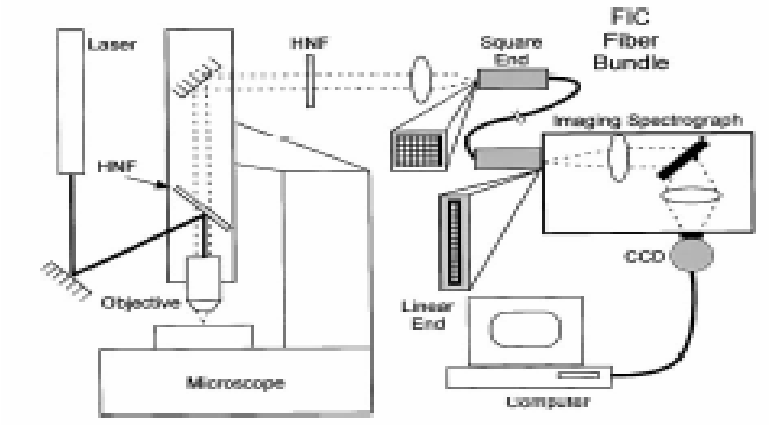

Figure 5.8: Raman imaging microscopy [184]

5.3.2 Raman spectroscopy and the optical characteristics of graphitisable carbon

Raman microscopy has been widely applied to the study of carbon materials and their graphitisation behaviour at high temperature [184]. The hexagonal graphite structure (space group D^4_{6h}) is characterised by two Raman active vibrational modes with E_{2g} symmetry (E_{2g1} and E_{2g2}). Both modes correspond to the in-plane vibrations of carbon atoms. Whereas the former mode corresponds to shear displacement of whole graphene layers (νE_{2g1} = 42 cm^{-1}, not considered here), the latter involves the stretching of the sp^2 C-C bond. Owing to the C-C covalent bond (as compared with the weak interlayer --bonding), the E_{2g2} mode (commonly referred to as the G band) is characterised by a much higher frequency (νE_{2g2} = 1 582 cm^{-1}). With disordered carbons (e.g. turbostratic), the Raman spectra commonly show an additional feature at about 1 350 cm^{-1} (D band or A_{1g} mode), as well as, in some cases, another weak band around 1 620 cm-1 (D' band), close to the G band. Both the D and D' bands are generally associated with a broadening of the G band. They are assigned to defects within the carbon microtextures (edge, distorted graphene layers, etc.) with regard to ideal graphite structure [185, 186, 187]. The 1 350cm^{-1} band is attributed to the

finite crystal size. The intensity ratio of the 1 350 cm^{-1} band to the 1 580 cm^{-1} band can be used to measure the crystal size, L_a, of the graphite sheet [122].

Structural defects have been observed in mechanically ground graphite by Raman microscopy. The interlayer spacing was found to increase during the grinding process with the reduction of the crystallite size, La, Lc. Smaller values of full width at half maximum (FWHM) of the 1 350 cm^{-1} peak in heat-treated carbon and ground carbon were observed [188].

It has been found that the lower the plasticity of the softened coal, the lower the degree of orientation of the aromatic nuclei. Inversely, the higher the plasticity of the coal, the larger the zone of anisotropy in the coke. The latter zone of anisotropy could be interpreted as a zone within the aromatic lamellae having approximately the same orientation. Higher rates of heating lead to a lower viscosity and subsequently an increased zone of anisotropy. Inversely, a sharp reduction in the rate of heating, viz. 0.5 – 1 ^{o} C/mm, can result in a higher degree of viscosity, and a reduction in the size of the zones of anisotropy and sometimes even in isotropy [189].

CHAPTER 6

EXPERIMENTAL

This chapter describes the starting material, chemicals, apparatus and experimental procedures used in obtaining the graphitisable carbon.

6.1 Chemicals used

The chemicals, all pure grade, used were: N, N-dimethylformamide (DMF) 99.9 % AR (Samsung Fine Chemicals); NaOH CP in pearl (Bio-Zone Chemicals); hydrated Na_2S 60 - 62 % (PAC Chemicals), KCN analytical grade (Rochelle Chemicals), $Na_2S_2O_3 \cdot 5H_2O$ (Acros Organics) and polyethylene glycol-400 (PGA-400). The carbon black and acetylene black, i.e. the carbon additives, were supplied by Ferro Industrial Chemicals Ltd and SA Dow (Pty) Ltd respectively. (See Appendix D.)

6.2 The solvent of choice

N-methylpyrrolidone being a relatively expensive solvent, the solvent of choice is defined by the general equation (2.5), where R_2 and R_3 = the methyl group, M = carbon, R_n = H and R_1 = 0. The structure takes the form of N, N-dimethylformamide or formic acid dimethylamide (Fig. 6.2.1), which is inexpensive and readily available in South Africa

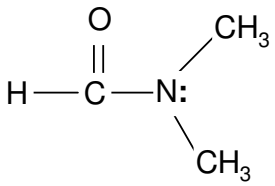

Figure 6.2.1: N, N-dimethylformamide (DMF)

N, N-dimethylformamide is a suspected carcinogen, hygroscopic and has the following physical properties (Table 4.1): density of 0.957 g/ml; Mp~ -61 ^{o}C; boiling point ~ 152 - 154 ^{o}C; flash point ~ 59 ^{o}C; viscosity/20^{o} ~8 m Pa; dipole moment/20^{o} ~ 36.7; saturation concentration/20 ^{o} ~36.7; explosive limits 2.2 - 16 vol. %; miscible with water; residue upon evaporation ≤ 0.0005 % [190, 191, 192]. The impurity levels identified include the following:

- Free acid (CH_3COOH) ≤ 0.003 %
- non-volatile matter ≤ 10 ppm
- Free alkali (NH_3) ≤ 0.005 %
- Water ≤ 0.15 %
- Residue upon evaporation ≤ 0.005 %

Table 6.2: Traces of elements present in N, N-dimethylformamide [190, 191, 192]

Element symbol	Amount mg/kg	Element symbol	Amount mg/kg	Element symbol	Amount mg/kg
Al	0.50	Cu	0.02	Ni	0.02
Ba	0.20	Fe	0.10	Pb	0.10
Bi	0.10	K	0.50	Sr	0.10
Ca	0.50	Li	0.10	Zn	0.20
Cd	0.05	Mg	0.10	Sn	0.10
Co	0.02	Mn	0.02	Mo	0.10
Cr	0.02	Na	1.00		

6.3 Coals studied

The Tshikondeni coal (ash content ~ 10 %, particle size distribution < 150 µm passing, obtained from Tshikondeni coal mine and supplied by Kumba Resources, RSA) was chosen for this research because of its availability and

solubility in dimethylformamide (DMF). Analyses of coal (air-dry basis) were done by the SABS Coal Exploration Technology Section. Table 7.1.1 gives the proximate analysis, Table 7.1.2 gives the ultimate analysis, Table 7.1.3 gives the ash analysis and Table 7.1.4 gives the petrographic characteristics of the coals.

6.4 Apparatus

This section lists the apparatus used. All electrical appliances, viz. furnaces, ovens and balances, were calibrated by Microsep Co. and Intercal Co., affiliated to the SABS's International Calibration Laboratory.

1. Outline of the reactor used in the extraction process

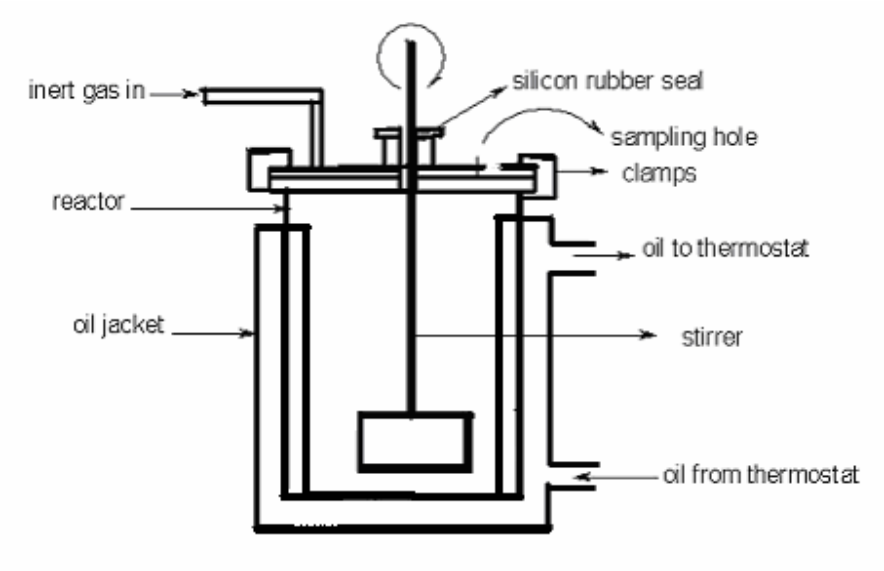

Figure 6.4.1: The reactor used for coal dissolution

2. Oven: model Labcon EFDO, supplied by Merck, equipped with an inlet for nitrogen flow which is used for drying.
3. Beckmann model GPR Centrifuge with a maximum speed of about 5 000 r/min

4. LKB Bromma 2160 Midispin Centrifuge with a maximum speed of 4 000 r/min
5. Clements GS 150 Centrifuge with a maximum speed of 2 000 r/min
6. Ohaus Explorer balance, 2 100 g full-scale capacity with a resolution of 0.001 g.
7. Mixer: Ultra-TURRAX TIZ5, IKA-Labortech, max. speed 2 400 r/min
8. Stirrer: Heilddph-Labortech, 140 – 1 100 r/min
9. Furnace system (used in pyrolysis): supplied by Prestige Furnace and Engineering, with nitrogen blanketing and automated temperature programmer important in carbonisation (Fig. 6.4.2).

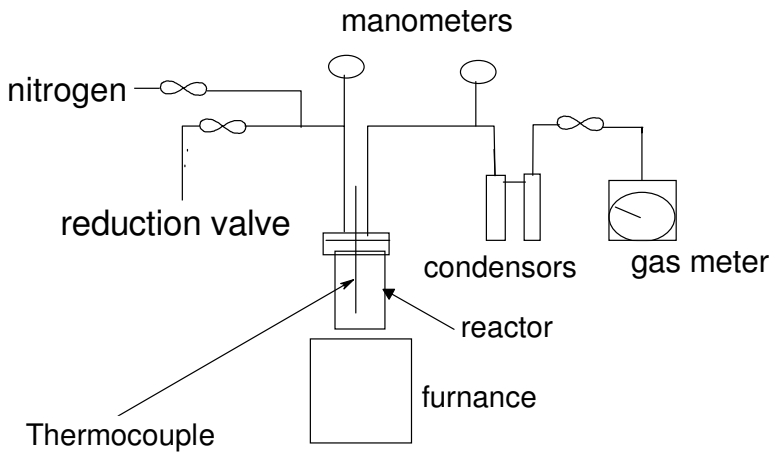

Figure 6.4.2: Furnace system used for pyrolysis

6.5 Instruments used to analyse the results

The instruments described in this section were used in the analysis of the results. In each case, the method of analysis is also described.

6.5.1 Spectronic Genesis - 5 Ultra-Violet Spectrophotometer

This instrument was used to measure the degree of extraction by measuring the optical transmission of the diluted samples at 600 nm.

6.5.2 Optical microscopy

To obtain optical micrographs and reflectance, an optical microscope equipped with a computerised digital camera (Olympus DP B10 with soft imaging system) was used to observe the surface characteristics of the coke (courtesy of the Department of Geology University of Pretoria). Reflectance measurements were taken on each of the samples in accordance with the ISO Standards 7404-5 of 1994 by the Petrology Section of Coal and Mineral Technologies (Pty) Ltd at the SABS. An assessment of the microscopically recognisable coke textural characteristics was made with reference to the AS Standards D 5061-92 (courtesy of the SABS, Coal and Mineral Technologies (Pty) Ltd). For each set of two measurements, the object stage was turned through an angle of 90 ^{o}C and the maximum and minimum reflectance values recorded.

In order to view the samples under an optical microscope, it is necessary to prepare a highly reflecting, polished surface. To facilitate the polishing of the very brittle samples, a cross-section of each sample was mounted in Bakelite resin. In order to expose the sample and prepare a flat surface, the initial grinding was carried out on a grinding disc fitted with 120, 600 and 1 200 grades of diamond disc, over which water was flowing continuously. Grinding was carried out on the successively fine grades until a flat, even surface ready for polishing was obtained.

Polishing was done using successive grades of diamond pastes (9, 6, 3 and 1 microns), starting with the coarsest and finishing with the very fine grade. A rotating lap was used for the final polishing using the diamond paste. The laps

were covered with cloth (Poly Pan 2) and water continuously dripped on the cloth. When polishing was considered to be satisfactory, the samples were mounted on a glass slide with plasticine using a hand mounting press to enhance evenness. The polished surface was protected from abrasion during the mounting by a soft tissue. Samples of the cokes produced were examined under polarised light in a reflectance optical microscope. The samples were then placed on the rotating stage of the microscope (Standard Universal-Carl Zeiss) and examined by reflected polarised with an Antiflex-epi Zeiss objective lens (Figs 7.2.14 to 7.2.17, courtesy of the SABS). The optical micrographs shown in Figs 7.3.9, 7.3.10, 7.3.16, 7.3.17, 7.4.1 and 7.4.2 were taken with a digital Olympus camera.

6.5.3 Thermogravimetry

The thermogravimetric analyser (Mettler Toledo TGA/SDTA 851^e thermal analyser) was equipped with an additional sensor to record the temperature difference between the temperature measured directly at the sample and the model reference temperature. Thermogravimetric analysis monitors the weight losses as the temperature is increased [187]. Weight losses occur as a result of water and the other volatiles being driven off. About 10 mg of sample was placed in aluminium crucibles, 70 µl capacity, and heated in a thermo balance at the rate of 10 $^oC\ min^{-1}$ to 900 ^oC, in a nitrogen flow of 50 ml/min. The weight loss of each sample as a function of temperature is shown in Figs 7.3.4, 7.3.5, 7.3.6, 7.3.7 and 7.3.8.

6.5.4 X-ray diffraction analysis

The series of graphite samples, about 2.0 g each, were ground together with about 0.150 - 0.20 g of silicon (99.9% Merck with crystallite sizes up to 45 µm to pass through a 240 BSS mesh sieve). About 0.6 g (16 drops of PEG) and 1 to 2 ml of ethanol as a wetting agent were added to the mixture. After thorough

mixing, the ethanol was evaporated. The ground sample was placed in a 0.3 mm silica glass capillary and an X-ray powder photograph was taken using a 57.4 mm camera fitted to a Phillips PW 1010/30 X-ray diffraction unit operating with filtered CuKα radiation.

The X-ray line profiles were plotted out on graph paper and the width of the (002) and the adjacent silicon peak determined at half the peak intensity. The instrument broadening and the broadening due to small crystalline sizes were merely additive. The peak intensity and the crystalline sizes (L_c) determined from the corrected broadening (β) were calculated and the results are shown in Tables 7.2.7, 7.3.2 and 7.4.1 and Figs 7.2.19, 7.3.14. 7.3.15, 7.4.3 and 7.4.4.

6.5.5 Raman spectroscopy

Raman spectra were recorded with an XY Raman spectrometer from Dilor®, using the λ = 514.5 nm laser line of a Coherent Innova®90 $Ar^{\pm}$ laser, with a resolution of at least 2 cm^{-1}. The samples were recorded in a backscattering configuration under the microscope attached to the instrument, using a 50 x microscope objective. The presence of the confocal pinhole before the spectrometer entrance ensures a sampling of 1 - 3 µm diameter area using the objective, with the final laser power of about 1-4 mW at the sample surface. Acquisition time is about 20 – 300 s and 15 - 20 spectra are recorded for each sample. A liquid-nitrogen-cooled CCD detector was used with the laser power 200 mW at the laser exit, resulting in a laser power of < 20 mW at the sample. The spectra were baseline corrected, using the Labspec software program supplied by Dilor®. Raman microscopy was performed on the graphitised samples. The Raman spectra of the graphites are depicted in Figs 7.2.20, 7.2.21, 7.3.11, 7.3.12, 7.3.13, 7.4.1 and 7.4.6 and in Tables 7.2.7, 7.3.2 and 7.4.1.

6.5.6 Scanning electron microscopy (SEM)

Images and identification of some phases of the coal extracts samples were obtained on a JEOL JSM-6300 Scanning Microscope. SEM photomicrographs are shown in Figs 7.3.1, 7.3.2 and 7.3.3.

6.6 Experimental procedures

This section describes the procedures used in obtaining the data.

6.6.1 Measurement of the degree of extraction

A 0.7 litre reactor of stainless steel tubes equipped with a lid, fitted with a small metal stirring plug and operated at room temperature, was charged with coal (7 g), fresh DMF (70 g), NaOH (0.7 g), and different amounts of the nucleophile (A^{-1}) with NaOH:A^- (where A^- is S^{-2}, CN^{-1}, and $S_2O_3^{-2}$) mole ratios of 4:1, 2:1 and 1:1, and tumbled end to end for 24 h. The solution was then centrifuged and filtered using a pre-weighed sintered glass funnel. The residues were washed five times with fresh DMF, centrifuged (LKB Bromma 2160 Midispin Centrifuge, speed 5 000 r/min) and the supernatant decanted. Thereafter, the residues were washed with deionised water and filtered in the pre-weighed sintered glass. They were then dried to constant weight in an oven at 60 ^oC, weighed, and analysed for C,H,N,S. The degree of extraction was calculated as follows:

$$\% \text{ Carbon extraction} = \frac{W_t \text{ of carbon in coal} - W_t \text{ of carbon in residue}}{W_t \text{ of carbon in coal}} \times 100$$

The results are shown in Tables 7.2.4, 7.2.5 and 7.2.6 (data obtained from Appendix A1) and Figs 7.2.10 and 7.2.11.

6.6.2 The scaled-up extraction process

To a 1-litre reactor equipped with a hot water or oil jacket (Fig. 6.4.1) (Jalabo MD, Laborteck) and operated at temperature of 90 ± 2 ^{o}C, 80 g of coal was charged together with 800 g of fresh DMF. The mixture was stirred at 700 r/min (Heilddph Labortech stirrer, 140 – 1 100 r/min) and allowed to reach operating temperature. At that operating temperature, 8 g of sodium hydroxide (in pearl form) was added. To maintain an absolutely inert environment within the reactor, a slow stream of nitrogen was flushed into the dissolver to maintain a slight positive pressure. A near-perfect seal of the reactor was effected by means of silicone rubber tubing around the stirrer shaft. The extraction period was 4 – 5 min. The inorganic mineral components and undissolved coal were separated by centrifugation (Beckman GPR Centrifuge, speed 5 000 r/min) for 1 h.

6.6.3 Monitoring the progress of extraction

Samples of about 2 ml of the slurry in the reactor were taken at regular suitable intervals. The samples were centrifuged (Clements GS 150 Centrifuge, maximum speed of 4 000 r/min) for 4 min. About 0.1 g of the supernatant solution was weighed into a 50 ml volumetric flask and made up to the mark with fresh DMF. The absorbance at 600 nm was read on a Spectronic Genesis - 5 UV Spectrophotometer. The nitrogen-purged coal solution was then tightly sealed and centrifuged at 3 000 r/min for 1 h to separate the ash and insoluble organics from the coal solution. The decanted coal extract solution was then immediately used in the recovery process. (See Section 6.5.4). The reproducibility of different separate extraction runs is shown in Fig. 7.2.1. The various curves showing the progress of extraction are given in Figs 7.2.2, 7.2.3, 7.2.4 and 7.2.6. The extraction properties of the coal extract solution are shown in Figs 7.2.5 and 7.2.7 and in Table 7.2.1.

6.6.4 Recovery of the coal extracts from the solution

To a 1-litre Teflon bottle containing deionised hot water (60 °C, 100 g), purged with nitrogen for 10 min, about 400 g of the Refcoal solution (constant ratio of 1:2) obtained as described in Section 6.6.2 was added and thoroughly mixed. The mixture was then centrifuged (4 000 r/min for 30 min). The gel obtained after decantation of the supernatant solution was thoroughly washed with deoxygenated water (process repeated x 4), filtered (Buchner funnel) under nitrogen, and dried overnight in a slow stream of nitrogen at 60 °C. The washing efficiency calculated from equation 6.1 was kept consistent at 33 %. The characteristics of the coal extract are shown in Tables 7.2.2, 7.2.3, 7.2.4, 7.2.5, 7.2.6 and 7.3.1 and in Figs 7.2.7 and 7.2.8.

$$WashingEfficiency = \left(\frac{M_{gel}}{M_{gel} + M_{supernatant}} \right)^{n} \qquad (6.1)$$

Where

M_{gel} = mass of the coal extract gel

$M_{supernatant}$ = mass of the decanted supernatant solution.

N = number of washings

6.6.5 Dissolution of coal into DMF, with NaOH and Na_2S

The same procedure described in Section 6.6.2, but with the addition S^{-2}, was followed. The reactor was charged with coal (80 g), fresh DMF (800 g), NaOH (8 g) and different amounts of sodium sulphide in separate extraction runs, and each was stirred for 6 to 7 h. The molar ratios of NaOH: Na_2S were 4:1, 2:1 and 1:1. Following the monitoring and recovery procedures, described in Sections 6.6.3 and 6.6.4 respectively, the coal extracts and their blend of sodium sulphide were carbonised using the method described in Section 6.6.6. The results with

regard to the behaviour of the coal extracts are shown in Tables 7.2.1 and 7.2.3, and the elemental analysis is given in Table 7.3.1.

The plastic properties of the coal extracts obtained were measured in accordance with SABS Method 933 by Kumba Resources laboratories using a constant–torque Gieseler plastometer. Samples of the coal extracts were sent to the SABS (Coal and Mineral Technologies laboratory) for measurement of the swelling index. The Gieseler fluidity test measures the rotary speed (in dial divisions per minute, ddpm) of a stirrer under a constant torque in a compacted 5-g charge, heated at 30 ^{o}C/min from 300 ^{o}C until it resolidifies (Table 7.2.3.)

6.6.6 Dissolution of coal at room temperature

To a 1-litre Teflon bottle charged with coal (80 g), fresh DMF (800 g) and NaOH (8 g), and purged with nitrogen for 10 min, sodium sulphide of molar ratios (NaOH:Na_2S) 4:1, 2:1 and 1:1 were separately added and continuously stirred at 600 r/min over a magnetic stirrer for 72 h. The same procedure was then followed again, but without the addition of sodium sulphide. The mixtures were each charged separately into the reactor. The procedure described in Section 6.6.4 was then followed to recover the organic solids. The results obtained are shown in Fig. 7.2.9.

6.6.7 Carbonisation of the coal extracts

The coal extracts were carbonised by step heating in a nitrogen atmosphere to 480 ^{o}C at a rate of 10 ^{o}C min^{-1} and held at the maximum temperature for 1 h, then heated to 900 ^{o}C at the same rate and held for 2 h. The flow diagram of the furnace used in the pyrolysis is shown in Fig. 6.4.2. The samples were weighed before and after pyrolysis, and the percentages of weight loss or volatiles are shown in Figs 7.2.13 and 7.2.18. The process of mounting the resultant cokes in a thermosetting resin for sectioning and polishing is described in Section 6.5.2.

The optical textures of the cokes were characterised in terms of the size and domain texture of the observed areas. The optical micrographs of the cokes are shown in Section 6.5.2.

6.7 Control of the flow texture of the coke obtained from pyrolysis of the S^{-2} derived coal extracts

To a 500 ml Teflon bottle, about 0.044 g, 0.088 g and 0.160 g each of the carbon additive corresponding to 76 % carbon in the coke was added into 200 g of the prepared coal extract solutions at room temperature. The additive was dispersed by a high-shear mixer (Turrax TIZ5 mixer, max. speed 2 400 r/min) into the coal extract solution for 10 min. During mixing, a continuous flow of nitrogen was purged into the mixture and additional stirring allowed over a magnetic plate. The dispersed carbon additive was observed through a transmission electron microscope (Figs 7.3.1, 7.3.2 and 7.3.3). Recovery of the organic extract solids was achieved by mixing a definite proportion of the coal extracts with deionised hot water (~ 60 ^{o}C), purged with nitrogen (see Section 6.6.4). The precipitates were thoroughly washed, then filtered under nitrogen. The process was repeated four times with a consistent washing efficiency of 33 % (calculated from equation 6.1). The resulting cake was dried overnight at 60 ^{o}C under nitrogen. The chemical composition of the dry coal extracts (C, H, S, N and O by difference) determined is given in Table 7.3.1. The dry coal extracts were then carbonised as described in Section 6.6.7. The carbon yield (CY) was obtained from the weight difference of the carbon substrate and corrected for the amount of carbon additives added. The cokes produced were evaluated in terms of the optical texture of the polished surface. The results of the weight loss (%) and optical texture are given in Figs 7.3.4, 7.3.5, 7.3.6, 7.3.7 and 7.3.8, and in Figs 7.3.9 and 7.3.10 respectively.

6.8 Addition of carbon black and iron (III) to the coal extract solution prepared at room temperature without the addition of sodium sulphide

The coal extracts without S^{-2} were prepared as described in Section 6.6.6 in a 1-litre Teflon bottle. Small amounts of about 0.015 g, 0.022 g and 0.044 g each of the carbon black, corresponding to about 75 % carbon in the coke, were added into 200 g of the coal extract solution. The mixture was stirred with a high-shear mixer (Turrax TIZ5 mixer, max. speed 2 400 r/min) under nitrogen for 10 min and over a magnetic stirrer. The organic solids were recovered as described in Section 6.6.4 and coked using the method described in Section 6.6.6. Similarly, using prepared room-temperature coal extract solution, small amounts of about 0.01 g and 0.03 g of iron (III) gel were mixed into 200 g portions of the solution and the resin-mounted polished cokes were observed under an optical microscope. The graphitised cokes at 2 950 ^{o}C were characterised by Raman microscopy and X-ray diffraction spectrometry.

6.9 Graphitisation

Samples of cokes were graphitised by means of a Thermtron at 3000 ^{o}C under a total nitrogen flow of 17 kg/h for 2, 3 and 6 h, in a Plasma furnace (Plasma burner 80 kW, 150 kW DC, water-cooled resistor 0.28 Ω). The graphitised cokes were assessed by means of Raman spectroscopy and X-ray diffraction. The behaviour of the graphitised cokes and their blends of carbon additives was characterised in terms of percentage weight loss and the results are given in Fig. 7.3.18. The micro-textures of the graphites are given in Figs 7.3.16 and 7.3.17.

CHAPTER 7

RESULTS

7.1 Major ash components and petrographic characteristics

The coal used was analysed for ash content, and for proximate, ultimate and petrography characteristics. The oxygen content (%)was obtained by difference.

Table 7.1.1

Proximate analysis of the coals used

	Content (% wt)				
Coal	**Moisture**	**Ash**	**Volatile matter**	**Fixed carbon**	**Total sulphur**
Tshikondeni	0.9	9.4	23.3	66.4	0.81
Moatize	1.0	7.9	16.8	74.3	0.85

Table 7.1.2

Ultimate analysis of the coals used

Element	Amount %	
	[a](Tshikondeni)	[b](Moatize)
Hydrogen	4.38	4.19
Carbon	81.5	83.5
Nitrogen	1.86	2.01
Sulphur	0.81	0.85
Oxygen	1.15	0.59

[a] $(C/H)_{atomic\ ratio}$, 1.54 [a] $(C/O)_{atomic\ ratio}$, 0.37

[b] $(C/H)_{atomic\ ratio}$, 1.65 [b] $(C/O)_{atomic\ ratio}$, 0.74

Table 7.1.3

Ash analysis of the coals used

	Amount %	
Component	**Tshikondeni**	**Moatize**
SiO_2	51.4	68.4
Al_2O_3	25.5	22.5
Fe_2O_3	6.00	1.11
P_2O_5	0.82	0.34
TiO_2	2.24	1.46
CaO	5.05	1.31
MgO	2.52	0.65
K_2O	1.46	1.60
Na_2O	0.36	0.13
SO_3	4.45	0.64

Table 7.1.4

Petrographic characteristics of the coals

	Tshikondeni	**Moatize**
Rank (degree of maturity)	Meta-bituminous	Per-bituminous
ACE-UN in-seam classification	(Medium rank B)	(Medium rank A)
Mean random reflectance (%)	1.33	1.63
Vitrinite-class distribution	V10 – V16	V13 – V19
Standard deviation (σ)	0.117	0.106
Abnormalities	Extended vitrinite-class distribution	Slightly extended vitrinite-class distribution
Petrographic composition – Analysis of macerals		
Vitrinite content (%)	93	82
Liptinite content (%)	<1	<1
Total reactive macerals (%)	94	87
Total inertinite (%)	6	18
More highly reflecting materials (%)	1	0
Cracks and fissures	occasionally observed	Very frequent
Signs of advanced weathering	Very occasionally seen or thermal effects	rarely seen

7.2 High-temperature extraction runs on addition of different dosages of sodium sulphide and carbonisation of the coal extracts

The dosage of the nucleophile used in the extraction process is based exclusively on the molar ratio of NaOH:Nu^{-1} (Nu^- = nucleophile). 'Refcoal' is synonymous with, and used interchangeably with, the coal extracts. Each photomicrograph is labelled with a code, e.g. RSF-25 RT, which signifies that it is representative of the sulphide-derived Refcoal (R), containing 25 g Na_2S (NaOH:Nu^{-1} molar ratio of 1:1) and obtained at room temperature (RT). For the corresponding coke and graphite, the codes are CSF-25 RT and GSF-25 RT respectively. The other labels follow the same pattern. Room-temperature extraction means extraction at 25 ± 1 °C, while high-temperature means extraction at 90 ± 2 °C.

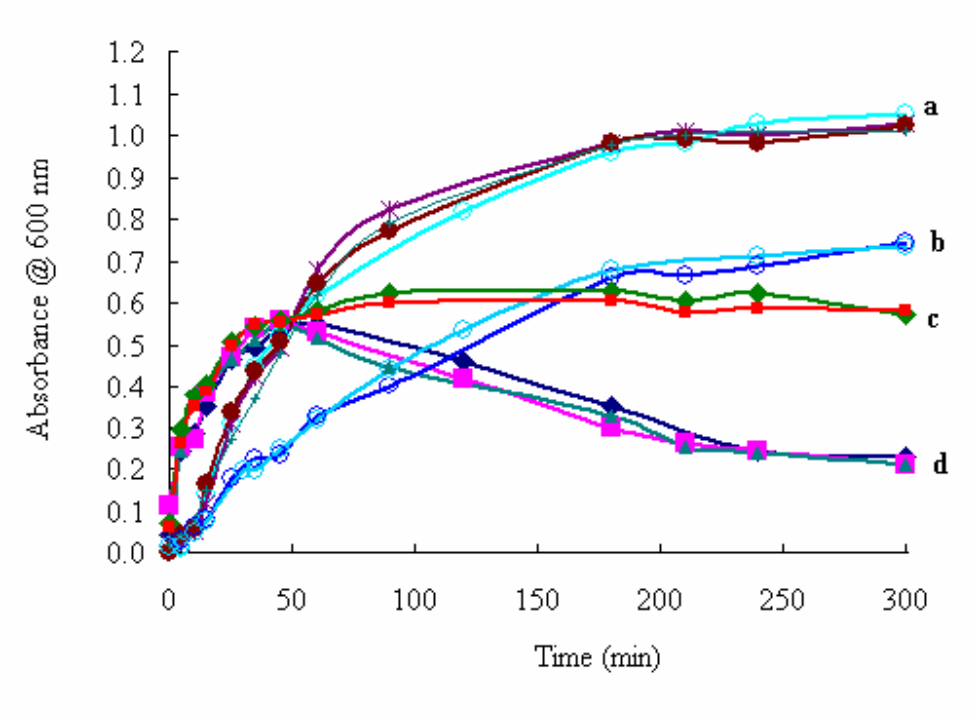

Molar ratios of NaOH:Na_2S [a](1:0), [b](4:1), [c](2:1), [c](1:1)

Figure7.2.1: Reproducibility curves for various extraction runs at high temperature. The ratio of DMF:coal:NaOH was 100:10:1. The standard deviation was 0.1 and a variance 0.004

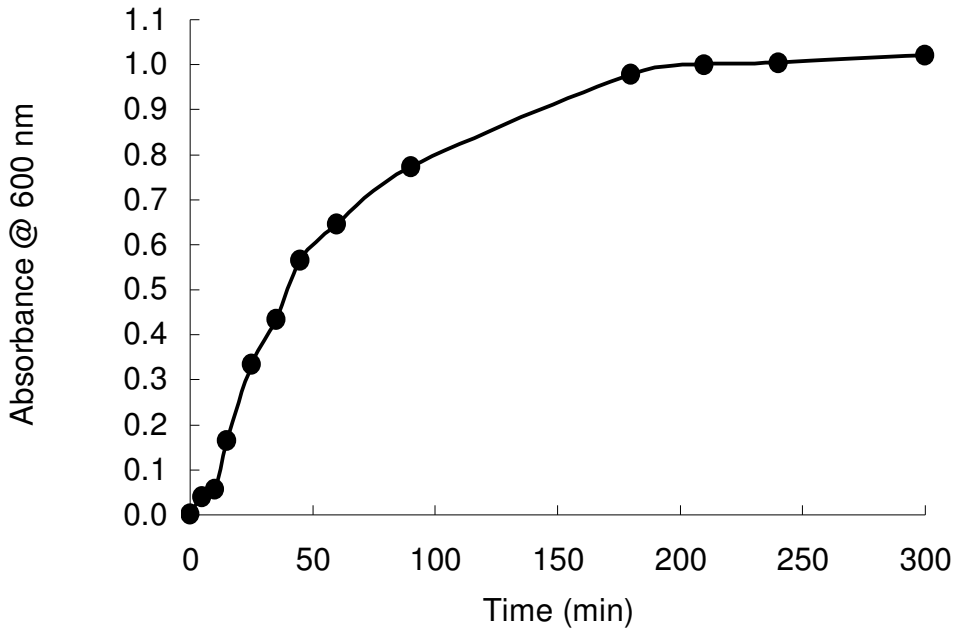

Figure 7.2.2: Progress of extraction at high temperature. The ratio of DMF:coal:NaOH was 100:10:1

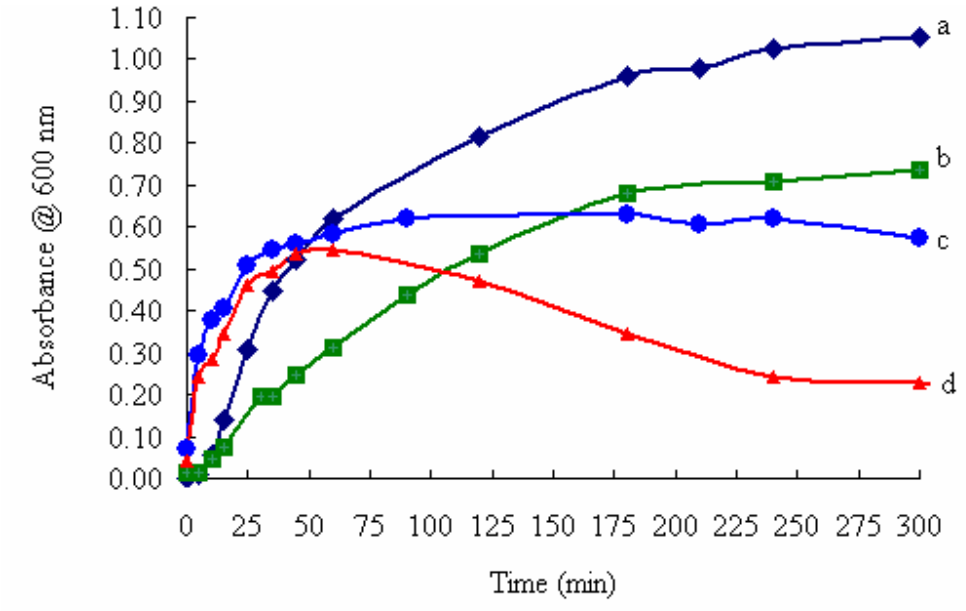

Ratios of NaOH:Na_2S [a] (1:0), [b] (4:1), [c] (2:1), [d] (1:1)

Figure 7.2.3: Optimisation results from separate extraction runs with the addition of various amounts of Na_2S. The mass ratio of DMF: coal: NaOH was 100:10:1

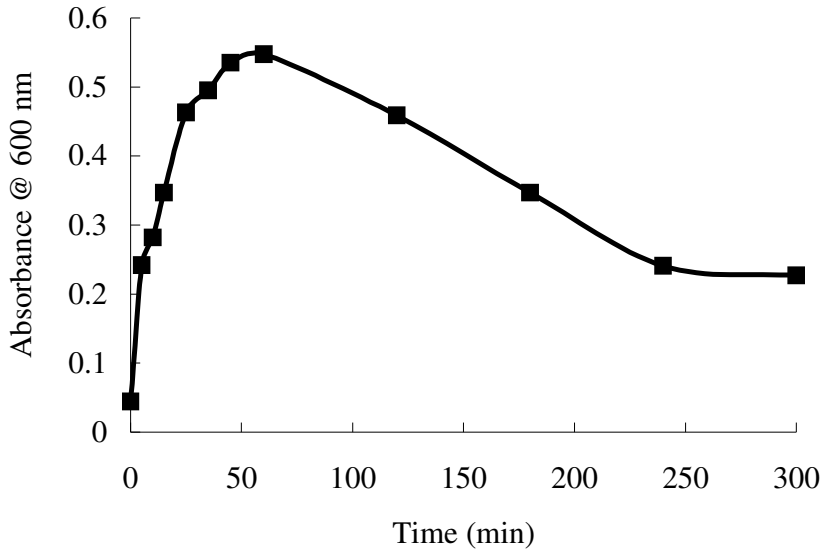

Figure 7.2.4: Progress of extraction at high temperature when the molar ratio of NaOH:Na_2S was 1:1. The mass ratio of DMF: coal: NaOH was 100:10:1

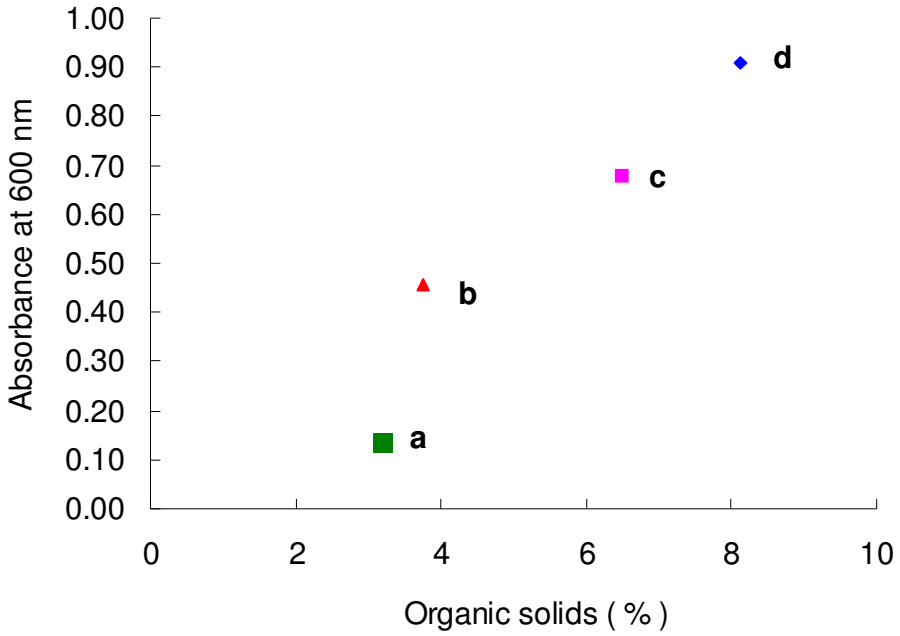

Figure 7.2.5: Comparison of the optical absorbance of the coal extract solution with its organic solids content obtained at high temperature on the addition of different amounts sodium sulphide. The molar ratios of NaOH:Na_2S were [a] (1:1), [b] (2:1), [c] (4:1), [d] (1:0)

Table 7.2.1

Characteristics of the Refcoal solution obtained at high temperature for 5 h on the addition of different amounts of Na_2S. The mass ratio of DMF: coal: NaOH was 100:10:1

Molar ratio NaOH: Na_2S	Mass of Na_2S (g)	Organics recovered	Abs (λ_{max})	Abs/g coal dissolved	Observed Colour	Swelling index	Fluidity observed
0.2:0	0.00	8.20	1.00	0.013	Black	4.5	Viscous
4:1	6.30	6.40	0.74	0.009	Black	9.0	Less viscous
2:1	12.00	4.90	0.57	0.007	Black	9.0	Fluid
1:1	25.20	2.75	0.23	0.003	Brown	9.5	Too fluid

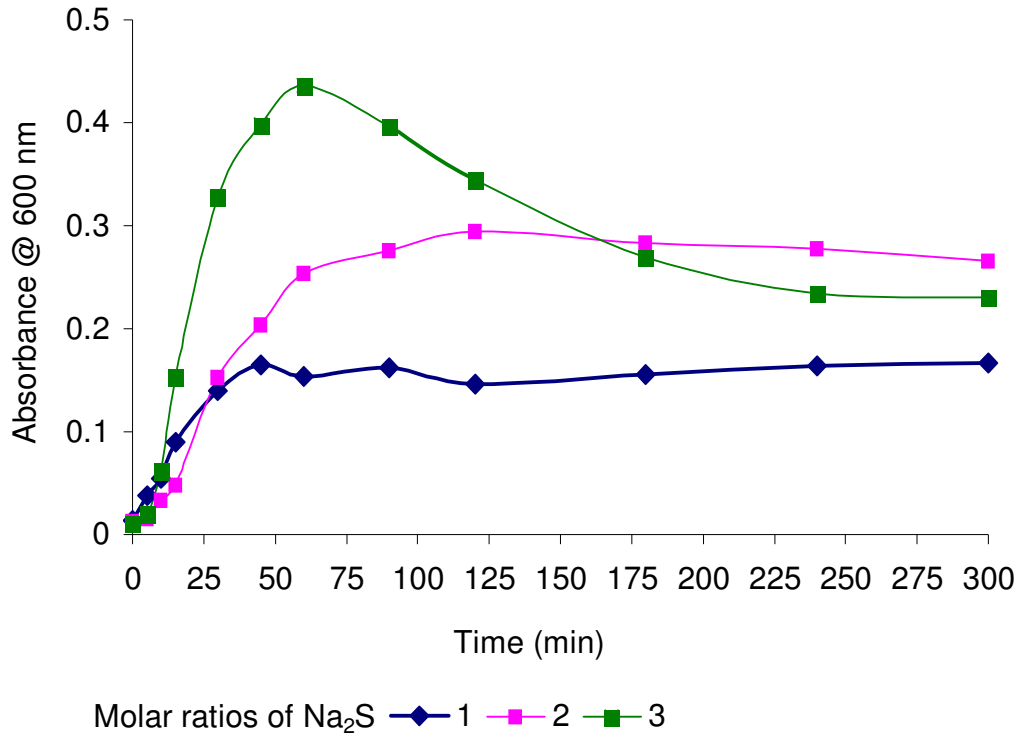

Figure 7.2.6: Progress of extraction obtained at high temperature on the addition of different amounts of Na_2S only. The mass ratio of DMF: coal was 100:10

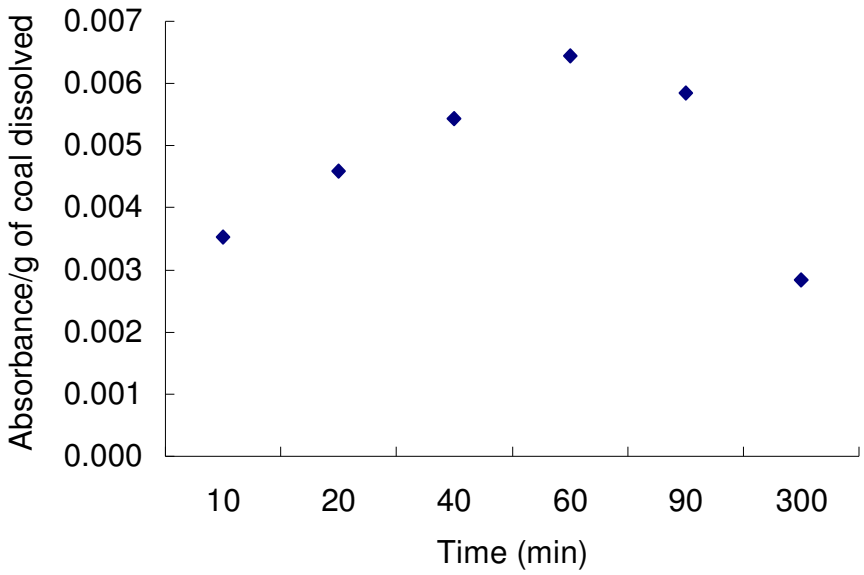

Figure 7.2.7: Absorbance per gram of coal dissolved for extraction at high temperature. The molar ratio of NaOH:Na_2S was 1:1

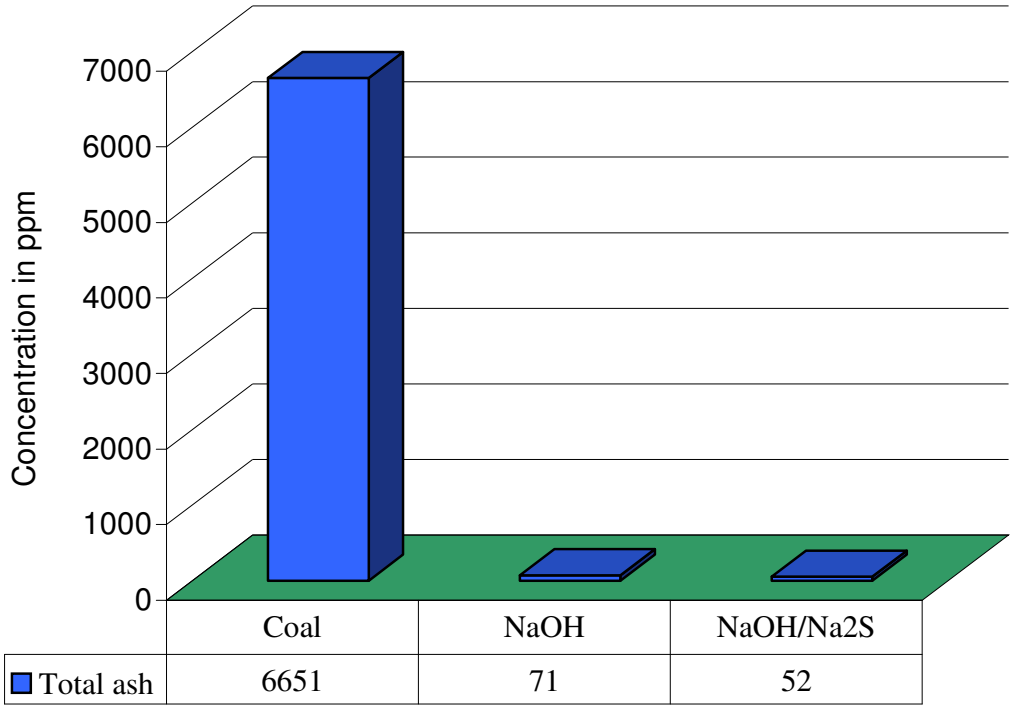

Figure 7.2.8: Extent of purification[1] of Tshikondeni coal

[1] Ash removal – mainly inorganic elements

Table 7.2.2

Elemental analyses of the S^{-2} derived coal extracts at high temperature on the addition of different amounts of Na_2S

Molar ratio	Elemental analysis (wt %)							
NaOH:Na_2S	C	H	N	O[a]	S	Ash	C/H[b]	C/O[c]
2:0	85.2	4.43	2.06	7.49	0.86	1.60	1.591	0.059
4:1	84.5	5.53	3.35	5.78	0.82	1.30	1.265	0.076
2:1	85.2	5.45	2.80	5.72	0.85	1.00	1.293	0.078
1:1	86.5	5.53	2.19	5.04	0.75	0.70	1.294	0.089

[a] By difference

[b] Carbon/hydrogen atomic ratio

[c] Carbon/oxygen atomic ratio

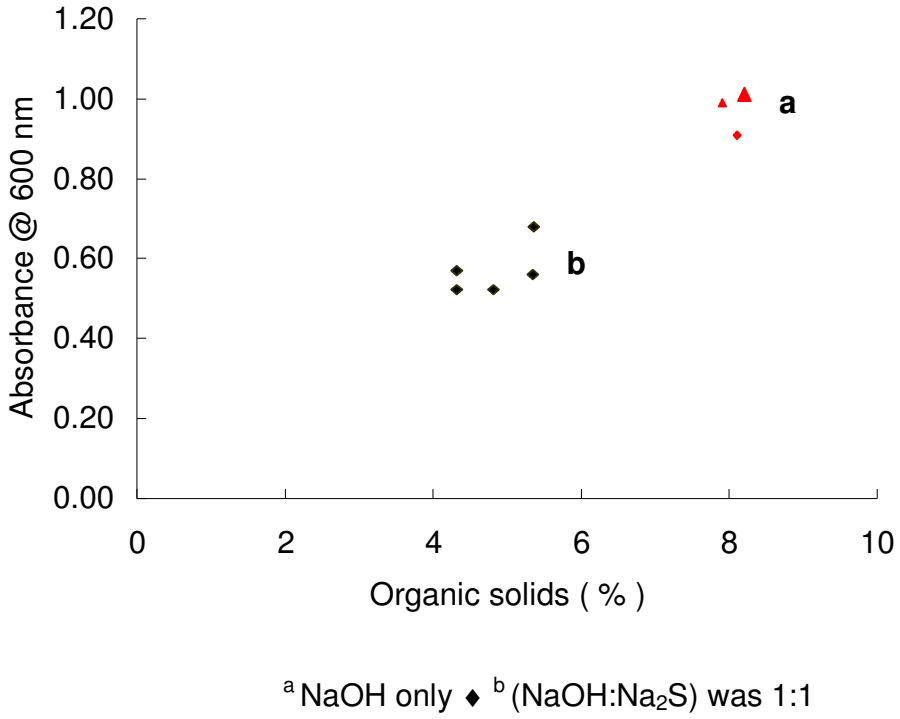

Figure 7.2.9: Absorbance of the coal extract solution obtained at room temperature plotted against its organic solids content

Table 7.2.3

Elemental analyses of coals extracts residues obtained at room temperature on addition of different amounts of sodium sulphide

Sample ID	molar ratio	Contents (%)					Atomic ratios		Absorb	(OEXT) [c]
(Residue, g)	NaOH:Na_2S	C	H	N	S	O	(C/H)[a]	(C/O)[b]	λ (nm)	
RSF (1.39)	1:0	41.8	2.26	1.09	1.13	5.72	3.29	0.082	1.00	89.80
RSF (1.35)	4:1	45.1	2.19	1.03	1.27	6.54	3.36	0.071	0.87	88.97
RSF (1.74)	2:1	55.5	2.91	1.33	1.27	9.93	2.41	0.044	0.82	84.56
RSF (2.33)	1:1	65.9	3.57	1.73	1.47	22.8	1.63	0.016	0.51	70.47

[a] Carbon/hydrogen atomic ratio, [b] Carbon/oxygen atomic ratio, [c] Organics extracted (%)

Table 7.2.4

Elemental analyses of coal extract residues obtained at room temperature on the addition of different amounts of potassium cyanide

Sample ID (Residue, g)	Molar ratio NaOH:KCN	Contents (%)					Atomic ratios		Absorb	(OEXT)[c]
		C	H	N	S	O	(C/H)[a]	(C/O)[b]	λ (nm)	
RCN (1.39)	1:0	41.75	2.26	1.09	1.13	5.72	3.29	0.082	1.00	89.80
RCN (1.19)	4:1	46.53	2.59	1.25	0.76	5.88	2.86	0.079	0.97	89.52
RCN (1.57)	2:1	40.82	2.30	1.34	0.95	6.06	3.21	0.077	0.99	89.35
RCN (1.34)	1:1	41.92	2.38	1.31	0.89	7.54	3.06	0.061	0.58	87.88

[a] Carbon/hydrogen atomic ratio, [b] Carbon/oxygen atomic ratio, [c] Organics extracted (%)

Table 7.2.5

Elemental analyses of the coal extract residues obtained at room temperature on the addition of different amounts of sodium thiosulphate

Sample ID (Residue, g)	Molar ratio OH^- : $S_2O_3^{-2}$	Contents (%) C	H	N	S	O	Atomic ratios (C/H)[a]	(C/O)[b]	Absorb χ (nm)	Organ [c] extract
RTS (1.39)	1:0	41.75	2.26	1.09	1.30	5.55	3.29	0.084	1.00	89.80
RTS (1.19)	4:1	41.23	2.44	1.23	0.47	5.42	3.07	0.087	1.01	90.44
RTS (1.57)	2:1	42.13	2.52	1.21	1.09	4.98	2.96	0.094	0.97	90.20
RTS (1.34)	1:1	41.16	2.345	1.24	1.06	5.95	3.16	0.078	0.95	89.41

[a] Carbon/hydrogen atomic ratio, [b] Carbon/oxygen atomic ratio, [c] Organics extracted (%)

Table 7.2.6

The characteristic of the S^{-2} derived coal extracts showing Geissler fluidity and foaming volume per gram of Refcoal pyrolysed

Sample ID	Volatiles %	Maximum Fluidity [a] (ddmp)	Maximum Fluidity [b] (ddmp)	Temperature (°C)		Estimated Volume [c]
				Solidification	Max. fluidity	
Coal	22	13550	13550	496	464	27
RSF-0	25	> 30 716	4	492	480	16[b] (13)
RSF-6	27	35 700	18	498	476	18
RSF-12	31	700	280	500	476	27
RSF-25	25	>35 693	> 4 392	514	466	> 46

[a] Room-temperature coal extracts [b] High-temperature coal extracts

[c] Volume/g of coal carbonised

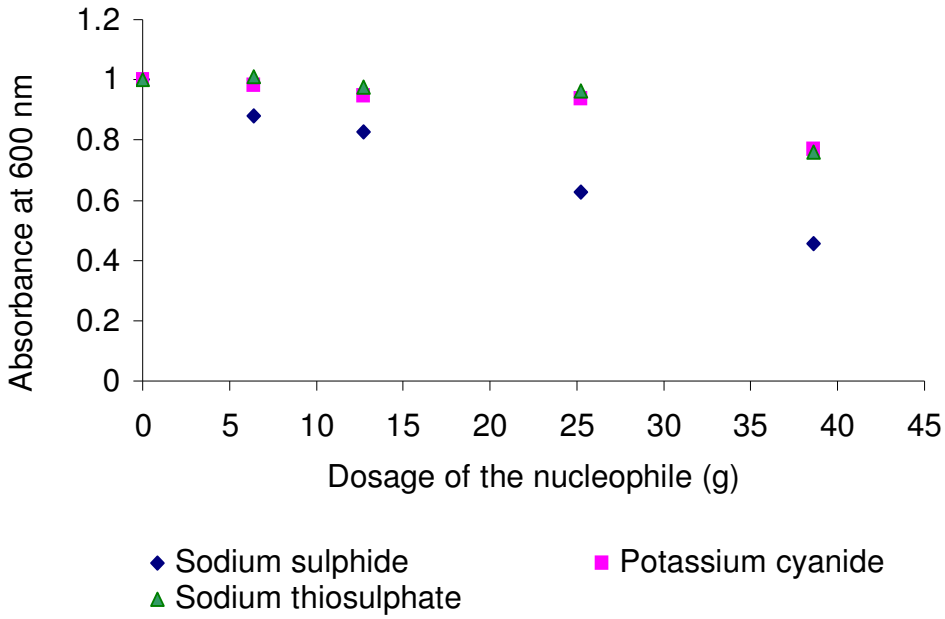

Figure 7.2.10: Comparison of the solubility of the coal at room temperature on the addition of different amounts of the nucleophiles Molar ratios of NaOH:Nu^- were [a] (1:0), [b] (4:1), [c] (2:1), [d] (1:1)

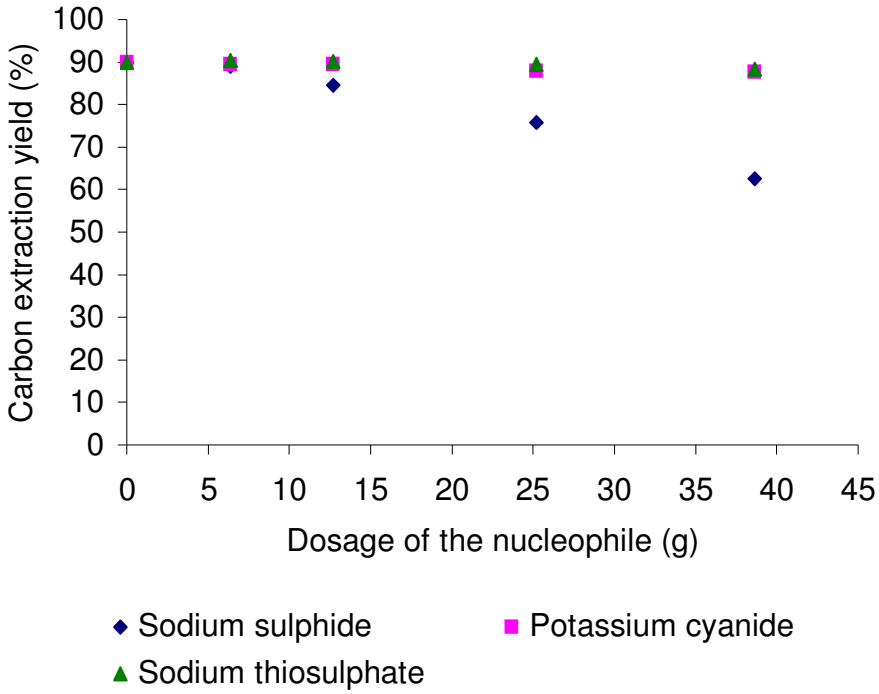

Figure 7.2.11: The carbon extraction yield (%) obtained at room temperature on the addition of different amounts of the nucleophiles The molar ratios of NaOH:Nu^- were [a] (1:0), [b] (4:1), [c] (2:1), [d] (1:1)

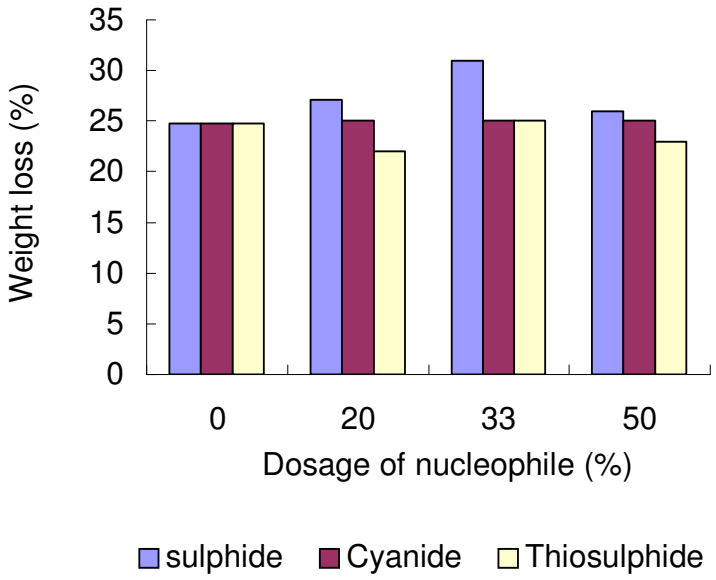

Figure 7.2.12: The average weight loss (%) of the heat-treated coal extracts containing different amounts of the nucleophiles
The molar ratios of (NaOH:Na_2S) were (1:0); (4:1); (3:1); (1:1)

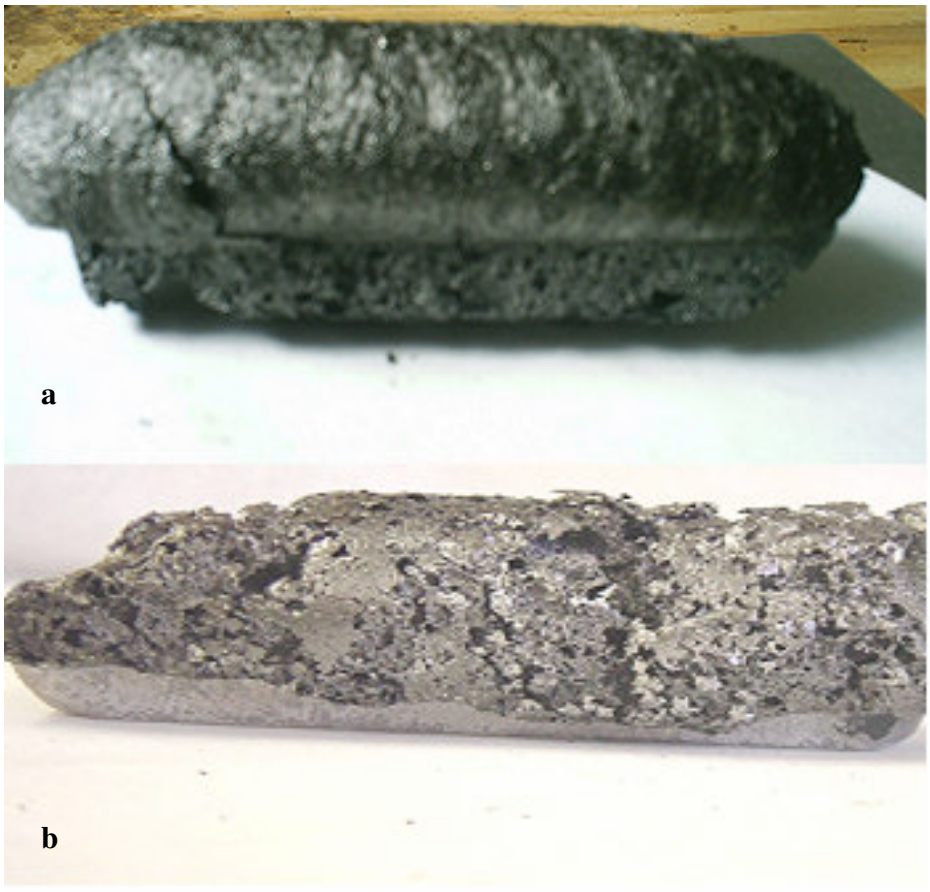

Figure 7.2.13: Foamed coke obtained from carbonisation of the coal extract derived at room temperature. The rate of carbonisation was 10 ^{o}C/min to 480 ^{o}C for 1 h, then to 900 ^{o}C for 2 h. (a) CSF-0RT, without S^{-2}, volume + 17 cm^3/g Refcoal coked (b) CSF-25RT shows a volume > 45 cm^3/g of Refcoal coked (Molar ratio of NaOH: Na_2S was 1:1)

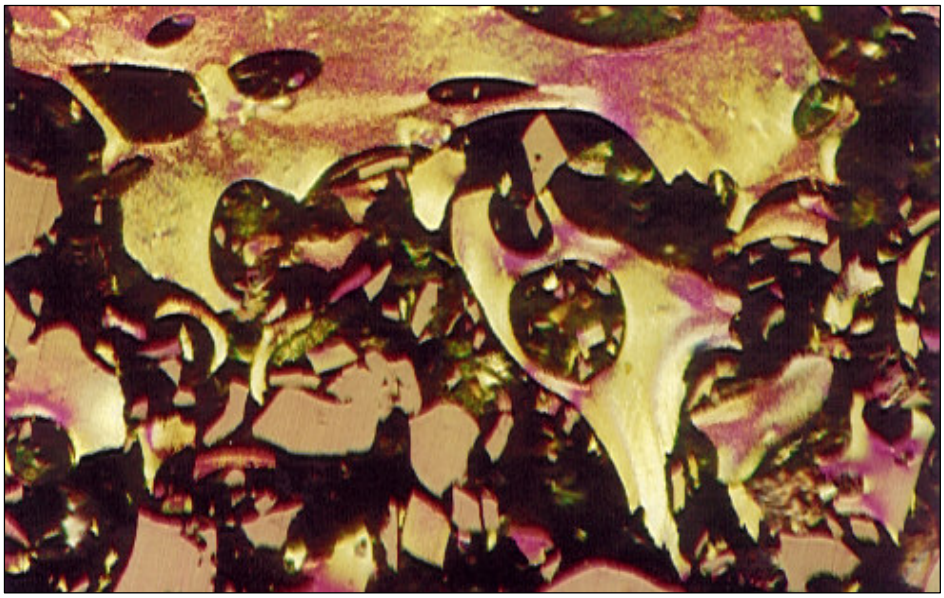

Figure 7.2.14: Micrograph of the coke CSF-0RT
The optical character of the coke shows (a) poorly developed pores with thickened walls, and (b) low level of anisotropy and a rich isotropic domain

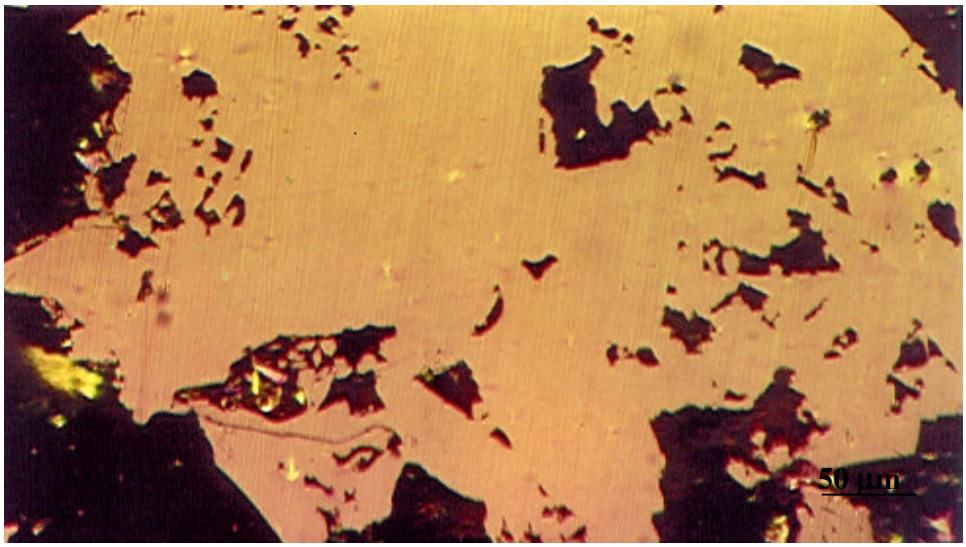

Figure 7.2.15: Micrograph of the coke CSF-0HT
The optical character shows isotropic carbon with poor devolatilisation.

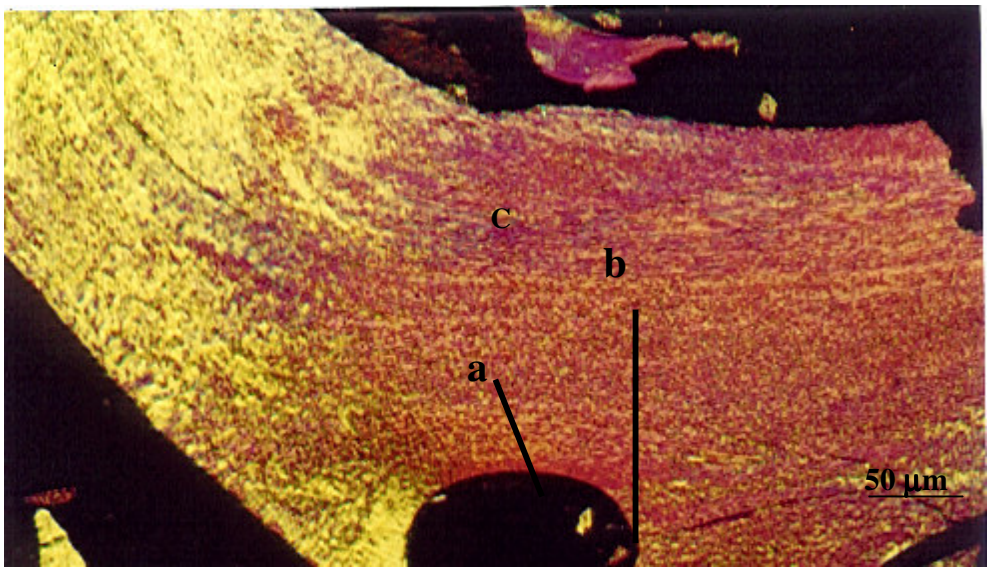

Figure 7.2.16: Micrograph of the coke CSF-25 RT

The optical character of the coke shows (a) thickened walls, (b) a well-marked devoletilisation pores, and (c) coarse-grained anisotropy with stacks of parallel lamellae and flow domain texture

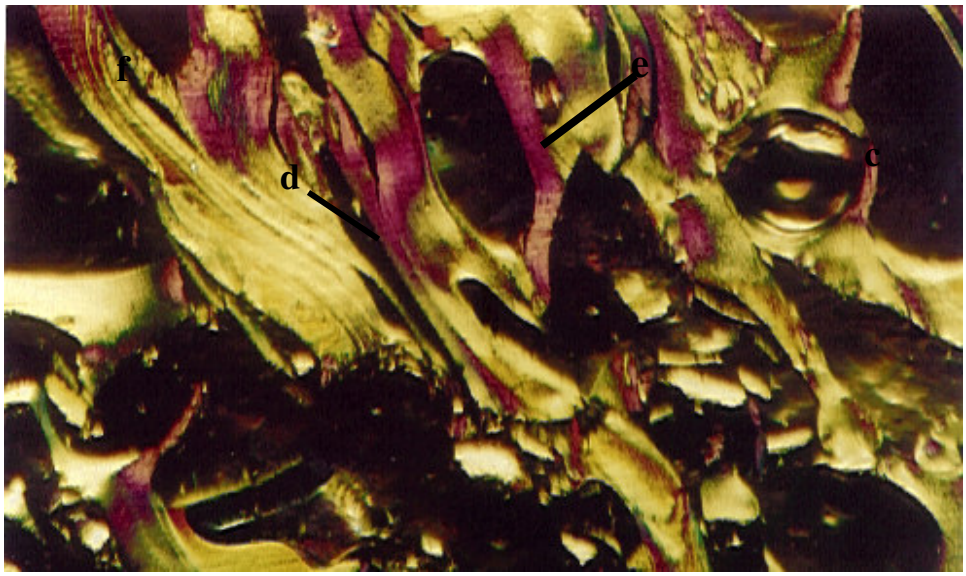

Figure 7.2.17: Micrograph of the coke, CSF-25 HT

The optical character of the coke shows (d) thinner walls, (e) well-marked devolatilisation pores, and (f) fine to coarse-grained anisotropy with some flow structure

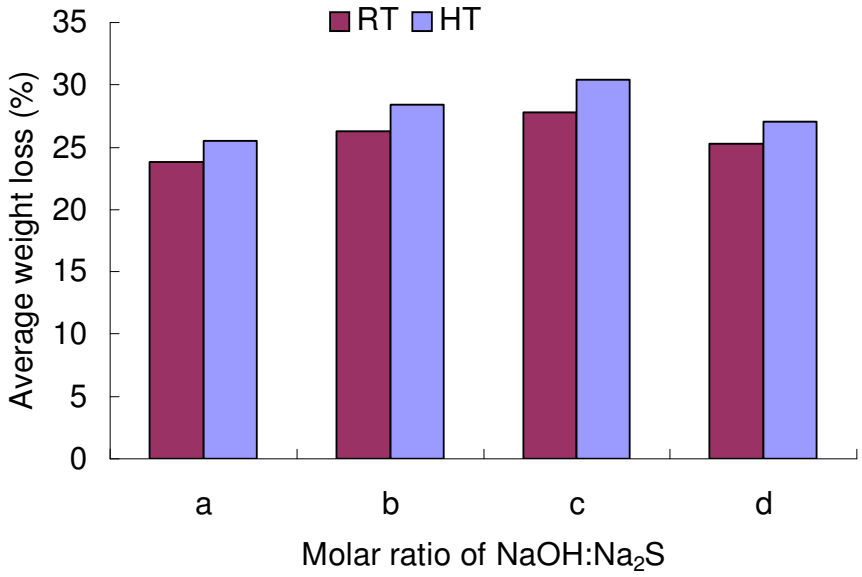

Figure 7.2.18: The weight loss (%) of the heat-treated S^{-2} derived coal extracts obtained at room temperature (RT) and high temperature (HT) The molar ratios of (NaOH: Na_2S) were [a] (1:0); [b] (4:1); [c] (2:1); [d] (1:1)

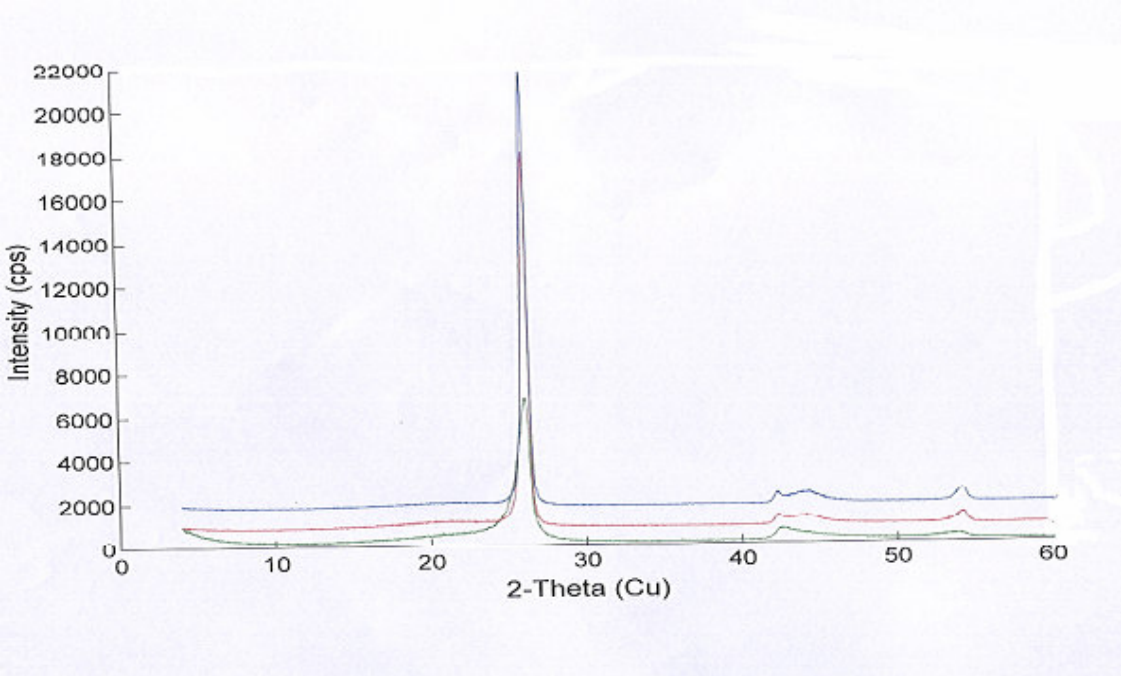

Figure 7.2.19: XRD of the graphitised cokes. The $d_{(002)}$ value of the graphites is in the order GSF-25RT (3.37Å) < $d_{(002)}$ GSF- 25HT at $d_{(002)}$ GSF-0RT at 3.38Å.

Table 7.2.7

The Raman and XRD results of the graphitised cokes, listing the intensity ratio, R, of the g-peak and d-peak, the interlayer thickness $d_{(002)}$ and the Graphitisation factor, g

Sample ID	Extraction conditions	Raman [a] R	XRD $d_{(002)}$ value	[b] L_a	g [c]
GSF-0.0HT	90 °C, no S^{-2}	0.79	3.419	5.41	25
GSF-0.0RT	RT, no S^{-2}	3.53	3.385	1.22	64
GSF-25HT	90 °C, $+S^{-2}$	2.53	3.376	1.70	74
GSF-25RT	RT, $+ S^{-2}$	4.69	3.372	0.92	79

[a] $R = g/d$ [b] $L_a = 4.3/R$ [c] $g = (3.44 – d_{(002)})/0.086$

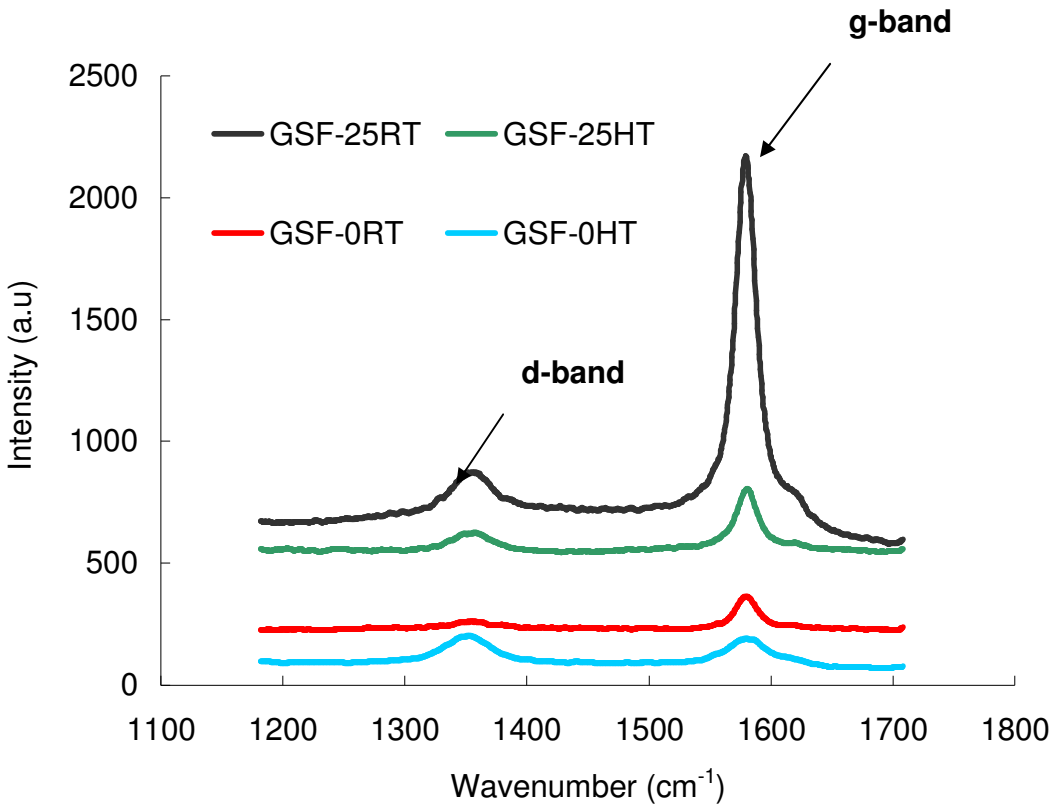

Figure 7.2.20: Raman spectra of the graphitised cokes showing bands at intensities of 1360.5 cm^{-1} and 1579.1 cm^{-1} for the d-peak and g-peak respectively

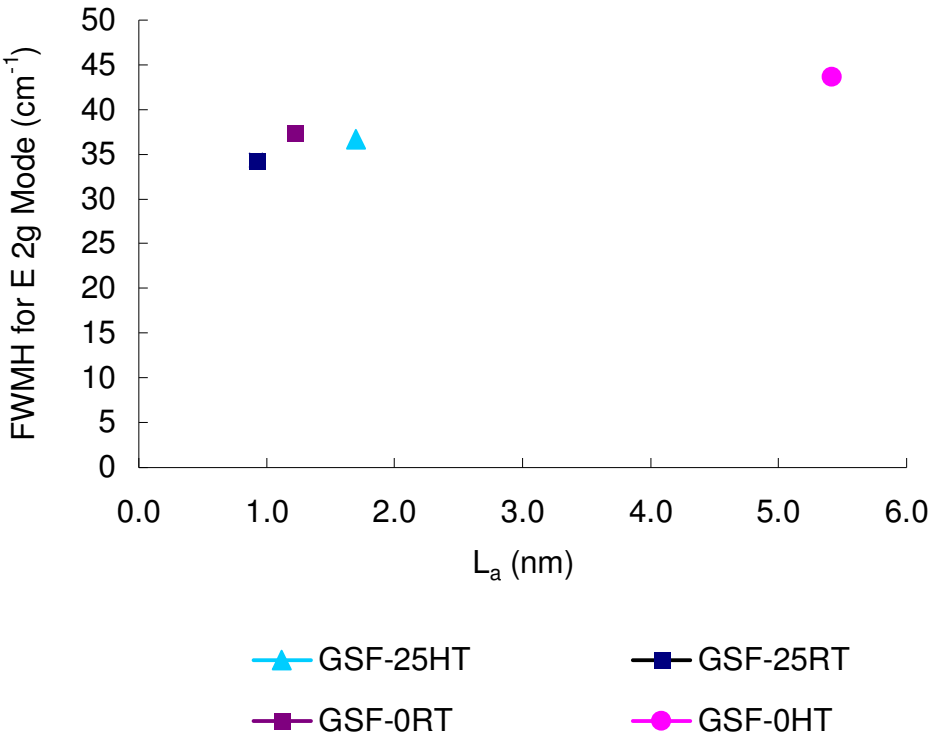

Figure 7.2.21: The average full width at half maximum (FWHM) of the E_{2g} mode (1580 cm^{-1}) as a function of the crystallite size (L_a) of the graphitised cokes

7.3 The control of coke flow texture on the addition of carbon additives to the sulphide-derived coal extracts at room temperature

This section details the results obtained on controlling the coke flow texture of the sulphide-derived coal extracts. The additives used were dispersed in the coal extract solution prepared at room temperature only. Each sample is labelled with a code identified by the first letter R for Refcoal, C for coke, G for graphite and S for sulphide. The number attached at the end of the code signifies the amount of the additive (%) in the coal extract solution.

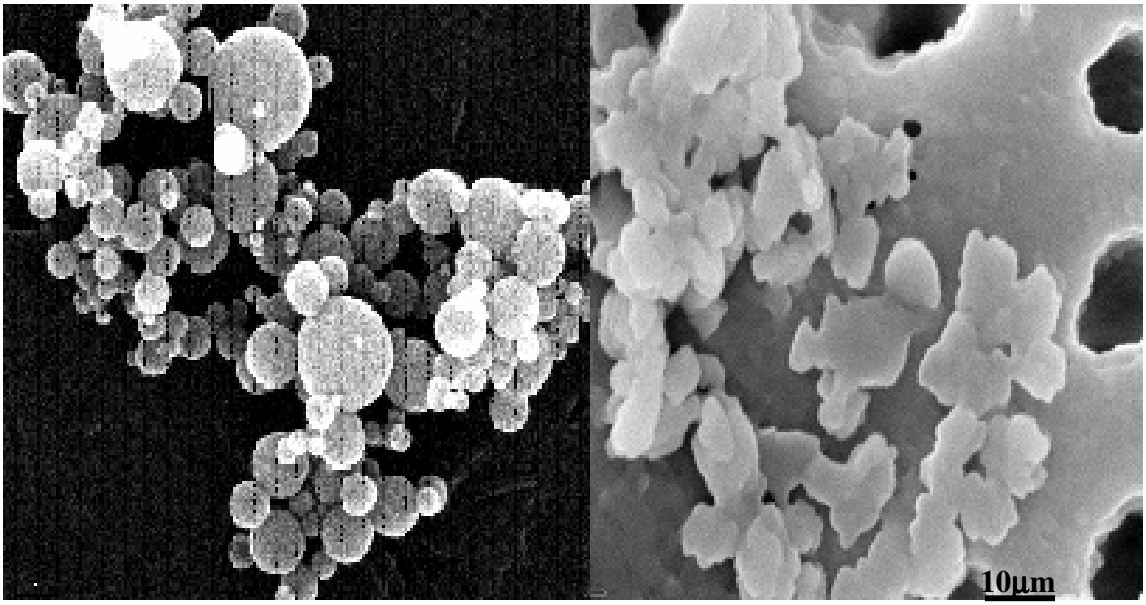

Figure 7.3.1: SEM photomicrograph of carbon additive
(a) Carbon black, spherically shaped chains of aggregates are visible, and (b) acetylene black, with its flat surface and chains of aggregates, makes it difficult to disperse in a viscous coal solution.

Table 7.3.1

Elemental analysis of the coal extracts on addition of the carbon additive

Sample ID	Elemental analysis (wt %)					C/H [a]	C/O [b]	RY [c]
	C	H	O	N	S			
RSF-0.00 AB	89.45	7.40	0.06	2.27	0.82	1.00	7.76	64.50
RSF-0.44 AB	96.79	0.71	0.09	1.65	0.76	1.09	5.60	67.13
RSF-0.88 AB	87.03	7.44	1.92	2.77	0.84	0.97	0.24	67.93
RSF-1.60 AB	94.84	0.73	2.09	1.63	0.71	1.06	0.24	68.48
RSF-0.00 CB	89.35	6.88	0.06	2.03	0.68	1.07	0.44	64.50
RSF-0.44 CB	96.26	0.89	0.21	1.90	0.74	1.08	2.39	67.66
RSF-0.88 CB	95.93	0.74	0.69	1.93	0.71	1.08	0.72	68.56
RSF-1.60 CB	96.14	0.87	0.69	1.62	0.68	1.07	0.73	68.44

[a] Carbon/hydrogen atomic ratio [b] Carbon/oxygen atomic ratio

[c] Residue yield, TGA data (%)

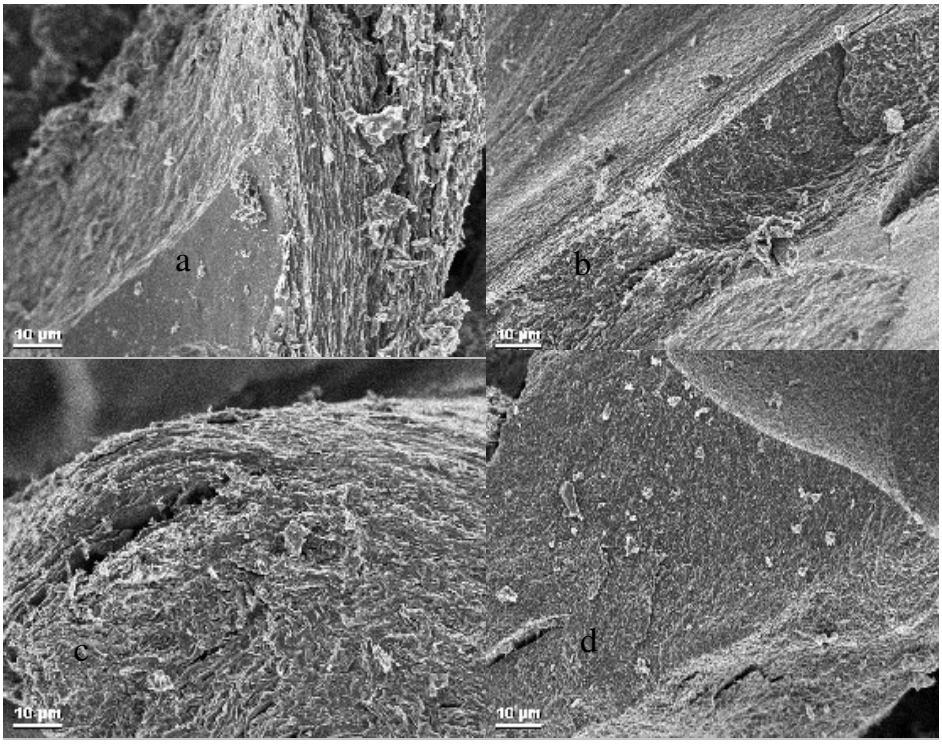

Figure 7.3.2: SEM photomicrograph of the carbon black dispersed cokes

(a) CSF-0.0 CB shows the coarsest textured surface

(b) CSF-0.44 CB, shows a fine textured surface

(c) CSF-0.88 CB shows a coarse texture

(d) CSF-1.60 CB shows a very fine textured surface.

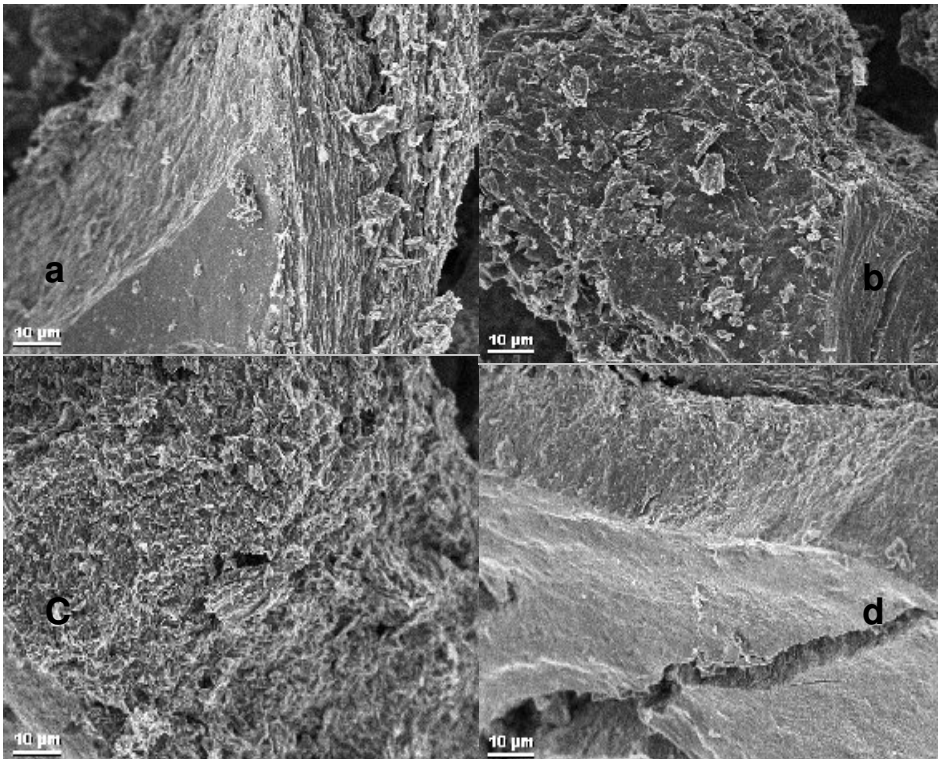

Figure 7.3.3: SEM photomicrograph of the acetylene dispersed cokes

(a) RSF-0.0 AB shows an extremely coarse textured surface

(b) CSF-0.44 AB shows a coarse textured surface

(c) CSF-0.88 AB, shows a coarse textured surface

(d) CSF-1.60 AB shows the finest textured surface.

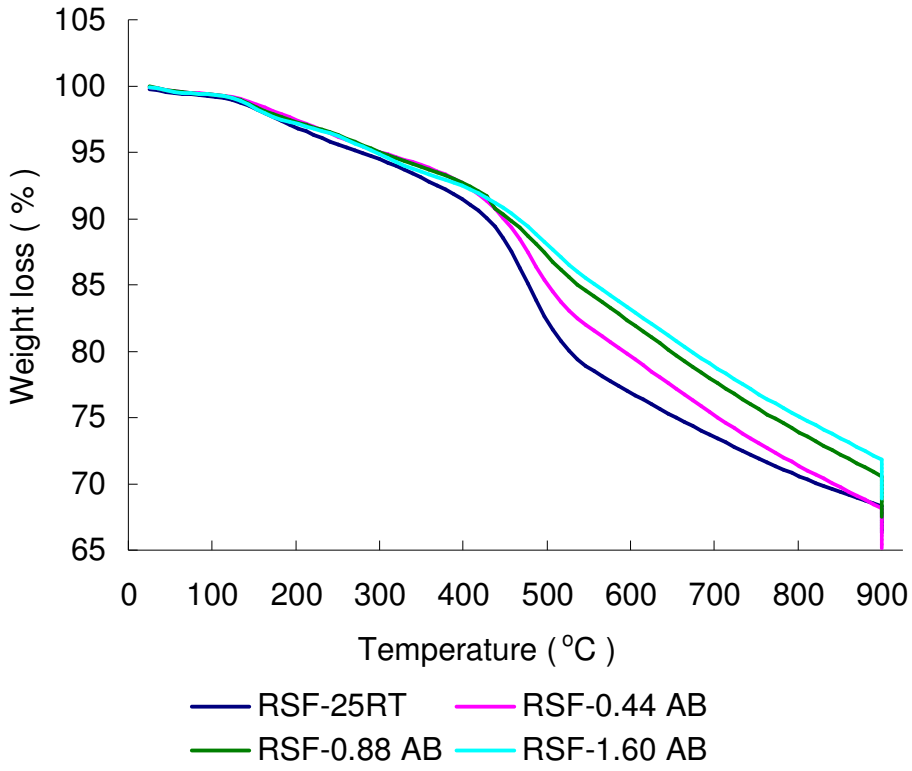

Figure 7.3.4: Thermogravimetric (TGA) analysis of the acetylene black dispersed in the coal extracts

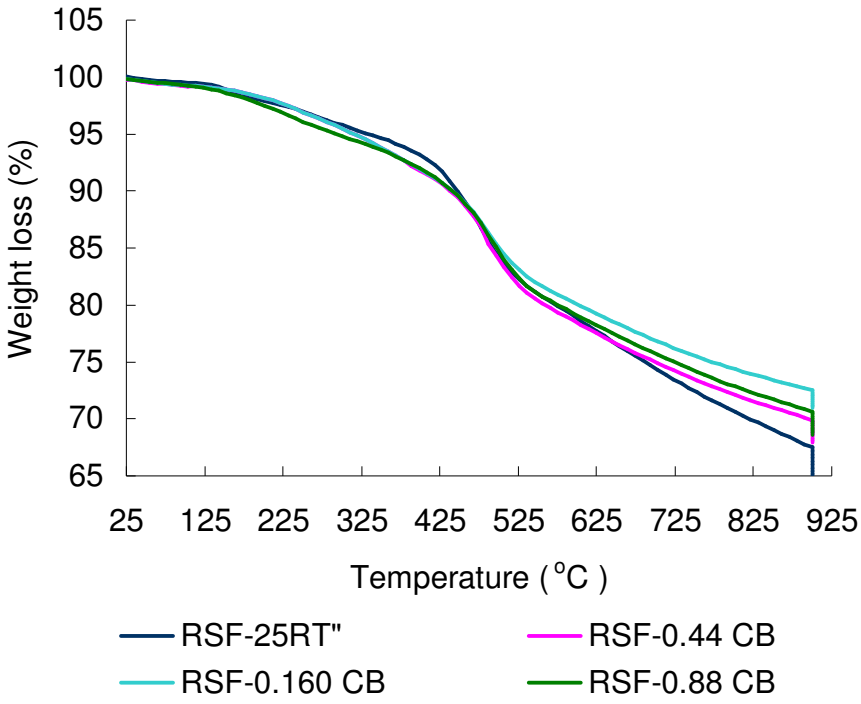

Figure 7.3.5: Thermogravimetric (TGA) analysis of the carbon black dispersed in the coal extracts

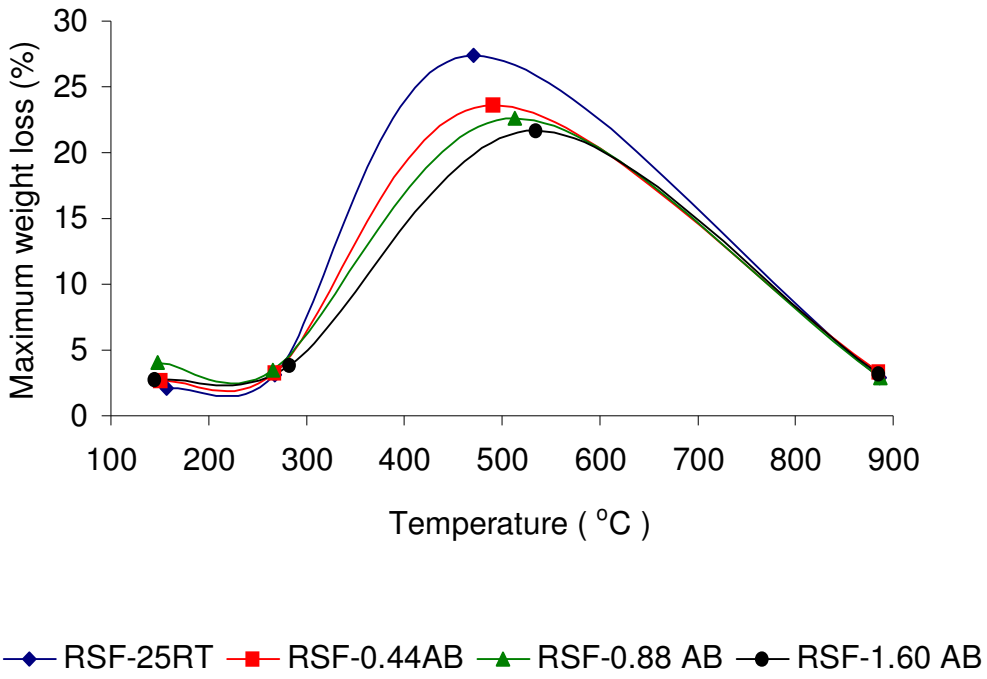

Figure 7.3.6: The TGA curves showing weight loss at 300-550 °C of the heated coal extracts with acetylene black. The coal extracts were:

- RSF-0.00 AB shows 27 % at 471 ± 1°C.
- RSF-0.44 AB shows 24 % at 491 ± 1 °C
- RSF-0.88 AB shows 23 % at 593 ±1 °C
- RSF-1.60 AB shows 21. % at 535 ± 1 °C.

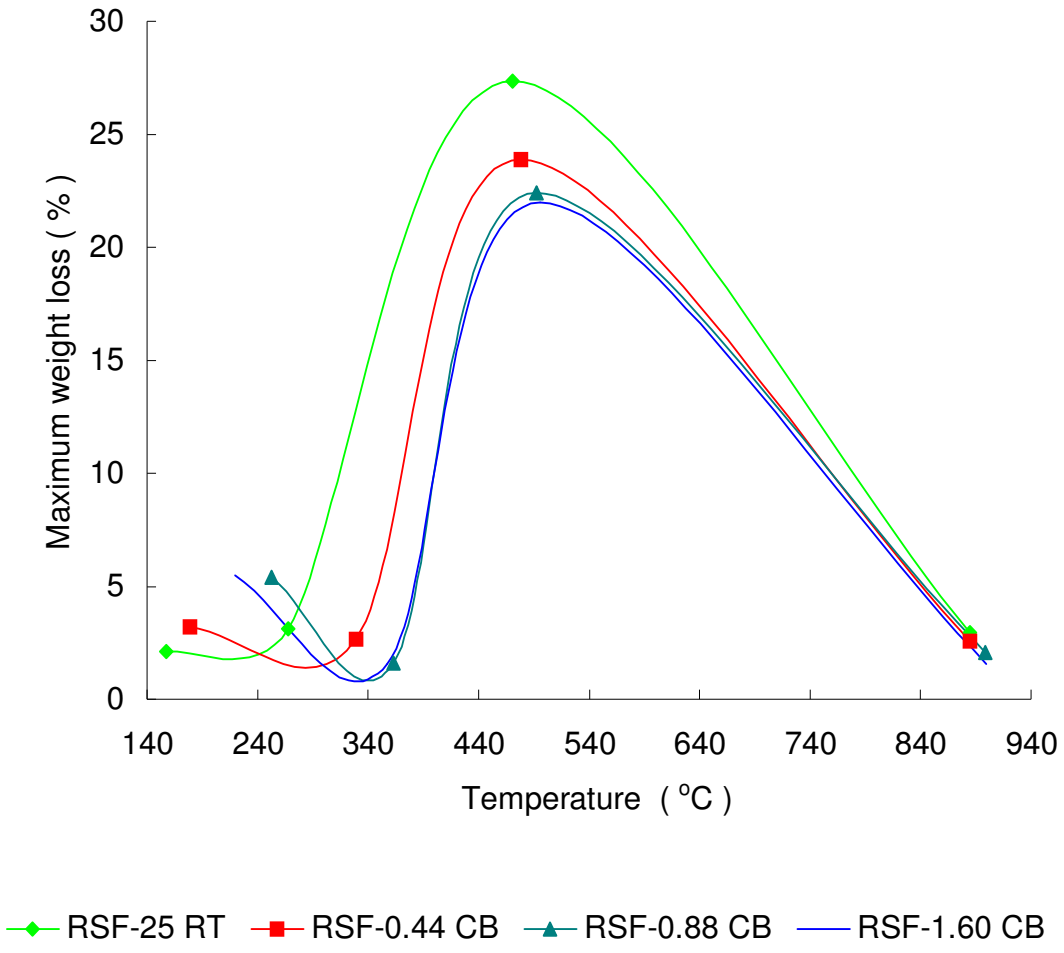

Figure 7.3.7: The TGA curves showing weight loss at 300-550 °C of the heated coal extracts with carbon black

The coal extracts were:

- RSF-0.00 CB shows 27 % at 471 ± 1 °C
- RSF-0.44 CB shows 24 % at 479 ± 1 °C
- RSF-0.88 CB shows 23 % at 492 ± 1°C
- RSF-1.60 CB shows 22 % at 496 ± 1 °C.

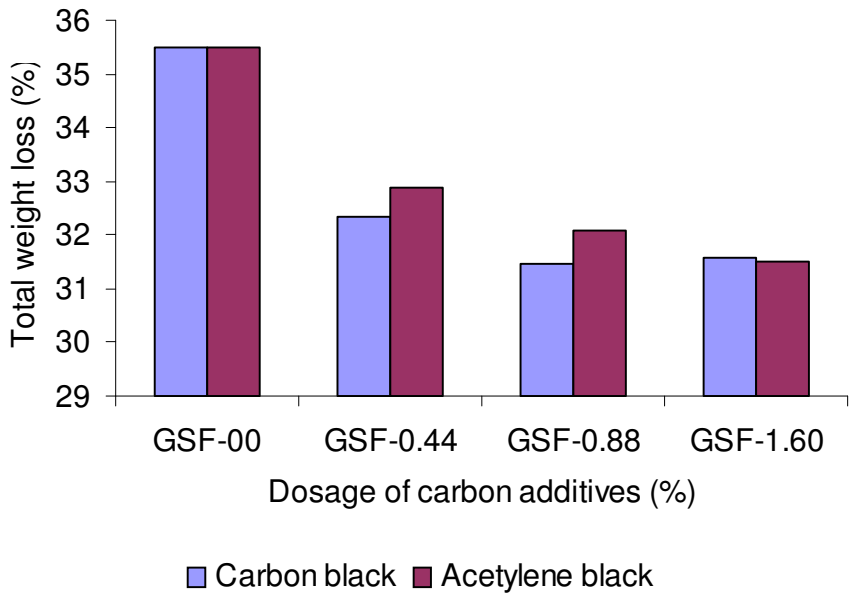

Figure 7.3.8: The total weight loss (%) of the heat-treated S^{-2} derived coal extracts on the addition of different amounts of the carbon additives

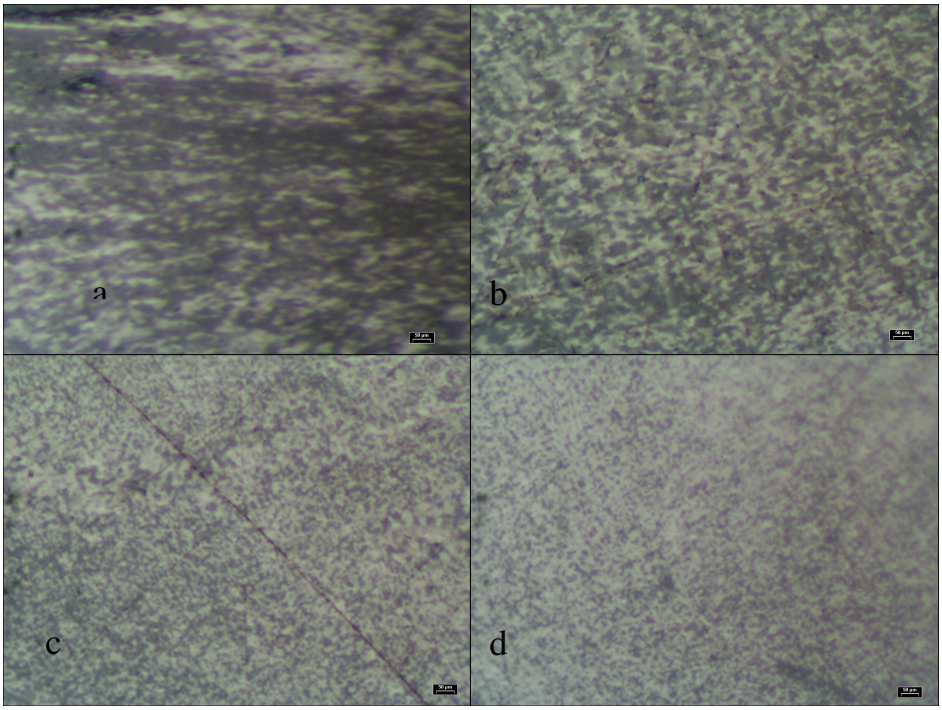

Figure 7.3.9: Optical micrographs of the carbon black blended cokes

(a) CSF-0.00 CB, coke is very crystalline with extensive flow texture.

(b) CSF-0.44CB shows high crystallinity and reduced flow texture domain. The coke is homogeneously anisotropic.

(c) CSF-0.88CB shows no flow texture but reduced mosaic texture domains.

(d) CSF-1.6CB shows extremely small granular anisotropic domains.

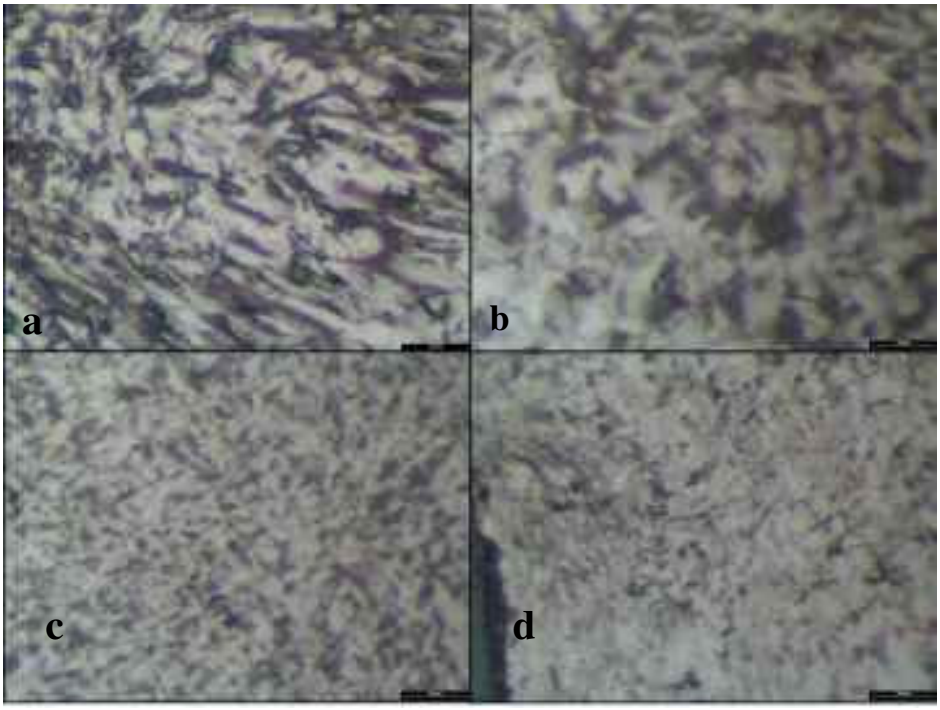

Figure 7.3.10: Optical micrographs of the acetylene black blended cokes

(a) CSF-0.0AB is highly crystalline with extensive continuous flow texture.

(b) CSF-0.44 AB shows high crystallinity with visible fragmented patches of flow texture

(c) CSF-0.88 AB – coke shows no visibility of the flow texture. Reduced size of fragmented granular but coarse mosaic texture.

(b) CSF-1.60 AB shows extremely small but coarse anisotropic domains. No flow texture.

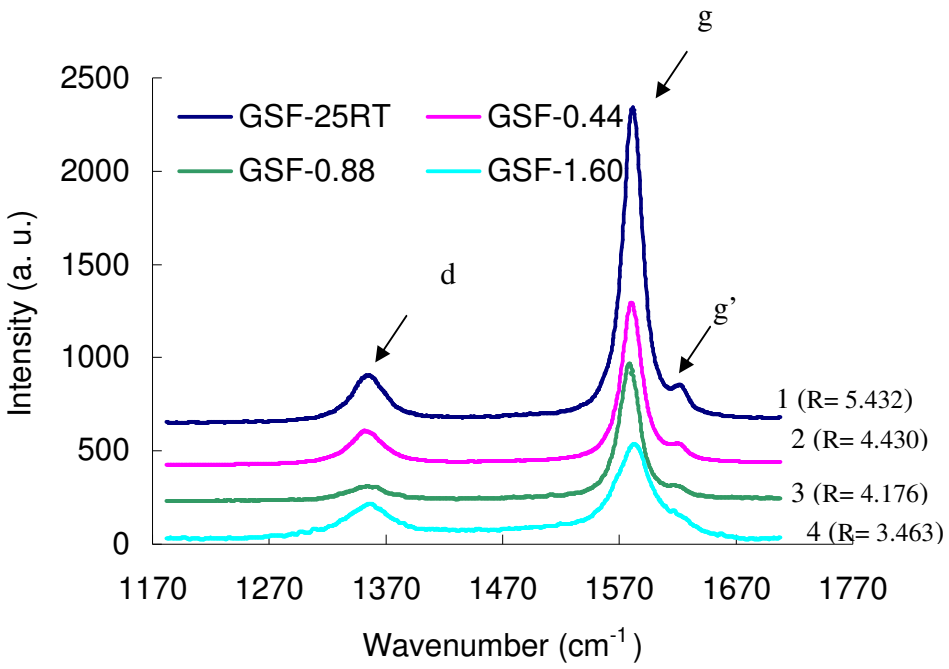

Figure 7.3.11: Raman spectra of the graphitised cokes prepared with the addition of carbon black, showing the intensity ratios of the area under the peak

(1) GSF-25RT shows the d-peak at 1354.56 cm^{-1} and a split of the g-peak into 1579.79 cm^{-1} and 1612 cm^{-1}.

(2) GSF-0.44 shows the d-peak at 1351.31 and the g-peak splits into 1580.69 cm^{-1} and 1617.81 cm^{-1}.

(3) GSF-0.88 shows the d-peak at 1 349.92 $cm^{-1}$and a split in the g-peak into 1579.64 cm^{-1} and 1 618.35 cm^{-1}.

(4) GSF-1.60 shows the d-peak at 1349.52 cm^{-1} and the g-peak slightly lowered to 1582.26 cm^{-1}.

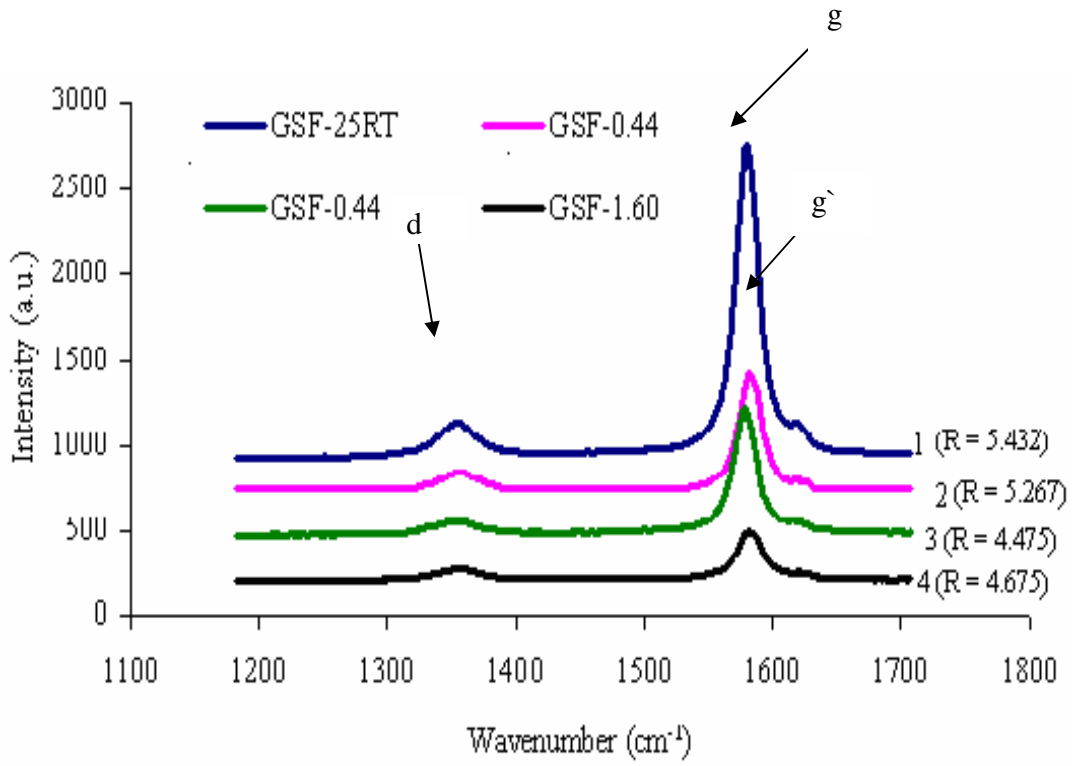

Figure 7.3.12: Raman spectra of the graphitised cokes prepared with the Addition of acetylene black, showing the intensity ratio, R = I_G/I_D, of the area peaks

(1) GSF-0.00 % AB shows the d-peak at 1 353.86 and the g-peak at 1567.19 cm^{-1}.

(2) GSF-0.44 % AB shows the d-peak at 1 352.98 and the g-peak at 1580.69 cm^{-1}.

(3) GSF-0.88 % AB shows the d-peak at 1 355.44 $cm^{-1}$and the g-peak at 1 582.58 cm^{-1}.

(4) GSF-1.60 % AB shows the d-peak at 1 354.10 cm^{-1} and the g-peak slightly lowered to 1 583.84 cm^{-1}.

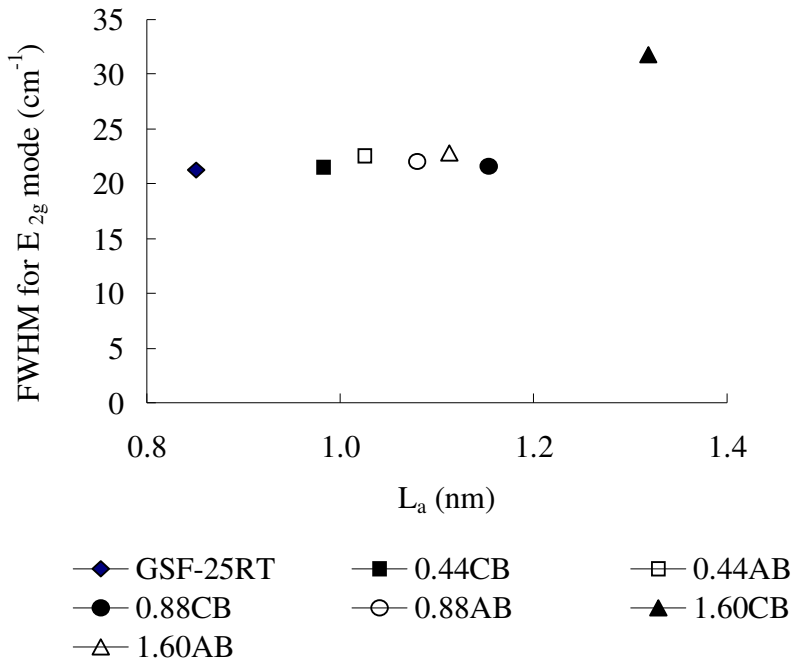

Figure 7.3.13: The average full width at half maximum (FWHM) of the E_{2g} mode (1 580 cm^{-1}) as a function of the crystallite size, L_a, of the graphitised cokes

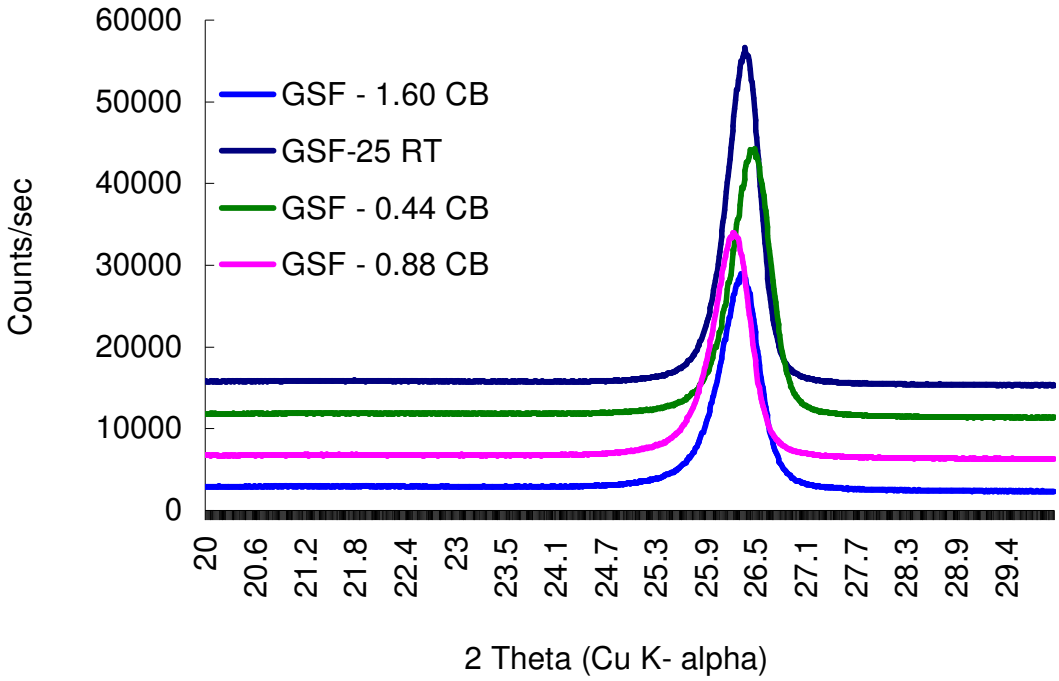

Figure. 7.3.14: XRD spectra (002 reflection) of the graphitised cokes on the addition of carbon black

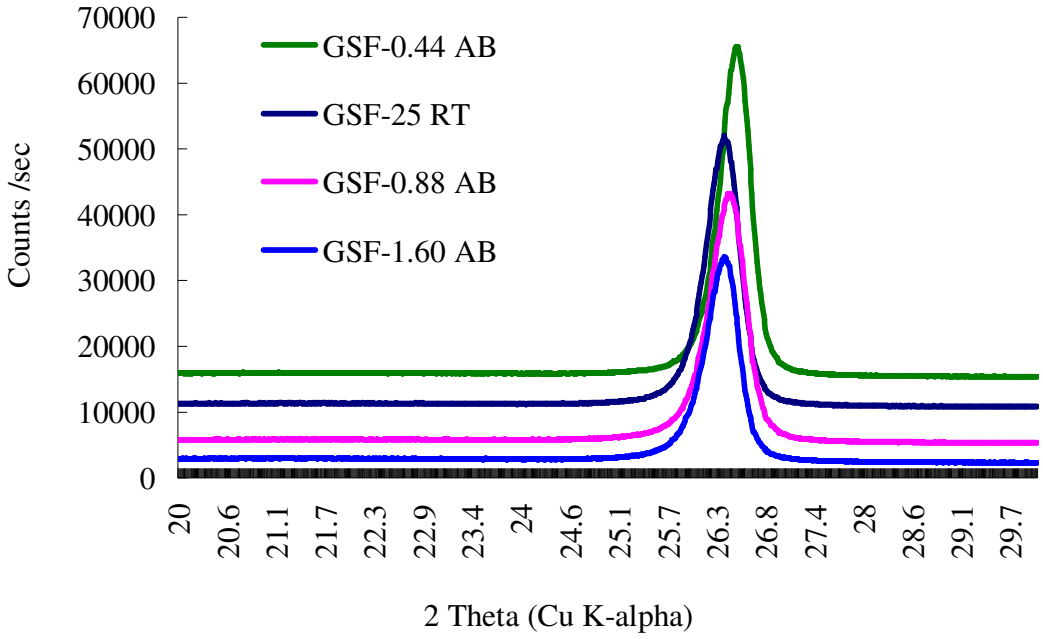

Figure 7.3.15: XRD spectra (002 reflection) of the graphitised cokes on the addition of acetylene black

Table 7.3.2

The effect of carbon additives on the properties of the graphitised coke

Sample ID	Raman R	L_a	XRD $d_{(002)}$ value	g
Additive AB				
0.00 %	5.4	0.796	3.38888	66
0.44 %	5.3	0.811	3.38113	69
0.88 %	4.8	0.896	3.38435	61
1.60 %	4.7	0.915	3.38666	61
Additive CB				
0.00 %	5.3	0.811	3.38981	58.0
0.44 %	4.4	0.977	3.39038	57.7
0.88 %	4.2	1.023	3.39143	56.5
1.60 %	3.5	1.229	3.39570	51.5

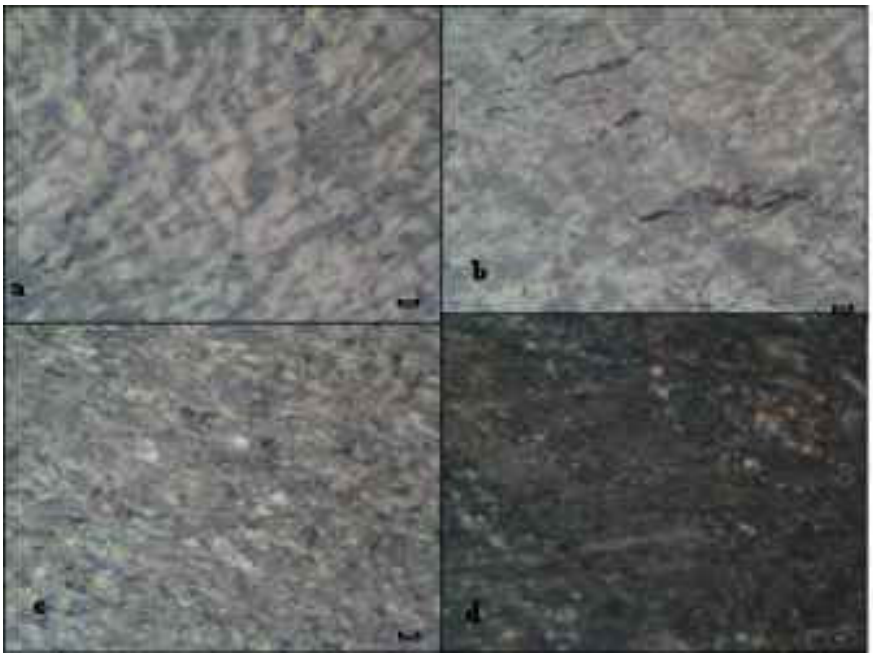

Figure 7.3.16: Optic micrographs of the graphitised cokes showing poor graphitised surface as the dosage of acetylene black is increased
(a) GSF-25RT (b) GSF-0.44 AB
(c) GSF-0.88 AB, (d) GSF-1.60 AB

Figure 7.3.17: Optical micrographs of the graphitised cokes showing poorly graphitised surface as the dosage of carbon black is increased (a) GSF-25RT showing graphitic interconnected parallel lamellae. Samples are poorly graphitised (b) GSF-0.44 CB (c) GSF-0.88 CB (d) GSF-1.60 CB

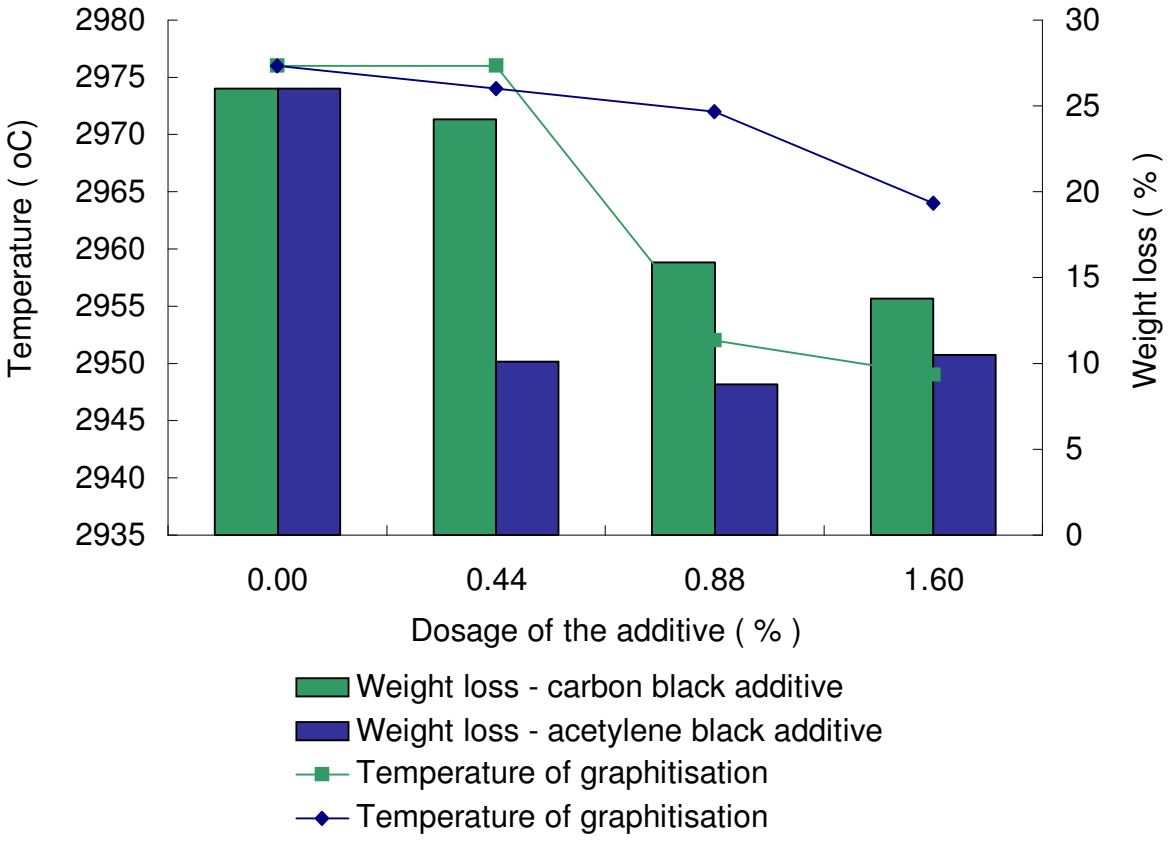

Figure 7.3.18: The graphitisation behaviour of the carbon additive cokes, showing the total weight loss (%) as a function of temperature obtained during graphitisation for 2h

7.4 The control of coke flow texture on the addition of carbon additives and iron (III) compound

This section details the results obtained when the coke flow texture was controlled with carbon additives. The additives were dispersed in the coal extracts solution prepared at room temperature and without the addition of sodium sulphide. Each sample is labelled with a code identified by the first letter R for Refcoal, C for coke, G for graphite and Fe for iron. The number attached at the end of the code signifies the amount of the additive (%) in the coal extract solution.

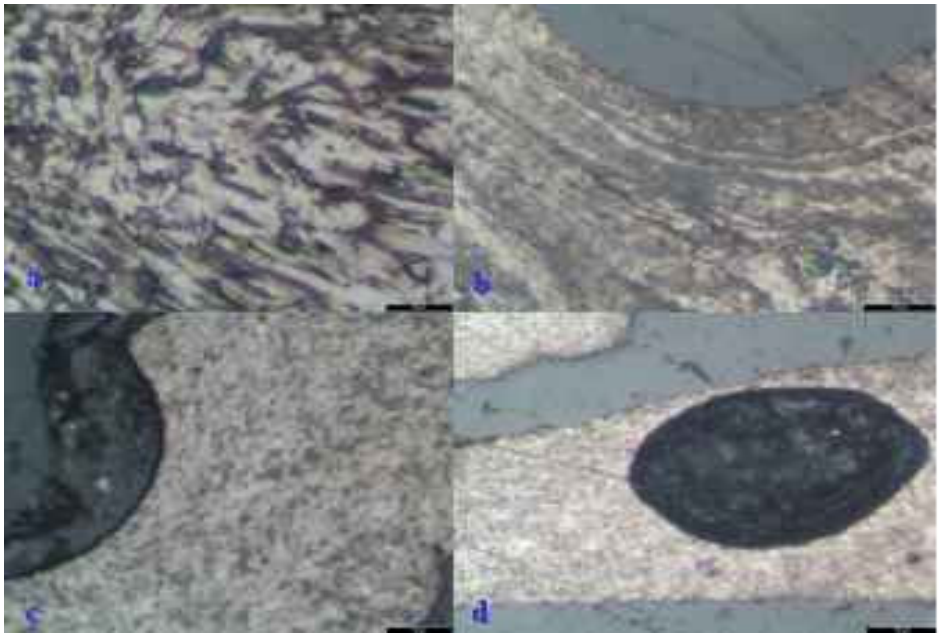

Figure 7.4.1: Optical micrographs of the acetylene black blended cokes obtained on pyrolysis of the coal extracts prepared at room temperature without S^{-2} (a) CCB-0.00 shows lamellae suggestive of flow texture.
(b) CCB-0.15 coke shows highly crystalline domain texture.
(c) CCB-0.22 coke shows coarse-grained mosaic texture.
(d) CCB-1.60 AB CCB-0.44 is essentially isotropic.

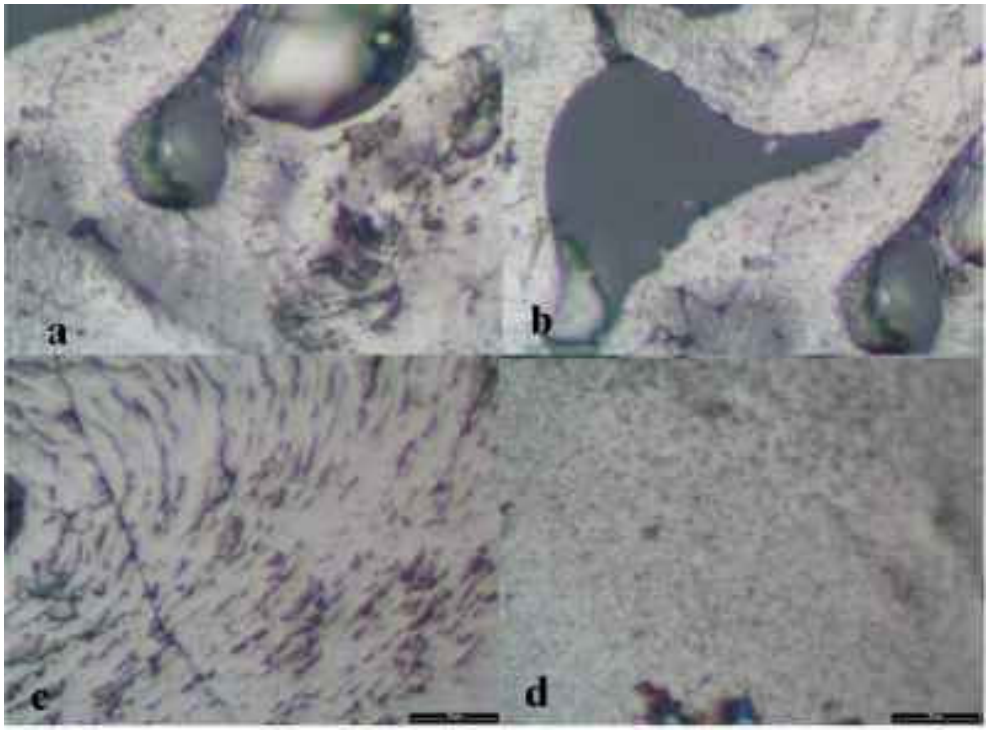

Figure 7.4.2: Optical micrographs of the cokes containing iron (III) compound (a-b) CFe-0 cokes show very fine crystalline domain texture. The coke is homogeneously anisotropic.
(c) CFe-1 coke shows a high crystalline flow domain texture in a concentric pattern. (d) CFe-3 coke has no flow texture mosaic and is essentially isotropic.

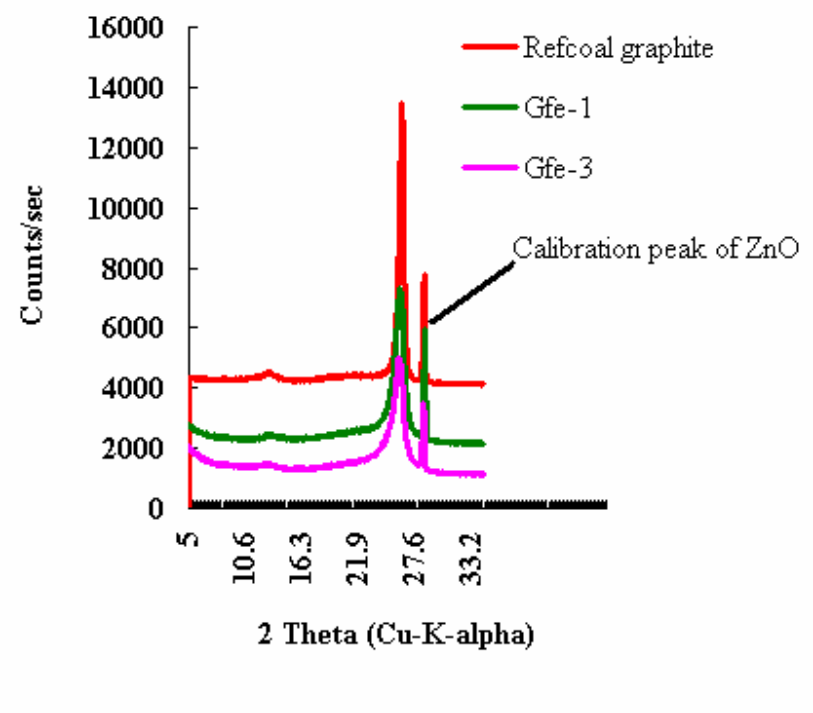

Figure 7.4.3: X-ray diffraction (002 reflection) spectra of the graphitised cokes on the addition of the iron (III) compound

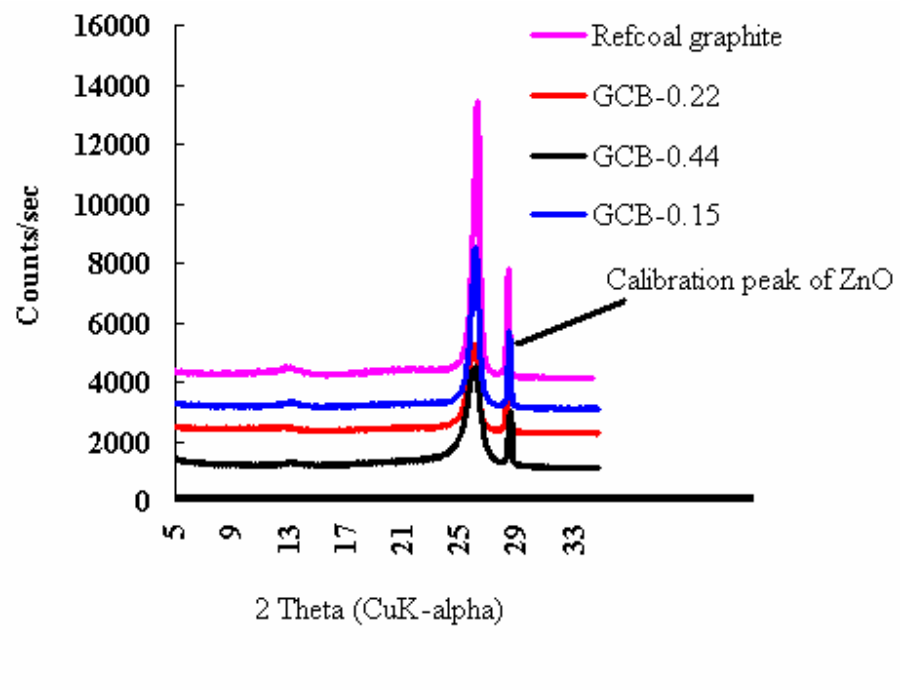

Figure 7.4.4: X-ray diffraction (002 reflection) spectra of the graphitised cokes on addition of carbon black

Table 7.4.1

Analysis of the graphitised cokes by Raman spectroscopy and X-ray diffraction
The graphitised cokes contain carbon black and iron (111) compound

Sample ID	R	$d_{(002)}$ value	L_a	G (%)
With carbon black				
No carbon black	3.89	3.38800	1.11	60.47
GCB-0.05	3.39	3.38997	1.27	58.17
GCB-0.10	3.07	3.42947	1.40	60.87
GCB-0.15	3.36	3.39434	1.28	53.09
GCB-0.22	2.47	3.40834	1.26	36.81
GCB-0.44	2.62	3.43134	1.64	10.07
Inorganic additive				
Gfe-1	0.54	3.42	7.96	21
Gfe-3	0.76	3.41	5.66	27

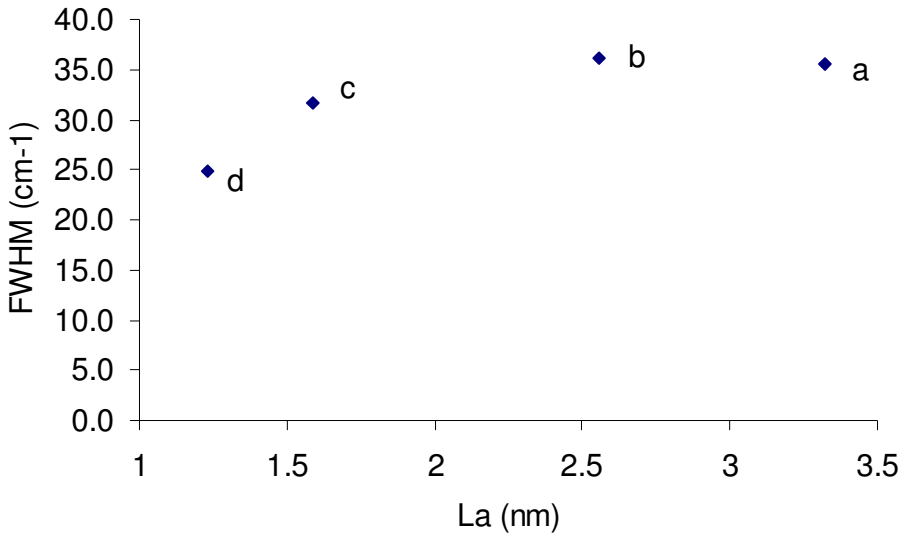

[a] No carbon black [b] GCB-0.15 [c] GCB-0.22 [d] GCB-0.44

Figure 7.4.5: The average full width at half maximum (FWHM) of the E_{2g} mode (1 580 cm^{-1}) as a function of the crystallite size L_a of the graphites prepared from the coal extracts obtained on addition of carbon black

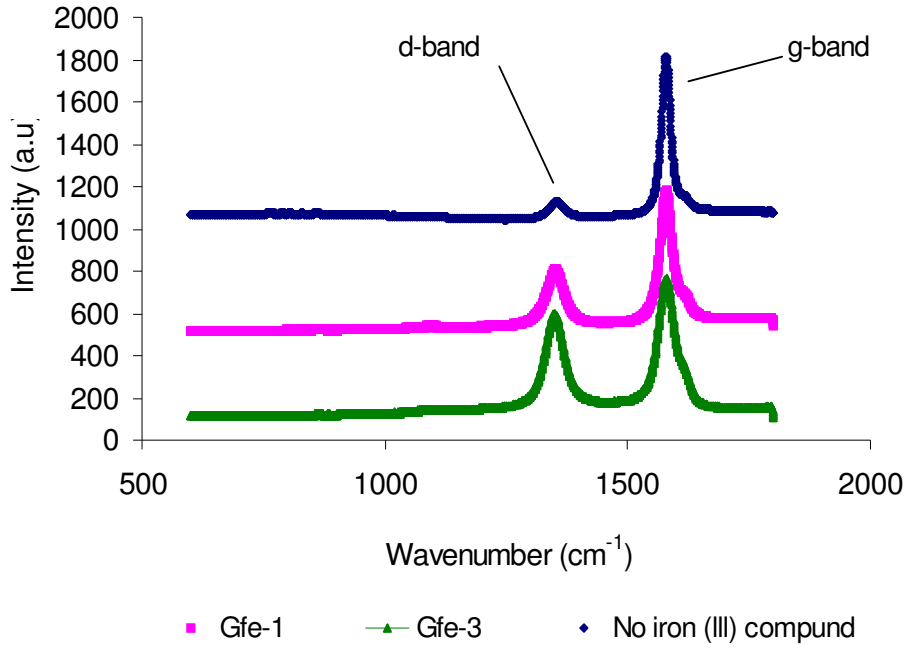

Figure 7.4.6: Raman spectra of the graphitised cokes on addition of iron (III) compound

CHAPTER 8

DISCUSSION

8.1 The coals studied

The coals studied were submitted to Coal and Mineral Technologies (Pty) Ltd for proximate, ultimate and major ash analysis and for determination of the major petrographic characteristics. The coal used was kept in nitrogen-purged plastic bags to minimise the intrusion of moisture and oxygen. Moisture is an undesirable component in coal. Its existence in the solvent greatly reduces the solubility effect of the solvent on coal. Existing moisture in the solvent is driven off as the heated reactor attains operating temperature prior to addition of the base. Tables 7.1.1 and 7.1.2 list the results of the proximate analysis and the ultimate analysis (air-dry basis) respectively. Table 7.1.3 lists the major ash components. The major petrographic characteristics of the Tshikondeni and Moatize coals are shown in Table 7.1.4. Tshikondeni coal has the highest vitrinite content of 93 %. However, both types of coal could be classified as meta-bituminous (see Table 7.1.4). Such coals have a hydrogen-rich vitrinite content [16]. The high C/H atomic ratio of 1.65 and the C/O atomic ratio of 0.74 shown by Moatize coal relative to Tshikondeni coal (C/H atomic ratio of 1.54 and C/O atomic of 0.37) suggest better extractability. However, Moatize coal is not readily available since it has been largely worked out. This makes Tshikondeni coal the primary important raw material in this project.

8.1.1 The coal dissolution process

Figure 7.2.1 shows the progress of extraction for various extraction runs at high temperature for 5 h with different amounts of sodium sulphide. The data for the different extraction runs are given in Appendix A2. The standard deviations and variances of the different extraction runs with sodium hydroxide, and with

different amounts of sodium sulphide at various time intervals are 0.1 and 0.004 respectively (see Appendix A3). The marginal deviation and variation order from the data shows reproducibility of the extraction process.

Figure 7.2.2 shows the progress of extraction at high temperature with sodium hydroxide only. The curve appears to be S-shaped with an absorbance of about 1.00 obtained over 5 h. The curve shows an induction period of 15 minutes, suggesting slow interaction of the reagent suit (see data in Appendix A2). The sharp rise in the curve after 15 minutes is thought to result from the coal solvent-base chemical interaction in which bond cleavage occurred to release organics into the solution. The reaction plateau when the maximum absorbance of about 1.00 was reached over 180 minutes. The maximum absorbance obtained corresponds to an 8 % organic content and is consistent with the literature value [54]. This was found to correspond to more than 90 % of the organic part of a 10 % ash flotation product dissolving in dimethylformamide, on addition of 10 % sodium hydroxide (Fig. 7.2.12) [54].

Hydrogen sulphide is known to aid in the metallation of porphyrins. To demineralise the coal further and obtain the very pure coal extracts needed for producing a highly crystalline coke, Na_2S was introduced into the extraction medium to help complex out the heavy metal ions released during chemical comminution. Unlike hydrogen sulphide, which is effective under controlled pH, the activity of sodium sulphide under a strongly basic solution is complex. It releases S^{-2} into the medium, which precipitates out certain heavy metals in solution, thereby forming an insoluble metal-sulphide complex [52, 53].

Figure 7.2.3 shows the optimisation results from separate extraction runs with various amounts of Na_2S. The maximum absorbance (λ_{max}) decreased with an increase in the dosage of sodium sulphide. The decreasing order of absorbance for the molar ratio mixture of NaOH: Na_2S (1:0) > (4:1) > (2:1) > (1:1), correspond to absorbances of 1.052 > 0.746 > 0.573 > 0.227 over 5 h respectively. The

addition of sodium sulphide caused a sudden rise in the curve, then a plateau after 60 minutes, suggesting that the maximum extraction is achieved within one hour and that sodium sulphide alone is not desirable in the coal dissolution process, which the author believes is attributable, partly, to the combined strength of the nucleophile. Sodium sulphide is a weaker nucleophile than sodium hydroxide. Its addition to the extraction medium appeared to promote a synergy, which enhanced a faster chemical interaction in which the induction period disappeared. The coal matrix softened and broken bonds instantly allowed organics into the solution. The mineral matters dropping out of the coal structure are thought to have formed insoluble complexes entangled to the insoluble organics in the solution. Coal dissolution in which the combined effects of swelling and bond cleavage weakened the coal matrix has been reported [22]. It is the author's view that some of the minerals released were precipitated out and trapped as insoluble sulphide complexes in the coal residue. However a high dosage of sodium sulphide adversely affected the degree of extraction with subsequent loss in the colour intensity and low yield of the coal extracts (Figure 7.2.4 and Table 7.2.1).

High organic rich coal solution produces coal extracts, which on heat treatment form cokes of high carbon content. Figure 7.2.5 shows a comparison of the optical absorbance of the coal extract solution with its organic solids content at various doses of sodium sulphide. The decrease in absorbance is related to the organic solids content of the coal extract solution. Without sodium sulphide, an absorbance of about 0.95, corresponding to the organic solids content of 8.2 (wt %), was obtained. With the addition of a small dosage[2] of sodium sulphide, the absorbance decreased to 0.64 with a corresponding organic solids content of 6.56 wt %. Further addition[3] of sodium sulphide lowered the absorbance to 0.16 and the organic solids content to 3.89 wt %. It can be generally inferred that

[2] NaOH:Na_2S molar ratio of 4:1

[3] NaOH:Na_2S molar ratio of 1:1

when the amount of sodium sulphide is increased, the organic solids content of the coal extract solution is decreased.

Optimisation of the coal extracts yield appeared to be far too low with the addition of sodium sulphide only. Figure 7.2.6 shows the progress of extraction at various amounts of Na_2S only (data obtained from Appendix A). The lower absorbance curves observed plateau at 0.30 after one hour suggested an extremely poor extraction yield and that sodium sulphide alone is not desirable for extraction of organics from coal. Sodium sulphide is a weaker nucleophile and its effect in extraction appears to be far less relative to sodium hydroxide. And the loss in colour intensity may be due to moisture released by sodium sulphide reagent, which inhibits the extraction of coal or may be due to chemical reaction or back-precipitation of the dissolved coal as explained in figure 7.2.7.

Figure 7.2.7 shows a curve of the absorbance per gram of coal dissolved over 5 h on addition of Na_2S and NaOH. The curve illustrates the loss in colour intensity at high dosage of sodium sulphide then a decline to 0.002 absorbance/g of coal dissolved. The addition of sodium sulphide to the extraction medium greatly lowered the absorbance and subsequently the amount of organic solids in the coal extract solution. Table 7.2.1 lists the characteristics of the coal extracts solution at high temperature over 5 h with different amounts of Na_2S. The loss in colour observed accompanies the decrease in the organic solids content of the coal extract solution. The bulk of the organic solids appear to have back - precipitated to form part of an insoluble ash. The extraction optimisation process was then limited to an hour to obtain high yields of the coal extracts.

8.1.2 The coal extracts or Refcoal

Table 7.2.2 lists the elemental analyses of the high-temperature coal extracts obtained on addition of different amounts of sodium sulphide. The C/H atomic ratio of coal extracts with no S^{-2} additives is high. The addition of sulphide lowers

the ratio. Such behaviour is believed to favour hydrogenation of the coal extracts. Coal being rich in aromatics, it is surely hydrogen-deficient. Hydrogenation of the coal extracts is reported to stabilise the free radicals generated in situ, thus favouring its dissolution [180]. It is pointed out in the literature that a solvent should have a hydrogen donor capability to stabilise the free radicals generated and thereby reduce the undesirable re-polymerisation process [39]. However, the solvent used in this project is N, N-dimethylformamide, a hydrogen donor. The increase in hydrogen could have been generated in situ by complex mechanisms and these could have accounted for the observed instant dissolution of the coal on the addition of S^{-2}, which resulted in the elimination of an induction period.

The oxygen content of the coal extracts decreases with increasing dosage of S^{-2} relative to the coal extracts without S^{-2} (Table 7.2.2). The decreasing order in oxygen content of the coal extracts is 7.49 > 5.78 > 5.72 > 5.04 wt %, corresponding to NaOH:Na_2S molar ratios of (1;0) > (4:1) > (2:1) > (1:1) respectively. The results suggest the removal of insoluble carbon containing oxygen. This behaviour favours the development of the mesophase.

The amount of ash in the coal extracts greatly affects the foaming and swelling during pyrolysis. The gradual decrease in the ash content following an increase in the dosage of S^{-2} provides the coal extracts with the purity favourable for producing the required graphitisable carbon. The decreasing order in the ash content of 1.30 > 1.00 > 0.70 wt % corresponds to the addition of NaOH:Na_2S molar ratio of (4:1) > (2:1) > (1:1) respectively. Without sodium sulphide, the coal extracts showed the ash content of 1.60 wt %.

Figure 7.2.8 shows the extent of purification of the Tshikondeni coal extracts. The total ash has been lowered from 6 651 ppm in the coal, to 71 ppm in the coal extracts on extraction with sodium hydroxide only. The addition of sodium sulphide to the extraction medium lowered the total ash further to 52 ppm, suggesting the effectiveness of sodium sulphide in coal purification. The removal

of complexed ash, such as kaolin with free silica entangled in a macromolecular structure (SiO_2 constitutes the highest ash content of the coal, see Table 7.1.3) of condensed aromatics rings, insoluble carbon, other inorganic elements and sulphide-metal complexes during the organic solids recovery process forms the basis for the high fluidity in the S^{-2} derived coal extracts [22, 24]. The result is differential swelling of the coal macerals and stresses that contribute to chemical comminution. The destruction of cross-linkages in a well-purified coal by cleavage of hydrogen bonds facilitates the reorganisation of aromatic units into a graphite-like structure during pyrolysis of the extracts [23, 24]. It is the purity of the coal extracts that determines the degree and graphitisability of carbon on heat treatment.

However, the method of recovering the coal extract remains important in lowering the ash content. Solvent evaporation produced extremely poor foaming of the coal extracts on pyrolysis, partly because of the high ash content still entangled within the coal matrix. Recovery of the coal extracts by water precipitation with a washing efficiency of 33 % produced well-foamed cokes. The washing efficiency of > 33 % could even provide the purity needed to promote foaming of the coal extracts, but there is a risk of the intrusion of oxygen during the solids recovery process. The resident time of water in the coal gel greatly affects the foaming of the coal extracts. An estimated amount of 86 % water was lost from the wet cake (formed after the filtration process) on heat drying in an oven at 60 ^{o}C under nitrogen flow. This huge loss of water could severely oxidise the coal extracts if drying is allowed at room temperature under nitrogen.

Table 7.2.3 lists the elemental analyses of the coal extract residue obtained at room temperature with different amounts of sodium sulphide. The degree of extraction on the addition of different doses of sodium sulphide and without the S^{-2} additives are listed. Without sodium sulphide, over 90 % of the organics are extracted. The addition of sodium sulphide to the extraction medium severely decreased the organic yields. The decreasing order of organics extracted is

90 > 89 > 85 > 71 wt % corresponding to NaOH/Na_2S molar ratio of 1:0, 2:1, 4:1 and 1:1 respectively. The intensity of the colour corresponds to the organic solids content of the coal extract solution.

Figure 7.2.9 shows the absorbance of the coal extract solution obtained at room temperature against its organic solids content. An absorbance of about 1.00, corresponding to an organic solids content of 82 %, is obtained. The addition of sodium sulphide reduced the absorbance to 0.58, corresponding to an organic solids content of about 6 %. However, the absorbance obtained at room temperature on the addition of sodium sulphide is higher relative to absorbance obtained from a high-temperature-derived coal extract solution (Fig. 7.2.5).

The (C/H) and (C/O) atomic ratios decrease with an increase in the dosage of sodium sulphide. Such systems are known to increase the solubility of the coal in different solvents, and the results are similar to those obtained in petroleum pitches in which a low C/H ratio favoured solubility in different solvents and reduced condensation of the hydrogen-rich aromatic molecules [34]. The residue without sodium sulphide showed lower hydrogen, oxygen and sulphur contents. The elemental composition of the coal shows (C/H) and (C/O) atomic ratios of 1.54 and 0.37 respectively (Table 7.1.2). These ratios are higher than in the sulphide-derived coal extract residues (Table 7.2.3). Such a pronounced decrease in hydrogen and oxygen could result from the induced dehydrogenation process, either from the coal or from the formation of water molecules [52].

The sulphur content is reduced from 0.81 % in the coal to 0.75 % in the coal extracts (Table 7.2.2). The decrease in sulphur content of the coal on the addition of the sodium sulphide, suggests efficient washing during the organics recovery process. The removal of minerals as a metal sulphide complex, together with insoluble carbon, cannot be ignored. The improvement in the purity of the coal observed on addition of sodium sulphide is a recipe for a better foaming of the extracts on heat treatment [150].

High sulphur content is commercially undesirable since it causes puffing of the graphite during heat treatment. Its existence in the coal extracts suggests the possibility of dehydrogenation during heat treatment. Polycyclic aromatic hydrocarbons, aliphatic materials and their derivatives result from the dehydrogenation process. Incorporation into the aromatic rings as thiophenic rings through radicalisation of the aliphatic chains, formation of conjugated chains, then cyclisation in which sulphur becomes part of the aromatic ring can occur. Research has shown that above 200 ^{o}C, sulphur extracts hydrogen from aromatic compounds, during which the thioether, C-S bonds are broken to release active fragments that participate in radical polymerisation, addition and substitution reactions [17, 95].

The effects of different nucleophiles in extraction viz. cyanide and thiosulphate did not make substantial difference to the degree of extraction. Table 7.2.4 and Table 7.2.5 show the elemental analyses of the coal extract residue obtained at room temperature with different amounts of potassium cyanide and sodium sulphate respectively. The degree of carbon extraction remains marginally the same, with no clear-cut difference in the percentage of carbon extraction. An absorbance of approximately 1.00 is observed.

However, the inconsistent low carbon-hydrogen and carbon-oxygen atomic ratios obtained favoured hydrogenation and formation of the mesophase. The inconsistency is thought to come from the sample homogeneity. The trend observed is that the (C/H) and (C/O) atomic ratios decrease with increasing dosage of the nucleophiles. The sulphur content in the extract residue is lower that in the original coal extract residue.

Figure 7.2.10 shows a comparison of the solubility of coal at different amounts of the nucleophiles. The addition of cyanide and thiosulphate separately to the extraction medium slightly decreases the absorbance, suggesting ineffective chemical interaction of the nucleophiles with the sodium hydroxide and coal

particles in the solution. However, the addition of sodium sulphide decreases the absorbance. The decrease is consistent with the previously discussed results and suggests a strong chemical interaction between species in the solution.
Figure 7.2.11 shows the organic solids content of the coal extract obtained on the addition of different amounts of nucleophiles. The organic solid content (%) decreases slightly with increasing dosage of cyanide and thiosulphate. The decrease is abrupt on the addition of sulphide. The purification of coal with the addition of cyanide and thiosulphate was discontinued because of not only safety reasons but also availability of the reagents.

8.2 Pyrolysis of the coal extracts or Refcoal

Figure 7.2.12 shows the average weight loss (%) of the heat-treated coal extracts obtained on the addition of different amounts of cyanide, thiosulphate and sulphide. The highest amount of wt % loss was obtained on the addition of sulphide. However, the carbon yield was relatively low. High carbon yield in the coke is desirable for the density and tensile strength of the graphite. The coal extracts obtained from the addition of sodium sulphide swells better than the coal extracts with sodium hydroxide only. The better swelling implies that the coal extracts with both NaOH and Na_2S goes through a more liquid phase. This suggests the formation of a better size of the mesophase region.

The swelling was determined at Coal and Mineral Technologies (Pty) Ltd by measuring the change in volume as the sample is taken from a low temperature to about 500 ^{o}C in an inert atmosphere. The swelling number for the coal extracts with sodium hydroxide only is 4.5, while a mixture of NaOH and Na_2S (molar ratio 1:1) gave swelling numbers of 9 and 9.5 (Table 7.2.1).

Swelling is thought to put a strain on the coal matrix, leading to the rupture of the hydrogen bonds, and the reorientation of the coal matrix allows reorientation of the hydrogen bonding structure [33]. It is believed that an appropriate hydrogen-

bonding agent, if allowed to penetrate the swollen coal structure, would be capable of "tying up" hydrogen bonding sites in the coal. The swelling index is related to the fluidity and is also used in this context to estimate the size of the mesophase. The higher the fluidity, the higher the swelling index, the larger is the size of the mesophase.

The addition of sulphide to the extraction medium greatly increases the fluidity of the coal extracts. Table 7.2.6 lists the fluidity data of the coal extract as a function of temperature. The S^{-2} derived coal extracts at room temperature show a fluidity of > 30 716 ddpm at 466 ^{o}C relative to the coal with fluidity of 13 550 (ddpm) at 464 ^{o}C. The high-temperature coal extracts show inconsistent fluidity at a slightly higher temperature of 480 ^{o}C. The observed inconsistency in fluidity on the addition of various dosages of sulphide is thought to come from oxygen intrusion during extraction or during the organic solids recovery process. Oxygen inhibits the extraction and foaming of the coal extracts during pyrolysis.

Figure 7.2.13 shows the foamed coke obtained on carbonisation of the room temperature prepared coal extracts. Without S^{-2}, the average foaming volume of +17 cm^3/g of Refcoal pyrolysed was obtained. However the room temperature prepared coal extracts[4] produced a coke with an average estimated volume of > 45 cm^3/g of Refcoal carbonised and far higher than the raw coal [5] at 27 cm^3/g coal pyrolysed. The high foaming volume is used as a measure of estimating the size of the mesophase region and is favourable for the formation of a crystalline anisotropic coke with intensive flow texture domains. The high temperature prepared coal extracts produced an estimated foaming volume of 13.2 cm^3/g of coal carbonised.

[4] NaOH/Na_2S molar ratio of 1:1

[5] Unpurified coal

Foaming of the coke depends on the pressure build-up within the melted coal. There is a minimum fluidity of the coal needed to entrap the volatiles to permit a high degree of foaming. A very fluidised coal allows the volatile matter to escape easily, thus reducing the foaming. Poor devolatilisation pores suggest that pressure built up within the coal mass to enhance foaming. Pyrolysis of the S^{-2} derived coal extracts produced a coke with far fewer devolatilised pores and improved foaming. However, sulphur in the coal extract is a problem as it causes puffing of the graphite on further heat treatment [53].

8.3 Optical texture of the cokes

Isotropy in this context is distinguished from anisotropy on the basis of changes in the surface characteristics of the resin-mounted polished sample when observed through an optical microscope rotated by 90^{o}. The dark purple or black colour changed to light yellow or white on rotation of the stage, which is indicative of anisotropic domains textures. However, when the colour remains unchanged on rotation of the stage it suggests isotropic texture. Figure 7.2.14 shows a micrograph of the polished coke, CSF-0RT. Microscopic examination of the resin-mounted polished sample under polarised light showed that the coke is essentially isotropic with isolated low levels of anisotropic domain, and poorly developed pores with thickened walls. The high plasticity of the coal extracts suggests a larger size of the mesophase. The black spherical bodies typical of pores in the coke suggest that the plastic mass formed was too fluid and is consistent with the observed swelling index.

Figure 7.2.15 shows a micrograph of the polished coke, CSF-0HT. The coke is essentially isotropic with poor devolatilisation pores. The limited coke porosity observed is thought to provide a coke density suitable for blast furnace operations and with the tensile strength required for nuclear carbon. The high

plasticity of the coal extracts in the sample RSF-0RT is suggestive of a large mesophase size, leading to the formation of anisotropic coke.

The number of pores observed in the coke suggested that a plastic mass formed, allowing gas bubbles to escape at relatively low pressure and thus forming microspores as suggested by the swelling index of 4.5. It is important to note that not all the domains of the sample show a change in their characteristic tints while the stage is being rotated, suggesting the less anisotropic character of the CSF-0RT. The measured bi-reflectance of 1.75 % is consistent with the texture of the coke. The coke yield is averaged at 76 %. However the related swelling index and foaming volume were low. The addition of S^{-2} to the extraction medium and the subsequent pyrolysis of the coal extracts changed the texture of the resultant coke.

Figure 7.2.16 shows a micrograph of the coke obtained on the addition of S^{-2}, CSF-25RT. The optical character of the coke showed thickened walls, poor devolatilisation pores with stacks of parallel lamellae and extensive flow texture pattern, and coarse flow-grained anisotropy of > 60 µm (scale ~50 µm). Rotation of the polished resin-mounted sample of coke on the microscopic stage resulted in a change in characteristic tints. The dark purple tints turned to yellow when the stage-mounted sample was rotated to an angle of 90^{o} [4, 5]. All the domains of the sample show a change in their characteristic tints when the stage is rotated, suggesting the 100 % anisotropic character of the CSF-25RT. The measured bi-reflectance of 5.45 % suggests a relatively high degree of ordered coke. The coke produced was anisotropic and the average carbon yield was 75 % – slightly lower than the coke without sulphide.

Additives alone do not determine foaming of the coal extracts during coking. The heating rate, which can be explained in terms of a competition between the evolution of volatile matter and thermal decomposition, is important in determining swelling [179]. The rate of heating of 10 ^{o}C/min to 480 ^{o}C for 1 h,

then to 900 ^{o}C for 2 h allows pressure built up within the fluidised coal mass and enhance foaming with formation of few microns. The accumulated volatiles escape to reduce the pressure built up. The soaking period allow maximum formation and coalescence of the mesophase spheres [179]. The high-temperature coal extracts with S^{2-}, CSF-25HT showed a medium-grained anisotropic domain with some flow texture. Devolatilisation of CSF-25RT is a factor of the rate (of carbonisation) and the amount of S^{-2} added.

Figure 7.2.17 shows a photomicrograph of the coke derived from the coal extracts prepared on the addition of S^{-2} at high temperature. The optical character of the coke showed a thinner wall, well-marked devolatilisation pores, and fine to coarse-grained anisotropy with some flow structure. The weight loss of the coal extracts prepared at various conditions is consistent with the formation of pores in the resultant cokes. Figure 7.2.18 shows a comparison of an average weight loss (%) of the heat treated coal extracts prepared at high temperature as a function of the amounts of sulphide added, with the room temperature prepared heat-treated coal extraction. Higher weight loss is obtained in the high-temperature coal extracts than in the room-temperature coal extracts. This favours the formation of coke with less carbon content than the cokes produced from pyrolysis of the coal extracts prepared at room temperature.

8.4 The graphitised cokes

Figure 7.2.19 shows an X-ray diffractogram of the graphitised cokes. For the same amount of S^{-2} but at different extraction temperatures, the d_{002} values of the graphites changed slightly. The d_{002} value of the graphite GSF-25RT is 3.37Å, while the d_{002} value of the graphitised cokes obtained from the coal extracts prepared at high temperature is slightly higher at 3.38 Å. Without sodium sulphide, the degree of graphitisation is low. However, with the addition of sodium sulphide to the extraction medium, the graphitised cokes showed improved degrees of graphitisation.

Figure 7.2.20 shows the Raman spectra of the graphitised carbons with a pair of bands at around 1350.5 cm^{-1} and 1579.1 cm^{-1} corresponding to the d-peak and g-peak respectively. Such Raman absorption frequency bands are very close to natural graphite. The difference in frequency is thought to come from the defects within the graphite structure. In natural graphite, the d-peak and g-peak are at 1350 cm^{-1} and 1580 cm^{-1} respectively. Such peaks are associated with well-ordered graphite lamellae [189].

Table 7.2.7 lists the ratio of g to d peaks, the interlayer spacing $d_{(002)}$ and the graphitisation factor, g. The ratio of the d-peak to the g-peak in the order GSF-0HT < GSF-0RT and GSF-25HT< GSF-25RT corresponds to 1.26 < 1.75 and 6.7 < 7.0 respectively. It appears that, for the same amount of sulphide added, the graphitised coal extracts prepared at room temperature showed a decrease in the area of the defect peak (d-peak) relative to the g-peak. The broad d-peak is indicative of the existence of disordered carbon in the distorted carbon network. This could be associated with the presence of hydrogen and alkyl groups at the edge of the planes thus decreasing the interactions between each molecule, which is thought to give rise to poor vibrational modes [188]. When these alkyl groups are between the planes, distortion of the carbon network occurs, resulting in some first-order bands as seen in Raman spectroscopy. In natural graphite, only a Raman band at 1580 cm^{-1} (E_{2g} mode) appears. However, in synthetic graphite, Raman bands appear at 1580 cm^{-1} and 1350 cm^{-1}. These bands have been used to measure the crystal size, La, of the graphite sheets [164].

In addition, this graphitised cokes showed a different degree of graphitisation. The graphites produced from the coal extracts prepared at room temperature showed the highest degree of graphitisation, as opposed to the graphites produced from the coal extracts prepared at high temperature. The order of graphitisation is GSF-0HT (25 %) < GSF-0RT (64 %) and GSF-25HT (74 %) <

GSF-25RT (79 %). High temperature of extraction appears to produce poorly graphitised cokes. Graphitised high-temperature-derived coal extracts showed low intensity ratio value ($R= I_g/I_d$) suggestive of a turbostratic structure. The highest intensity ratio values (R) were observed in graphites prepared from room-temperature prepared coal extracts suggesting a more ordered graphite structure.

Figure 7.2.21 shows a plot of average full width at half maximum (FWHM) of the E_{2g} mode (1580 cm^{-1}) versus L_a for the graphites and their blends of sodium sulphide under various conditions. The E_{2g} mode corresponds to the stretching vibration in the aromatic layers. Because the aromatic bond involves high energy, this mode occurred at a high frequency (1580 cm^{-1}). In perfect crystalline graphite, there is only the g-band in the first-order region. In poorly organised crystalline graphite, additional bands appear in the first-order region around 1150, 1350, 1500 and 1620 cm^{-1}. The A_{1g} /mode is called the defect band [150]. The crystallite size along the a-axis, L_a, was obtained by fitting the Raman intensity ratio (R) data into the equation [10]. The area ratio is used to estimate the crystallite size, $L_a = 4.3/R$ where R is the ratio of the E_{2g} mode (1580 cm^{-1}) to the A_{1g} mode (1350 cm^{-1}) in the Raman spectra (Fig. 7.2.20). From the equation $L_a = 4.3/R$ and $R = g/d$), it can be inferred that when the area of the degenerate peak (d-peak) becomes smaller, the area of the graphitic peak (g-peak) becomes larger, and the result is a bigger ratio (R) and a smaller crystal size, L_a in the a-axis. The g-peak becomes sharper and narrower in graphitised carbon obtained from room temperature prepared coal extracts. The addition of same dosage of S^{-2} improves further the intensity of the g-peak. Such inference is consistent with the increasing degree of graphitisation.

Extremely disorganised crystalline graphite may show a peak at 1350 cm^{-1}. Since graphitic material has a crystal structure consisting of flat layers in which the trivalent carbon atoms are connected with σ-bonds in sp^2 hybridised orbit in the plane containing the a – b axes, the layers are held by π-bond along the c-

axis. The presence of impurities material or heteroatom such as sulphur on the surface of the aromatic plane greatly affected the electronic environment and thus created defects within the crystal structure of the graphite, which is presumed to account for the existence of additional bands in the first-order region. A heteroatom such as sulphur, if it were attached to an alkyl carbon skeleton in the coal extract, would be released together with the volatiles during heat treatment. But if the sulphur is incorporated into the aromatic rings, it is difficult for it to be released with the volatiles at a coking temperature of about 500 ^{o}C. This may cause puffing of the graphite during further heat treatment and thus affect the quality of the resultant graphite.

Without the addition of sulphide, the graphite sample GSF-0RT showed the crystallite size, L_a, of 1.22 nm, corresponding to the FWHM of the E_{2g} peak at 37.39 cm^{-1}, while the graphite, GSF-0HT obtained from the high-temperature-derived coal extracts showed a larger crystallite size, L_a, of 5.41 nm, corresponding to a FWHM of 43.65 cm^{-1}. This suggests that the room-temperature-derived graphites are more ordered than the high-temperature-derived graphites. With the addition of sulphide, the FWHM of the E_{2g} peak in the Raman spectra of the sample GSF-25HT is bigger at 36.67 cm^{-1} corresponding to a crystallite size of 1.70 nm while the sample of graphite GSF-25RT showed FWHM of 34.37 cm^{-1} corresponding to a crystallite size of 0.92 nm. The smaller FWHM value suggests a sharp and narrower intensity of the g-peak (Table 7.2.7 and Appendix G1).

In general, the decrease in crystal size, L_a, of the graphite favours extraction at room temperature relative to high temperature. This favours the formation of a well-ordered graphitised carbon. High FWHM value of the E_{2g} peak may suggest various boundary conditions of the layer planes or a large number of defective structures introduced into the graphitic lattice within the layer planes, creating an environment that distorts the structure of the graphite.

8.5 Control of the coke texture

In carbonisation, bonds are broken and the active fragments formed participate in reactions of addition and substitution. The process of interstructural plastification takes place. The viscosity of the heat-treated coal extract and the high lability of the macromolecular fragments are determined by specific characteristics of the parent coal. Additives can influence the coal's thermoplastic properties but the effect depends on the nature of the additive used, the amount added and also the structure of the parent coal. The additives used in this work were carbonaceous.

8.5.1 The coal extracts prepared on the addition of S^{-2}

The coal extracts used were prepared at room temperature on the addition of sodium sulphide. The carbon additives used in blending the coal extracts were acetylene and carbon black, the properties of which are given in Appendix H. Mixing and dispersion of the carbon additives were described in Section 6.7.

Figure 7.3.1 shows SEM photomicrographs of a carbon additive and its surface characteristics. Carbon black is more spherical, while acetylene black is flat in shape. The carbon additives showed chains of aggregates that made it difficult to disperse uniformly in the viscous coal solution. As opposed to acetylene black, carbon black is relatively easier to disperse because of its structure (Appendix H).

Figure 7.3.2 shows SEM photomicrographs of the carbon black dispersed in the heat-treated coal extracts. The surface texture observed shows some ridges that become smaller with increasing amounts of carbon black. The fine surface texture is more visible with 0.88 % (by wt) of carbon black.

Figure 7.3.3 shows SEM photomicrographs of acetylene black dispersed in the heat-treated coal extracts. The surface texture observed remains coarse with increasing amounts of acetylene black. However, a fine texture was observed on the addition of 0.88 % (by wt) of carbon black. Such inconsistency could be attributable to the ease of dispersion.

Table 7.3.1 shows the elemental analysis of the coal extracts blended with carbon additives. The unblended coal extracts show lower C/H ratios relative to the extracts with carbon additives, suggesting the existence of hydrogen-rich molecules such as saturated hydrocarbons etc. With the addition of a carbon additive, the C/H ratio, however inconsistent, increases, suggesting the formation of hydrogen-deficient molecules. This favoured formation of radicals, which are important in dehydrogenative polymerisation [96]. However, the low C/O ratio observed in the blended coal extracts suggest poor formation of the mesophase on pyrolysis and formation of oxygen substituted aromatic hydrocarbons [14]

Pyrolysis of the sulphide-derived coal extracts produced an average of 64 wt % carbon yield. The addition of 0.44, 0.88, and 1.60 wt % of acetylene black produced on average 67, 67, and 68 % wt carbon yield respectively. A similar trend was observed with the addition of carbon black. The addition of about 0.44, 0.88, and 1.60 wt % carbon black produced 70, 71 and 69 % carbon yield respectively. The increasing trend in carbon yield of the cokes appears to happen albeit discounting the amount of carbon additives used prior heat treatment.

Figures 7.3.4 and 7.3.5 show TGA analysis of the coal extracts and their blends of carbon additives. The curves show significant weight loss (%) between 425 ^{o}C and 525 ^{o}C. The weight loss produced resulted from the physicochemical changes occurring in the thermoplastic stage during carbonisation and includes water, oxides of carbon and hydrogen, sulphide from thermally labile substituents or facile condensation reactions, breaking of cross-linkages comprising oxygen or non-aromatic carbon bridges between adjoining aromatic groups, etc. [135,

136]. The effect is more pronounced at a low dosage of the carbon additives. The difference in the amount of weight loss is more pronounced at 500 ^{o}C on the addition of carbon black relative to acetylene black, which shows sudden weight loss from 420 to 500 ^{o}C. Carbon black is more effective in suppressing the volatiles released during carbonisation relative to acetylene black. Such results complement the observed surface characteristics of the dispersed carbon additives in the coal extracts.

Figure 7.3.6 shows the curves of the maximum weight loss in the temperature region of 300 – 550 ^{o}C (obtained from Thermal analysis of the coal extracts) with the addition of acetylene black. The maximum weight loss excludes regions in which moisture and other light volatiles were released in the regions of < 300 ^{o}C and includes all volatiles released at the temperature of < 900 ^{o}C. Only the points on the TGA curves within these regions and up to 900 ^{o}C were used to produce curves. This is because the effect of carbon additive was reported to be more pronounced at the mesophase region of the pyrolysed coal extracts [114]. Without carbon black, the maximum weight loss of 27 % appears at a temperature of 471 ± 01 ^{o}C. The addition of 0.44 % carbon black slightly shifted the weight loss of 24 % to a temperature of 491 ± 01 ^{o}C. Further addition of 0.88 and 1.60 wt % acetylene black shifted the weight loss of 23 % and 21 % to temperatures of 592 ± 01 ^{o}C and 535 ± 01 ^{o}C respectively. Similar behaviour is observed with carbon black.

Figure 7.3.7 shows the curves of the maximum weight loss in the temperature region of 300 – 550 ^{o}C (obtained from Thermal analysis of the coal extracts, i.e. TGA curves) with the addition of carbon black. Without carbon black, the weight loss of 27 % appears at a temperature of 471 ± 01 ^{o}C. The addition of 0.44 % carbon black slightly shifted the weight loss of 24 % to a temperature of 479 ± 01 ^{o}C. Further addition of 0.88 and 1.60 wt % of carbon black shifted the maximum weight loss of 23 % and 22 % to the temperatures of 492 ± 01 ^{o}C and 495 ± 01 ^{o}C respectively. It appears that in the presence of carbon additives, the

start of the weight loss (temperature range 450 – 550 ^{o}C of the mesophase region) is delayed up to a slightly higher temperature during the heating process. This behaviour is similar in carbonisation systems of pitches in which carbon black delays the appearance of liquid crystals and causes the supersaturated mesogens not to precipitate. Supersaturated mesogens lead to a large number of smaller-sized spheres [113].

Figure 7.3.8 shows the total weight loss of pyrolysed coal extracts at different dosages of the carbon additives. The original coal extracts showed the highest weight loss (%) during pyrolysis. The addition of carbon black to the coal extract solution affected the weight loss (%). The decreasing order of weight loss (%) with dosage of carbon black is 35.50 > 32.34 > 31.48 >31.56 (by wt %), corresponding to RSF-0, RSF-0.44, RSF-0.88 and RSF-1.60 respectively. For acetylene black, the decreasing order of the total weight loss (by wt %) is 35.50 > 32.87 > 32.07 > 31.52 corresponding to RSF-0, RSF-0.44, RSF-0.88 and RSF-1.60 respectively. Both carbon additives are effective in reducing the amount of weight loss (%) during thermal analysis. However, the effectiveness of suppressing the weight loss (%) is more pronounced with the addition of carbon black relative to acetylene black. The results compare favourably with the observations made by Kanno *et al.* in which 5 % of carbon black addition in pitch was found to suppress the swelling of mesophase pitch sufficiently by initiating pyrolysis at lower temperatures, thus avoiding the intense evolution that may lead to severe swelling and increased size of the optical units [18, 127].

The slight increase in the maximum temperature at which the mesophase occurs is associated with the addition of carbon additives. Such a shift or delay in the maximum temperature corresponds to a gradual decline in the amount of weight loss and subsequently a reduction in the size of the crystalline domain of the coke. This is not favourable for graphitisation.

Figure 7.3.9 shows the optical micrographs of the cokes obtained from the coal extract blends of carbon black. The coal extracts alone show an extensive flow domain texture, as shown by the darkened parallel lamellae and the large crystalline domain units of about >10 microns. The extensive flow texture and high crystallinity of the coke result from severe expansion of the mesophase region within the temperature range of 470 – 520 ^{o}C, and characterise the size of the plasticity region formed during carbonisation. The addition of carbon additives significantly reduces the size of the optical units and provides mosaic domain texture. Perez *et al*. attributed this observation to insoluble solids offsetting the ability of petroleum pitch to generate large regions of the mesophase. The mesophase development is modified and affects the formation of new spheres, the growth of existing spheres and mesophase coalescence [126]. The size of the mosaic texture is influenced by the amount of the carbon additive present. Unlike acetylene black, a high dosage of carbon black produces a homogeneous fine mosaic coke texture, the reason being the effective dispersal of carbon black in the coal extract slurry. Dispersion of acetylene black has proved to be difficult. Chain-like aggregates that possess a cage structure have been observed (Fig. 7.3.1) and this structure has been reported to hinder the growth and stacking of mesophase molecules, leading to reduced size of the optical units to provide a fine-grained mosaic texture [120]. The disappearance of the flow texture domain is observed on the addition of the carbon additive and suggests interaction between the functionality of the carbon additive and the surface of the coal extract. Such interaction takes place within the temperature range of 470–520 ^{o}C in the early stage of carbonisation. The observation complements the weight loss (%) observed in the region of the plastic region formed during thermal analysis of the coal extracts and their blends of carbon additives.

Figure 7.3.10 shows the optical micrographs of the cokes obtained from the coal extract blends with acetylene black. A similar behavioural trend is observed with acetylene black. However, the poor dispersion of acetylene black in the coal extract slurry affected the homogeneity of the mosaic texture in the cokes

(Figs 7.3.2 and 7.3.3). There is inconsistency in the size of the domain texture. Reduced size of the optical units is also observed.

It can be concluded that the expansion (and subsequent flow texture) of the coke formed during carbonisation takes place as a result of gas evolution from the viscous liquid of the mesophase coal extracts during carbonisation and just before the solidification. The addition of carbon additives modifies the carbonisation properties of the mesophase coal extracts through chemical and physical interaction on their surface. Smaller size and larger number of crystalline domains in the coke were formed. The end result was the formation of a carbon with less flow texture and smaller domain texture units.

Figure 7.3.11 shows the Raman spectra of the graphitised cokes prepared with the addition of carbon black. The intensity ratio of the peak height, $R = I_G/I_D$, is a measure of the crystallinity of the graphitised coke (1). The unblended graphitised coke (1) shows a d-peak at 1351 cm^{-1} and a split of the g-peak into 1580 cm^{-1} and 1612 cm^{-1}. The largest intensity ratio (R) of 5.432 suggests a highly ordered graphite structure. The graphitised coke blend (2) shows a d-peak at 1355 cm^{-1} and a g-peak that has split into 1581 cm^{-1} and 1618 cm^{-1} with an intensity ratio of 4.430. The ratio of the g-peak to d-peak decreases in the order (1)[6] > (2)[7] > (3)[8] > (4)[9], corresponding to the intensity ratios of 5.432 > 4.430 > 4.176 > 3.463 respectively. This decrease in intensity ratio suggests the formation of a turbostratic graphite structure. In the graphitised coke blend (3) the d-peak has a frequency of 1350 $cm^{-1}$and the g-peak splits into 1580 cm^{-1} and 1618 cm^{-1}. Similarly, the graphitised coke blend (4) shows a d-peak at 1349 cm^{-1} and g-peak slightly lowered to 1582 cm^{-1}. The same observation holds for

[6] GSF-0 [4] GSF-0.44 [5] GSF-0.88 [6] GSF-1.60

graphitised coke blends of acetylene black. Such a split in the g-peak comes from some intrusions in the graphite structure.

Figure 7.3.12 shows the Raman spectra of the graphitised cokes prepared with the addition of acetylene black. Similarly, graphitised coke blends of acetylene black show decreasing order in the intensity ratio (I_D/I_G) of the peak height, i.e. 5.432 > 5.267 > 4.475 > 4.675, corresponding to graphite samples (1) > (2) > (3) > (4) respectively. The inconsistency in the intensity ratio of sample GSF-0.44 arises from the difficulty with which acetylene black disperses in the coal extract solution. The results obtained suggest a decrease in crystallinity with increasing dosage of carbon additives, leading to poor graphite formation. The graphites with less flow texture favoured a dosage below 0.22 % of carbon additives.

The relative intensity of the g-band increases from 1580 cm^{-1} to 1582 cm^{-1} as the graphitisation temperature decreases from 2976 to 2949 ^{o}C. In addition to the decreasing intensity ratio of the peak height in the coke blends, a second-order band occurring at approximately 1580 cm^{-1} tends to split into a double g-peak at ~1580 cm^{-1} and g` at 1617 cm^{-1}, suggesting structural disorder in the graphite. The subsequent doubling in the dosage of the carbon black to 0.88 wt % resulted in a similar split of the g-peak, indicating the occurrence of the triperiodic order.

The presence of carbon additives causes the qualitative differences in the Raman spectra of the materials. Since the properties of the graphite are determined largely by the quality of the starting material, the carbon additives present appear to be coating the mesophase spheres and affecting the crystal domain size and anisotropy of the graphites. The result is a decrease in the crystalline domain, which favours the formation of turbostratic carbon. The carbon additives decrease the graphitisability of the coke blends. The degree of graphitisability of the coke blends decreases with an increase in the dosage of carbon additives. The crystallite size, L_a (along the a-axis), is an important parameter in determining the spacing between the graphite layers.

The ratio of the peak area may be related to the crystalline size of the graphite along the a-axis. The crystallite size L_a was calculated from the calibration equation, $L_a = 4.3/R$ were R is the ratio of the g to the d peaks. It can be inferred that when the area of the degenerate peak (d) becomes bigger, the area of the graphitic peak (g) becomes smaller, and the result is a smaller ratio, R, and a bigger crystal size, L_a, in the a-axis. The area ratio is used to estimate the crystallite size, L_a. The crystallite size, L_a, is related to the FWHM (full width at half maximum) and its determination helps in the assessment of crystallinity.

Figure 7.3.13 shows the FWHM of the E_{2g} mode versus L_a over a temperature range from 2952 ^oC to 2976 ^oC. The FWHM is related to the crystallite size to allow a further assessment of the degree of crystallinity in each of the graphites. The FWHM of the E_{2g} peak in the coal extract blends becomes narrower and decreases with an increase in the dosage of carbon additives. Corresponding to the decrease in the FWHM, an increase in the L_a value is observed. These increase in graphite crystal size, L_a occurs when the dosage of the carbon additive is increased from 0.44 % to 1.60 %. The E_{2g} (1380 cm^{-1}) vibrational mode is affected by the distortion of the hexagonal graphite lattice near the crystal boundary; this originates from the reduced size of the crystalline domains within the coke blends. The carbon atoms at the crystal boundary are usually attached to chemical groups, such as a carbonyl group, hydroxyl group or carboxyl group, or to a hydrogen atom [11]. A rise in the FWHM of the E_{2g} peak with an increase in carbon black dosage may suggest various boundary conditions of the layer planes or a large number of defective structures introduced into the graphitic lattice within the layer planes.

Figures 7.3.14 and 7.3.15 show the XRD spectra of the graphitised coke blends with acetylene black and carbon black respectively. The degree of graphitisability (g), the interlayer spacing (d_{002} value) and the Raman intensity ratio (R) of the graphitic/degenerate peak are listed in Table 7.3.2. The crystallite size L_a

increases with the addition of the carbon additives while the d-spacing decreases accordingly. And the incipient asymmetry of the d_{002} peak was observed in the Raman spectroscopy of the graphitised samples, which gradually increased with increasing dosage of the carbon additive. This is thought to come from the introduction of defects into the lattice structure of the graphite, a similar result was reported by Wakayama *et al.* [188].

Table 7.3.2 lists the Raman spectrometry and XRD data on the graphitised carbons. The graphite produced without carbon additives shows the highest degree of graphitisability of 58 % to 66 %. The addition of carbon additive to the coal extracts decreases the degree of graphitisation. With increasing dosage of acetylene black from 0.05 through 0.88 to 1.60 wt %, the decreasing order in the degree of graphitisation is 69 %, 61 % and 62 % respectively. Similarly, carbon black shows the same trend and the decreasing order of graphitisability is 57.7 %, 56.5 % and 51.5 % respectively. Corresponding to this, the interlayer spacing, d_{002}, which decreases accordingly. The Raman intensity ratio of the g to the d peaks decrease with increasing dosage of the carbon additive. This suggests a broadening of the defect peak (d) resulting from induced defects within the crystal structure of the graphite.

Figures 7.3.16 and 7.3.17 show optical micrographs of the cokes graphitised with acetylene black and carbon black respectively. The effectiveness of the carbon additives hindered the graphitisability of the cokes as indicated by the char on the observed graphites' morphology.

Figure 7.3.18 shows the behaviour of the cokes with respect to weight loss during graphitisation. The temperature of graphitisation decreases with increasing dosage of the carbon additives and the weight loss (%) decreases accordingly. Figure 7.4.1 shows the behaviour of the graphitised coke blended with carbon additives at 2 000 ^{o}C for 2 h, and the relationship between the weight loss (%)and the temperature of graphitisation for the coal extracts and their

blends. Graphitisation of the coke labelled CSF-0 results in a weight loss of 26 % at 2 976 ^{o}C. The coke blends graphitised with carbon black, CSF-0.44, CSF-0.88 and CSF-1.60, show graphitisation weight losses of 24.2 % at 2976 ^{o}C, 15.9 % at 2952 ^{o}C, and 13.8 % at 2949 ^{o}C respectively. The same dosage of acetylene black gave 10.1 % at 2974 ^{o}C, 8.80 % at 2 972 ^{o}C, and 10.5 % at 2 964 ^{o}C respectively. The results indicate that the amount of weight loss (%) and consequently the graphitisation temperature (^{o}C) decrease with increasing dosage of the carbon additives. For the same period of graphitisation (2 h) and dosage of carbon additive, the cokes show similar behavioural trends during graphitisation. However, the main differences are those between the two carbon additives, the decreases in the graphitisation temperature and the weight losses, complementing the declining intensity ratio of the peak height, and these differences account, to a great extent, for the decrease in the graphite crystal size, and subsequently for the increase in induced defects within the graphite structure.

It could be inferred from this study that the reduction in the flow texture of the carbon favoured the formation of isotropic carbon. However, at large dosages of the carbon additives, graphitisation is severely hindered. Induced defects within the crystal structure of the graphite were observed on the addition of the carbon additives. It can be concluded that the addition of the carbon additives decreases the amount of the weight loss, and consequently the graphitisability of carbon.

8.5.2 The coal extracts prepared without S^{-2} additives

Figure 7.4.1 shows the optical texture of the cokes obtained from the coal extracts on the addition of carbon black. The coal extracts without additives show extensive flow texture domains. The addition of the carbon additives significantly reduces the size of the optical units and provides reduced mosaic texture domain. The size of the mosaic texture is determined by the amount of the carbon additive present. Higher dosages of carbon black produced

homogeneous fine mosaic texture cokes, which are essentially isotropic. The order of decreasing size of the optical units is CCB-0.0 > CCB-0.15 > CCB-0.22 > CCB-1.60. However, the degree of graphitisation is decreased. At very high dosages of carbon additive, graphitisation ceased altogether. Carbon black hinders the growth and stacking of mesophase molecules, leading to reduced size of the optical units providing a fine-grained mosaic texture [112, 113]. The size of the optical units is determined by the modification of the domain anisotropy of the blend's mesophase during the carbonisation process.

Table 7.4.1 lists the Raman spectroscopy and XRD data on the graphitised cokes containing carbon black and iron. The graphitised cokes without carbon black show the highest degree of graphitisation relative to the graphitised cokes with carbon black. The degree of graphitisation decreases in the order GCB > GCB-0.15 < GCB-0.22 > GCB-0.44, corresponding to 60 > 20 < 50 > 20 %. The inconsistency observed is thought to be associated with the effectiveness of dispersal of carbon black in the coal solution, as observed in GCB-0.15. The minimum amount of carbon black required to reduce the flow texture and produce an isotropic coke with a crystalline domain texture is < 0.22 % (by wt). Above this dosage of carbon black, the coke becomes essentially isotropic.

Figure 7.4.5 shows the average full width at half maximum (FWHM) of the E_{2g} mode (1580 cm^{-1}) as a function of the graphite crystallite size, L_a. The crystallite size, L_a, increases with increasing amount of carbon black. Additives such as carbon black and Al_4C_3 have been reported to lead to an increase in the crystallite dimension, L_c. These are thought to increase the density of the graphite and improve its neutron radiation stability [63, 72, 178].

8.6 The coal extracts on the addition of iron (III) compound

Figure 7.4.2 shows the optical micrographs of the coke containing iron (III) compound. The coke without iron (a and b) shows a small crystalline domain

texture. The addition of a small amount of iron (lll) compound (c, 1 % by wt) produced changes in the appearance of the crystalline domain to a concentric flow pattern. This is thought to emanate from dispersion of the iron (lll) gel in the coal extract solution during mixing. A high dosage of iron (lll) compound (d, 3 % by wt) produced an essentially isotropic coke. The degree of graphitisation was consequently decreased.

Figure 7.4.3 shows the XRD spectra of the graphitised cokes containing iron. Without iron (lll) compound, the degree of graphitisation appeared to be relatively high compared with the graphite with iron (lll) compound. However, the graphite Gfe-3 containing 3 % by wt of iron (lll) compound showed a slight improvement in the degree of graphitisation relative to Gfe-1.

Figure 7.4.4 shows the XRD spectra of the graphitised cokes containing carbon black. The calibration peak of ZnO is clearly visible. The d_{oo2} value appeared to be higher on the addition of carbon black, suggesting movement towards disordered graphites. In addition, the crystallite size and degree of graphitisation decreased with an increase in the dosage of carbon black (Table 7.4.1). Evidently, the addition of a high dosage of carbon additive hinders the formation of graphites.

Table 7.4.1 lists the data on the degree of graphitisation for each of the graphites. The coke with the highest dose of iron (lll) compound showed 27 % graphitisation relative to the coke with the lowest amount of iron (lll) compound, which is at 21 %. This is a promising step towards catalytic graphitisation and is a subject of interest for future research work. Oxygen intrusion during mixing could be a problem. Previous research work on oxygen-containing aromatics showed that oxygen substitution could result in both well-ordered and poorly ordered graphite [48, 49, 56, 103]. Poor graphitisation could be the result of the formation of quinines, which lost carbon monoxide (CO) on pyrolysis to give non-planar

radicals, leading to a dramatic decrease in the final graphitisability of the starting material.

The corresponding $d_{(002)}$ spacing increases accordingly and is consistent with the Raman spectroscopy results (Table 7.4.1). The intensity ratios (R = g/d) of the graphites Gfe-3 and Gfe-1 are 0.76 and 0.54 respectively. The intensity ratio of the degenerate peak (d) decreases with increasing amounts of iron. Subsequent to that, the $d_{(002)}$ value decreases with increasing amounts of iron.

Previous work showed that heat treatment of iron or iron compounds with amorphous carbon led to the formation of the carbide, cementite (Fe_3C) that decomposed on further heating to give graphite [169]. The formation of cementite was further reported to yield even better graphite when used in conjunction with silicon as ferrosilicon [169]. The effect of iron is consistent with the literature study in which iron was found to improve the graphitisability of hard carbons through the formation of cementite, as intermediate carbide, which decomposed on further heating to give graphite [67].

Further work on catalytic graphitisation needs to be done to improve the degree of graphitisation. However, it appears conclusively that iron or iron compounds catalyse the conversion of hard carbon into graphitisable carbon by firstly dissolving the intercellular hard carbon to form graphite via one of the mechanisms documented in the literature [168, 169].

It can be concluded that the thermal reactions during carbonisation can be altered considerably through the use of certain additives. These are chemical substances that influence the thermoplastic properties of coal. Their effect on the coal structure occurs via active centres of the coal macromolecules (functional groups, labile hydrogen) and they influence the condensation reactions at pre-coking temperatures with the evolution of free radicals at increasing

carbonisation temperatures. This effect depends on the nature of the additive used, the amount added and also the structure of the parent coal.

CHAPTER 9

CONCLUSIONS

High-ash coals are not suitable for efficient use in carbonisation. The Tshikondeni coal, like any other coal in South Africa, is ashed and contains polynuclear aromatic (hydrogen-deficient) structures bound to inorganic elements. The CSIR coal solubilisation process unlocked the elements by disrupting the bonds and allowed the bulk of the organic part of the coal into the solution. This lowered the ash content. The relatively pure coal extracts obtained through centrifugation and water precipitation provided a starting material suitable for carbonisation and graphitisation. The washing efficiency in the recovery of organic solids produced coal extracts with the desired purity. In addition, this method of carbon recovery offers advantages over other known coal purification processes used elsewhere. The solvent is relatively inexpensive and the coal extract solution produced can be beneficiated into numerous carbon end products. The addition of sodium sulphide lowered the ash level further with subsequent improvement in the coke texture. The well-purified coal extracts used in this project produced graphitisable and isotropic carbon, which is currently made from petroleum pitch. However, the carbon yield of the resultant coke was low. Coal being an abundant raw material in South Africa, it has the potential to be the future source of coke and graphitisable carbon needed in the pebble bed modular reactor (PBMR).

The low C/H atomic ratio observed in the coal extracts prepared at room temperature on the addition of S^{-2} enhanced hydrogenation of the coal extracts and increased the solubility of the coal in DMF. This was observed by the decrease in the delay time and the appearance of instant colour within a few minutes of extraction starting. Heat treatment of the purified coal extracts resulted in a high swelling index, extensive foaming and a highly plastic carbon material.

The coke formed was produced from the heat-treated coal extracts, which liquefied and formed domains of discoidal liquid crystal prior to cross-linking, with loss of volatile material. When polished specimens of the cokes were observed by reflectance microscopy, flow textures with domain sizes of a few to many microns were observed. Isotropic, poorly graphitising cokes showed little or no structure. Anisotropic cokes were produced when these domains of liquid crystal grew and coalesced. The cokes were found to be highly graphitisable. However, in the heat-treated coal extracts prepared at high temperature, the liquid crystal domains were graphitisable but appeared not to have coalesced. Nevertheless, the random orientation of the domains allowed isotropic blocks to be formed with extremely low crystallinity. The precursors that form these liquid crystals are generally materials known to have a high aromatic carbon content.

Extensive flow textures in the cokes obtained on the addition of sodium sulphide to the starting material produced coarse-grained, anisotropic graphites. The cokes produced were highly ordered, as suggested by the measured bi-reflectance. Such cokes were better when produced from the room-temperature-derived coal extracts than from the high-temperature-derived coal extracts. The degree of graphitisation increased on the addition of sodium sulphide. The highly anisotropic crystalline domains and the relatively high swelling index observed in the heat-treated room-temperature coal extracts complemented the measured foaming and fluidity, which was used as a measure for estimating the size of the mesophase.

The temperature at which the coal extract is prepared and the amount of sodium sulphide added determine the level of anisotropy. The highest degree of graphitisation was obtained in the coal extracts prepared at room temperature on the addition of sodium sulphide. The increase in the interlayer spacing (d_{002} value) of the graphites suggested the development of defects within the crystal lattice. This is a function of the method used to prepare the coal extracts.

Heat treatment of the coal extracts prepared at room temperature without the addition of sodium sulphide resulted in a low level of anisotropy and coarse flow texture. The addition of carbon black substantially reduced the coarseness of the flow texture. However, the effect of carbon black compromised the graphitisability of the carbon produced.

The carbon additives stimulated nucleation and restricted the growth and coalescence of spheres, resulting in the formation of smaller texture domains. Moreover, the carbon additives, especially acetylene black, agglomerated to restrict the diffusion of the mesogen molecules within the coal extracts. Such a hindrance reduced the size of the crystalline carbon domains and produced a large number of smaller spheres. The trend established was that when the amount of carbon additive increased, the sizes of the carbon domains tended to become smaller with uniform size distribution. The minimum threshold dosage of carbon additive required to reduce the flow texture without reducing the graphitisability of carbon was found to be very low. This is a significant step towards producing isotropic and crystalline graphite from coal.

Iron (lll) compound was also used with the purpose of influencing transition from liquid to solid reactions. The intention was to convert the intracellular hard carbons into soft carbons, thereby increasing the size of the mesophase around the mesophase temperature region. Iron (lll) compound showed insignificant but promising improvement in the degree of graphitisation. More attention is needed in future to improve the preparation methodology in order to improve the degree of graphitisation substantially.

REFERENCES

1 Nicholls D R, *The pebble bed nuclear reactor*, Eskom, 1996, pp 25 – 26.

2 Nicholls D R, *The pebble bed modular nuclear reactor*, South African Journal of Science, 2000, 96, pp 31 – 35.

3 Nicholls D R, *The pebble bed modular reactor*. South African Journal of Science, 1998, pp 31-32.

4 Cuesta A, Dhamelincourt P, Laureyns J, Martinez-Alonzo A and Tascon JMD, *Raman microprobe studies of carbon materials*, Carbon, 1994, 32, pp 1523 – 1532.

5 Jing, X, Xu X, Yang Y and Qu R, *Prediction calculations and experiments for the first criticality of the 10 MW high-temperature gas-cooled reactor test module,* Nuclear Engineering and Design, *2002,* 218, pp 43 - 49.

6 Kelly B T, Physics *of Graphite*, Applied Science Publishers, Englewood, London and New Jersey, 1981, p477.

7 Kelly B T, *Nuclear Reactor Materials in Material Science and Technology*, Vol 10A, Cahn R W, Haasen, P and Kramer E J, Academic Press, London, 1981.

8 Marsden L, *Irradiation damage in graphite due to fast neutrons in fission and fusion systems, International Atomic Energy Agency*, Report IAEA-TECDOC-1154, 2000.

9 Dekker M, Coal Handbook, Energy, Power and Environment Chapter 11, Academic Press, New York, 1981.

10 Snyman C P, *The petrological composition and origin of coal with special reference to South African coal*, Trans. Geol. Soc. South Africa, 1976, 79, pp 242- 252.

11 Valkovic V (Ed.), *Trace Elements in Coal*, Vol. 1, CRC Press Inc, Boca Raton, Florida, USA, 1983.

12. A.G.I. (American Geological Institute), *Glossary of Geology*, Washington D.C., USA, 1972, p805

13 Tatsch J H, *Coal Deposits* (Origin, Evolution and Present Characteristics), USA, 1980, pp 13-29.

14 Stach E, Mackowsky H-Th, Teichmuller M, Tailor G H, Chandra D and Teichmuller R, Stach's *Textbook of Coal Petrology*, Gebruder Borntraeger, Berlin, Edward Arnold, Stuttgart, 1982, 535 p.

15 Falcon R M S, Coal in South Africa – Part 2: *The Application of Petrography to the Characterisation of Coal*, Mineral Science and Engineering, 1978, 10 (1)

16 Teichmuller M and Teichmuller R, *Geological aspects of coal metamorphism: In: Coal and Coal-bearing Strata*, Murchison D G and Westoll T S (Eds), Oliver and Boud, Edinburgh and London, 1968, pp 233 - 268.

17 Van Krevelen D W, *Coal typology, Chemistry, and Physics and constitution*, Elsevier Scientific, New York, 1981 and Goedkoop M L, Palmel , Fuel, 1959, 38, p 256.

18 Haghseresht F, Lu G Q, Whittaker A K, *Coal structure and porosity of carbonaceous adsorbents in relation to their adsorption,* Carbon, 1999, 37, pp 1491 - 1497

19 Martinez-Escandell, Carreira P, Rodriguez-Valero M A and Rodriguez R, Self-sintering mesophase powder: *Effect on extraction/washing with solvent*, *Carbon,* 1999, 37, pp 1662 - 1665.

20 Marsh H, *Introduction to Carbon Science*, Butterworths, London, UK, 1989.

21 Hernandez J G, Hernandez- Calderon I, Luengo C A and Tsu R, *Microscopic structure and electrical properties of hard-treated coals and eucalyptus charcoal*, Carbon, 1982, 3, p 201.

22 Sapienza, T, Butcher W, Slegeir and Healy L, *Carbon dioxide/Water for coal beneficiation*, American Chemical Society, Series 301, pp 501 - 512.

23 Gonzalez D, Montes-Moran M A, Yong R J and Garcia A B, *Effect of temperature on the graphitisation process of a semianthracite*, Fuel Processing Technology, 2002, 79, pp 245-250.

24 Bodily D M, Wann J-P and Kopp V, *Solvent swelling of coal and coal macerals,* Poster session, Division of Petroleum Chemistry, American Chemical Society, Salt Lake City, 7 – 12 September 1986.

25 Berkowitz, N, *An Introduction to Coal Technology*, Academic Press, New York, 1979.

26 Schemer, R and DeRyuter, E, *Chemistry of coal utilisation*, John Wiley and Sons, New York, 1963.

27 Pitt G J and Millward G R, *An Introduction to Coal and Modern Coal Processing,* Academic Press, Philadelphia, 1979, pp 5-6.

28 Nandi B N, MacPhee J A, Ciavaglia L A, Chornet E and Arsenault R, *Enhancement of plastic property of inert-rich oxidised cretaceous coals via the water gas shift reaction*, Fuel, 1987, 66, pp 473 - 478.

29 Moodie B, *The maceral composition of the commercially available products prepared by collieries in the Republic of South Africa*, Report by the National Institute for Coal Research, CSIR, Pretoria, 1978.

30 Collin W R, *Coal geology and coal technology*, University of South Wales, Australia, 1984, p 123.

31 Mukherjee S and Borthakur P C, *Chemical demineralisation*, Fuel, 2001, 80, pp 2037 – 2040.

32 Rubiera F, Arenillas A, Pevida C, Garcia R, Pis J J, Steel K M and Patrick J W, *Coal structure and reactivity changes induced by chemical demineralisation,* Fuel Processing Technology, 2002, 79, (3), pp 273 - 279

33 Dryden I G C, *Solvent treatment of coal*, Fuel, 1973, 52, p86

34 Menendez R, Granda M and Bermejo J, *Relationship between pitch composition and optical texture of the coke,* Carbon, 1997, 35, pp 555 - 562.

35 Dryden I G C, *Coal conversion technology,* Fuel, 1976, 55, p366,

36 Nthembi P, *Coal purification*, Master's Thesis presented to the University of Pretoria, 2003, pp 43 – 45.

37 Stransberry P G, Stiller A H, Zondlo J W, Chenn C, Bland B and Fento D, *Carbon products from coal using an extractive process*, Research report, Department of Chemical Engineering, West Virginia University, USA, 2002.

38 Stiller A H, Sears J T and Hammack R W, Coal extraction process, US.Pat No 4.272,356, 1981

39 Darva C, de Oliveira J V, Vale M G R and Caramao E B, *Supercritical fluid extraction of high-ash Brazil coal*, Fuel, 1997, 76, p 485.

40 Olson E S, Swanson M L, Olson S H, and Diehl J W, *Reaction of low-rank coals in supercritical methanol,* American Chemical Society, Division of Fuel Chemistry, 31(4), p 64.

41 Swanson M L, Olson E S, Diel J W and Farnum S A, Extraction of low rank coal with supercritical water, *American Chemical Society, Division of Fuel Chemistry*, 1989, 31(4), pp 43 - 53.

42 Emanuel R, Aleksandra R and Wilhelm P, Influence of recycle solvent *properties on coal extraction*, ONB d/s, Pszczynska, Pol. Fuel, 1988, 67(8), 1143 - 1149.

43 Bean S D, Greenkorn R A and Cao K C, *Selective extraction of coal with supercritical solvent*, Proc. International Conference of Coal Society, School of Engineering, Purdue University, Indiana, USA, 1985, pp 238 – 241.

44 Barton P, *Supercritical separation in aqueous coal liquefaction with impregnated catalyst*, Ind. Eng. Chem. Process Des. Dev, 1983, 22, pp 589 - 594.

45 Anderson L L, Shifai Y M, Hill G R, *Activated extraction of coal using a hydrogen-donor solvent*, Fuel, 1974, 53 (1), pp 32 - 37

46 Gutmann V, *The Donor-Acceptor Approach to Molecular Interaction*, Plenum Press, New York, 1978.

47 Zuhiro T, Koyo N, Yoshihiro M and Masashi I. *Effect of addition of various salts on coal extraction with carbon disulphide/n-methyl-2-pyrrolidinone mixed solvent*, Energy and Fuels, 2001, 15 (1), pp 141 - 146.

48 Tatsushi I, Toshimasa T, Osamu I and Masashi I. *Effects of the additives on mixed solvent extraction for Argonne Premium coal samples*, Sekitan Kagaku Kaigi Happyo Ronbunshu, 1992, 29, pp 24 - 27.

49 Iino M, Liu H T, Ishizuka, T and Takanohashi T, *Noncovalent interactions in coal structures: Effects of additives on extraction yield and solubility of extracts*, Proc. Int. 7th Conf. On Coal Science, Michaelian, K H (Ed), Canada, 1993, pp 225-228.

50 Missal, PM, Quan H H and Cai G S, *Extraction of coal using toluene and water with and without the addition of H-donor tetralin, Erdoel, Erdgas, Kohle* 1992, 108 (6), pp 279 - 283.

51 Bland B W, Design, *Construction and evaluation of coal extraction pilot plant to manufacture coal-based carbon pitch*, thesis, Department of Chemical Engineering, West Virginia University, Morgantown, USA, 2000.

52 Lino M and Matsuda M, *Carbon disulphide-pyridine mixture, a new efficient extraction solvent for coal,* Fuel, 1983, 63, p 744.

53 Murray P R S, Dawson P R, *Structural and Comparative Inorganic Chemistry, (3rd edition),* Heinemann Educational Books, London, pp177 – 185.

54 Morgan D L, US patent No. 5120430, 1996.

55 Sharma D K and Gihar S, *Chemical cleaning of low grade coal through alkali- acid leaching employing mild conditions under ambient pressure*, Fuel 1991, 70, p 663.

56 Kara H and Ceylan R, *Removal of sulphur from four central Anatokan lignite by NaOH*, Fuel, 1998, 70, p 170.

57 Lino M, Takanohashi T, Ohsuga H and Toda K, *Extraction of coals with CS_2-N-methylpyrrolidone mixed solvent at room temperature*, Fuel, 1988, 67, pp 1639 – 1647.

58 Gerstner J A and Zondlo J W, *Gasification kinetics of residual coal produced from solvent extraction with N-methylpyrrolidone*. Fuel Science and Technology International, 1992, 10 (3), pp 335 – 346.

59 Kipling J J, Sherwood J N, Shooter P V and Thompson N R, Factors *influencing the graphitization of polynuclear carbons*, Carbon, 1964, 1, p 315.

60 Winslow F H, *Macromolecules: Introduction to polymer science 21*, Academic Press, New York, 1980, p850

61 Barton S S, Boulton G C, Dacey J R, Evans M J B, Harrison B H, *Heat of immersion studies on carbon from polyvinylidene chloride*, J. of colloid and interface science, 1973, 44, pp 50 - 56

62 Lewis I C and Edstrom T, *Thermal reactivity of polynuclear aromatic hydrocarbons,* J Org. Chem, 1963, 28 , p 2055.

63 Ruland W, *X-ray studies on the carbonisation and graphitisation of acenaphthylene and bifluorenyl*, Carbon, 1965, 2, pp 365 – 378.

64 Singer L S and Lewis I C, *An electron spins resonance study of carbonisation of aromatic hydrocarbons acenaphthylene*, Carbon ,1964, 2, p 115.

65 Edstrom T and Lewis I C, *Chemical structure and graphitization: X-ray diffraction studies of graphite derived aromatic polynuclear*, Carbon, 1969, 7, p85.

66 Fitzer K, Mueller L and Schaffer W, *Chemistry and Physics of Carbon*, 1971, 7, p 237.

67 Warburton A P, *Catalytic graphitisation*, PhD Thesis, University of Leeds, UK, 1973.

68 Marsh H, Mochida I, Scott E, Sherlock I, *Carbonisation of liquid-crystal (mesophase) development, Co-carbonisation of a solvent –refined coal with petroleum pithes and hydrogenated coal extracts solution.* Fuel, 1980, 59, pp 517 - 519.

69 Greinke R A and Lewis I C, *Carbonisation of naphthalene and dimethylnaphthalene,* Carbon, 1984, 22, pp 305 - 314

70 Marsh H, Mochida I, Macefield I, Scott E, *Carbonisation of liquid-crystal (mesophase) development. Carbonisation of soluble and insoluble fractions of coal extracts solution,* Fuel, 1980, 59, pp 514 - 516

71 Leung P S and Stafford G J, *An investigation of the early stage graphitisation process by neutron inelastic scattering*, Carbon, 1970, 8, p 527.

72 Evans S and Marsh H, *The chemistry of formation of semi-cokes from aromatic system using mass spectrometry*, Carbon, 1971, 9, pp 733 - 747.

73 Marsh H and Neavel R C, Carbonisation of liquid – crystal (mesophase) development. *Carbonisation of soluble and insoluble fractions of coal extracts solution.* Fuel, 1980, 59, p 511.

74 Brooks J D and Tailor G H, The formation of graphitising carbons from the liquid phase, Carbon, 1965, 3, pp 185 - 193.

75 Pierre D, *Graphite and precursors; World of carbon series*, Gordon and Breads, Amsterdam, 2001.

76 Montes-Moran M A, Crespo J L, Young R J, Garcia R and Moinelo S R, *Mesophase from a coal tar pitch: A Raman spectroscopic study*, Fuel Processing Technology, 2002, 78, pp 207 – 212.

77 Lewis I C, *Chemistry of carbonisation*, Carbon, 1982, 6, pp 519 - 529.

78 Yondo Y and Marsh H, In: Schults H D (Ed), *Coal Liquefaction Products*, Wiley, New York, Chapter 1983, 1, p 125.

79 Lewis I C and Singer L S, *Electron spin of aromatic compounds*, Carbon , 1967, 5, p 373.

80 Auguie D, Oberlin M and Oberlin A, *Microtexture of mesophase spheres as studied by high-resolution conventional transmission electron microscopy,* Carbon, 1980, 18, pp 337 - 346

81 Dumont M, Chollon G, Dourges M A, Pailler R, Bourrat X, Naslain R, Bruneel L and Couzi M, *Chemical, microstructural and thermal analyses of a naphthalene-derived mesophase pitch*, Carbon, 2002, 40, pp 1475 – 1486.

82 Brooks J D and Taylor G H, *The formation of graphitising carbons from liquid phase,* Carbon, 1965, 3, p 185.

83 Brooks J D and Taylor G H, *Chemistry and Physics of Carbon* 4, P L Walker (Ed.), Edward Arnold, London, 1968, p 243.

84 Honda H, Kimura H, Sanada Y, Sugawara S and Furuta T, *Optical mesophase texture and x-ray diffraction pattern of the early stage in carbonization of pitches,* Carbon, 1970, 8, p 181.

85 Marsh H, Dachille F, Melvin J and Walker P L, *The carbonisation of anthracene and biphenyl under pressures of 3 Kbar*, Carbon, 1971, 9, p 159.

86 Jager C, Henning Th, Schlogl R and Spillede Q, Spectral properties of carbon black, *J Non-crystalline Solids*, 1999, 258, pp 161 - 179.

87 Bacon G E, *The interlayer spacing of graphite*, Acta. Crst. 1951, pp 558 - 562

88 Becon G E, *The (hki) Reflexions of graphite*, Acta Cryst. 1954, pp 359 - 360

89 Bacon G E and Franklin R E, *The a dimension of graphite*, Acta Cryst., 1951, 4, p 561.

90 Diamond R, *A least square analysis of the diffuse x-ray scattering from carbons*, Acta Cryst. 1958, 11, p 129.

91 Tsuzuku T, Mechnical *damping in carbon and graphitisation at low temperature*, Pergamon Press Ltd, 1964, 1, pp 511-514.

92 Brooks J D and Stephen J F, *A test of diamond method for estimating size distribution of aromatic rings*, Carbon, 1965, 2, p 379.

93 Warren B E and Bodenstein P, *The diffraction pattern of fine particles carbon black*, Acta Cryst., 1965, 18, p 252.

94 Ergun S and Tiensuu V H, *Tetrahedral structure in amorphous carbons*, Acta Cryst., 1959, 12, p 1052.

95 Menendez R, Granda M and Bermejo J, *Relationship between pitch composition and optical texture of the coke,* Carbon, 1997, 35, pp 555 – 562.

96 Barr J B and Lewis I C, *Chemical changes during the mild air oxidation of pitches*, Carbon, 1978, 16, p 439.

97 Ihnatowicz M, Chiche P, Deduit J, Pregermain S and Tournant R, *Examination of cokes from coals and pitches by optic microscopy*, Carbon, 1966, 4, p 41.

98 Christu N, Fitzer E, Kalka J and Overhoff D, *Characterisation of carbons and graphites by X-ray examination*, Carbon, 1968, 6, pp 236 - 237

99 Blaydeen H E and Patric J W, *Studies of organic sulphur in coke: sulphur-carbons formed by pyrolysis in condensed phase* Fuel, 1970, 49, p 257.

100 Inagaki M and Radovic L R, *Nanocarbons*, Carbon, 2002, 40, pp 2263 – 2284.

101 Greinke R A and Lewis I C, *Twist desclinations in the carbonaceous mesophase,* Carbon, 1979, 17, p 471.

102 Lewis I C, and Greinke, J, *Pyrolysis studies on model aromatic sulphur compounds*, Carbon, 1977, 17, pp 471 - 477.

103 Fernandez A L, Granada M, Bermejo J and Menedez R, *Carbon precursors from anthracene oil. Insight into the reaction of anthracene oil and sulfur*, Energy and Fuel, 1988, 12, pp 949 – 957.

104 Lewis I C and Greinke R A, *Model compound studies of the role of sulphur in carbonisation*, Carbon 1982, 20, p 143.

105 Vasilyeva I G, *Handbook of physics and chemistry of rare earths* Elsevier, Russia, 2001, *32*, pp 567 - 609.

106 Shevkoplyas V N, *Coal carbonisation with addition of HCl as a way of improving coke quality*, Fuel, 2002, 81, pp 947 - 950.

107 Ergun S, *Determination of layer size in carbons*, Carbon, 1968, 6, p 7.

108 Fabry F, Flamant G and Fulvheri L, *Carbon black processing by thermal plasma. Analysis of the particle formation mechanism*, Chemical Engineering, 2001, 656, pp 2123 – 2132.

109 Jakab E and Blazso M, *The effect of carbon black on the thermal decomposition of vinyl polymers*, Journal of Analytical and Applied Pyrolysis, 2002, 64, pp 263 – 277.

110 Greinke R A and Singer L S, *Constitution of coexisting phases in mesophase pitch during heat treatment: Mechanism of mesophase formation*, Carbon, 1988, 26, p 665

111 Crammer J H, Plotzker I G, Peebles L H and Uhlmann D R, *Carbon mesophase-substrate interactions,* Carbon, 1983, 21,p 201.

112 Stadelhofer J W, *Examination of the influence of natural quinoline-insoluble material on the kinetics of mesophase formation,* Fuel, 1980, 59, p 360.

113 Forrest M, and Marsh H, *Growth and Coalescence of mesophase in pitches with carbon black additives and in coal,* Fuel, 1983, 62, p 612.

114 Menendez R, Gray E M,Marsh H, Pysz R W and Heintz G H, *Influence of primary QI on the development of secondary quinoline insolubles in coal tar pitches*, Carbon, 1991, 29, p 107.

115 Taylor G H, Pennock G M, FitzGerald J D and Brunckhorst L F, *Influence of QI on mesophase structure*, Carbon, 1993, *31* , pp 341-354.

116 Taylor G H, Pennock G M, FitzGerald J D and Brunckhorst L F, ,*Microstructure of hydrogenated coal-tar pitches*, Carbon, 1994, 32, pp 1389 - 1395.

117 Mochida I, Shimizu K, Korai Y, Otsuka H and Fujiyama S, *Structure and carbonisation proportion of pitches produced catalytically from aromatic hydrocarbons with BF/BF_3*, Carbon, 1988, 26, p 843.

118 Mochida I, Otsuka K, Maeda K and Takeshila K, Carbonisation of aromatic hydrocarbons VII: *The role of active carbonising species in the catalytic carbonisation of pyrene,* Carbon, 1977, 15, p 239.

119 Mochida I, Nakunura E, Maeda K and Takeshita K, *Carbonisation of aromatic hydrocarbons VII*, Carbon, 1976, 14, p 123.

120 Kuo K, Marsh H and Broughton D, *Influence of primary quinoline insoluble and particulate matter on pitch carbonisation*, Fuel, 1987, 66, p 1544.

121 Gentziz T, Rahimi P, Malhotra R and Hirschon A S, *The effect of carbon additives on the mesophase induction period of Athabasca bitumen, Fuel Processing Technology*, 2001, 69, pp 197 - 203.

122 Kanno K, Yoo K E, Fernandez K E J J, Mochida I, Fortina F and Korai Y, *Effect of carbon black on the carbonisation of mesophase pitch*, Carbon, 1994, 32, p 801.

123 Korai Y, Ishida S, Yoon S H, Wang Y G, Mchida I, Nakagawa Y and Mtsumura Y, *Efficient preparation of meso-carbon microbeads with uniform diameter from Ar-isotropic pitch in the presence of carbon black*, Carbon, 1996, 34, p 1569.

124 Korai Y, Wang Y G, Yoon S H, Ishida S, Mochida I, Nakagawa Y and Matsumura Y, *Effects of carbon black addition on preparation of meso-carbon microbeads*, Carbon, 1997, 35, p 875 – 884.

125 Mochida I, Korai Y, Cha-Hun Ku, Watanabe L and Sakai Y, *Chemistry of synthesis, structure, preparation and application of aromatic mesophase pitch*, Carbon, 1999, 38, pp 305 - 328.

126 Perez M, Granda M, Santamaria and Menendez R, *Preventing mesophase growth in petroleum pitches by the addition of coal-tar pitch,* Carbon, 2003, 41, pp 851 – 864.

127 Kanno K, Fernandez J J, Fortin F, Korai I and Mochida I*, Modification to carbonisation of mesophase pitch by addition of carbon black,* Carbon, 1997, 35, p 1627.

128 Machnikowski J, Machnikowska H, Brzozowska T and Zielinski J, Mesophase development in coal-tar pitch modified with various polymers, J. Analytical and Applied Pyrolysis, 2002, 65, pp 147 – 160.

129 Mendez A, Santamaria R, Granda M, Morgan T, Herod A A, Kandiyoti R and Menedendez R, *Influence of granular carbons on pitch properties*, Fuel, 2002, 20, pp 20 – 30

130 Yokono T, Obara T, Iyama S, Sanada Y, *Relationship between hydrogen donor abilities of pitches and coals and optical textures of cokes*, Carbon, 1987, 20, p144

131 Menedez R, Fernandez J J, Bermejo J, Cebolla V, Mochida I and Korai Y, *The role of carbon black/coal-tar pitch interactions in the early stage of carbonization.* Carbon,1996, 34 (7), p 895.

132 Otani S, Yamada S, Koitabashi T and Yokoyama A, *On the raw materials of MP carbon fibre*, Carbon, 1966, 4, p 425.

133 Lewis I C and Singer L S, *The formation of mesophase from acenaphthylene: kinetic and free radical studies*, Carbon, 13, 1975, p 546

134 Lewis I C, Kovac C A , *The role of free radicals and molecular size in mesophase pitch, Carbon,* 1975, 16, pp 425 - 429

135 Stein S E, Golden D M and Benson S W, *Predictive scheme for thermodynamical properties of polycyclic aromatic hydrocarbons*, J. Phys. Chem., 1977, 81, p 314.

136 Stein S E, *Thermodynamical kinetics of anthracite pyrolysis,* Carbon, 1981, 19, p 421.

137 Livingston R, Zeldes H and Conrade M S, *ESR of transient radicals during pyrolysis of fluids,* J. Am. Chem. Soc., 1979, 101, pp 4312- 4322.

138 Lewis I C, *Thermal polymerisation of aromatic hydrocarbons*, Carbon, 1980, 18, p 191.

139 Lewis I C and Edstrom T, *Further electron spin resonance studies of the pyrolysis of aromatic hydrocarbons*, Carbon, 1965, 3, p 327

140 Varma A K, *Thermogravimetric investigations in prediction of coking behaviour and coke properties derived from inertinite rich coals*, Fuel, 2002, 81, pp 1321 – 1334.

141 Romovacek G R, McCullough J P, Perrotta A J, *Formation of mesophase in coal tar pitches- Influence of pyrolytic carbon particles*, Fuel, 1983, 62, pp 1236 - 1239

142 Lewis I C and Singer L S, *Chemistry and Physics of Carbon*, Vol. 17, Marcel Dekker, New York, p 1.

143 Singer L S and Lewis I C, *An electron spins resonance study of the carbonisation of aromatic hydrocarbon acenaphthylene* Carbon, 1964, 2, p 115

144 Marsh H and Reinoso F R, *Sciences of Carbon Materials, University of Alicante*, Spain, 1977, pp 4 – 204.

145 Bragg R H, Crooks D D, Fenn R W and Hammond M L, *The effect of applied stress on the graphitisation of pyrolytic graphite*, Carbon, 1964, 1, p 171.

146 Knight D S and White W B, *Characterisation of diamond films by Raman spectroscopy*, J Material Res., 1989, 4 (2).

147 Mrozoski S, *Electron resonance and electron spin resonance in Turbocrystalline carbon,* Carbon, 1968, 6, p 841.

148 Houska, C R and Warren B E, *The structure of graphite carbons*, J. Applied Physics, 1954, 25, p 1503.

149 Franklin R E, *X-ray study of the graphitization of carbon black*, Acta Cryst, 1951, 4, p 253.

150 Yang Jianli, Stansberry, Zondlo J W and Stiller A H, *Characterisation and carbonisation behaviours of the coal extracts*, Fuel Processing Technology, 2003, 79, pp 207 – 215.

151 Mitchell S J and Thomas C R, *Crystallite parameter correlation for various polymer carbon*, Carbon, 1971, 9, p 253.

152 Konno H, Shiba K, Kaburagi Y, Hishiyama Y and Inagaki M, *Carbonisation and graphitisation of Kapton-type polyimide film having boron-bearing functional group*, Carbon, 2001, 39, pp 1731 – 1740.

153 Lauer G G and Bonstegt K P, *Factors influencing the performance of pitch binders in baking of small carbon electrode,* Carbon, 1963, 1, p 165.

154 Kipling J J, and Sherwood J N, Shooter P V and Thomas N R, *Factors influencing the graphitisation of polymer carbons*, Carbon, 1964, 2, p 315.

155 Otani S, *On the carbon fibre from the molten pyrolysis products*, Carbon, 1965, 3, p 31.

156 Otani S, Yamada K, Koitabashi T and Yukoyama A, *On the raw materials of MP carbon fibre*, Carbon, 1966, 4, p 425.

157 Dubois J, Agache C and White J L, *The carbonaceous mesophase formed in the pyrolysis of graphitisable organic materials*, Material Characterisation, 1997, 39, pp 105 - 119.

158 Mochida I, Shin-Ichi I, Maeda K, Takeshita K, *Carbonisation of aromatic hydrocarbon VI: Carbonisation of heterocyclic compound catalysed by $ALCl_3$*, Carbon, 1977, 15, pp 9 - 16

159 Gillot J, Lux B, Cornuault P and Du Chaffaut F, *Change in structure during desulphurisation of the coke,* Carbon, 1968, 6, p 389.

160 Korai Y and Mochida I, *Cocarbonisation process of petroleum asphalt and coal-derived liquids: an approach to co-carbonisation compatibility*, Fuel 1983, 62, pp 893 - 899.

161 Lewis I C and Singer L S, *Electron spin resonance of stable aromatic radical intermediates in pyrolysis,* Carbon, 1969, 7, p 93.

162 Austerman S B, *In chemistry and physics of Carbon*, P L Walker (Ed.), 1968, 4, Permagon Press, London, p 137.

163 Mitchel J S and Thomas C R, *Crystalline parameter correlations for various polymer carbons,* Carbon, 1971, 9, p 253.

164 Brooks L, US Patent 2734, 799, 1956.

165 Austerman E G, Myron S N and Wagner J W, *Growth and characterisation of graphite single crystal,* Carbon, 1967, 5, p 549.

166 Auguie D, Oberlin M and Oberlin A, *Microtexture of mesophase spheres as studied by high resolution conventional transmission electron microscopy*, Carbon, 1980, 18, pp 337-346

167 Orbelin A and Rouchy J P, *Transformation in non-graphitisable carbons,* Carbon, 1971, 9, p 3.

168 Acheson E G, US Patent 711, 031, 1902.

169 Baraniecki C, Pinchbeck F, Pickering B, *Some aspects of graphitisation induced by iron and ferro-silicon addition*, Carbon, 1969, 7, pp 213-218.

170 Parker W E, Merk R W and Woodriff E M, *Use of additives for graphite densification and improved neutron radiation stability*, Carbon, 1965, 2, pp 395-406.

171 Isaac L C, *The graphitisation of organic compounds-II, X-ray properties of carbons prepared from a series of alkylated carbazoles*, Carbon, 1969, 7, p 531.

172 Fitzer E and Kegel B, Reaction von kohlenstoffgesattigter vanadium carbidschmelzer mit ungeordnetem kohlenstoff *Carbon*, 1968, 6, p 433.

173 Edstrom T and Lewis I C, *Chemical structure and graphitisation: X-ray diffraction studies of graphites derived from polynuclear aromatics*, Carbon, 1969, 7, p 85.

174 Kirk-Othmer's Encyclopaedia of Chemical Technology 4th Ed, Executive editor Kroschwitz J, Vol 4, pp 949 - 1015

175 Zondlo J W, Stanberry P G, Seera M S, Pavlovic A S and Babu V S, *Measurement and control of anisotropy in ten coal-based graphites*, Carbon, 32 (3), 1996, pp 431 – 435.

176 Kirk-Othmer's Encyclopaedia of Chemical Technology 4th Ed, Executive editor Kroschwitz J, Vol 6, pp 424 - 594

177 Wakayama H, Mizuno J, Fukushima Y, Nagano K, Fukunaga T and Mizutani U, *Structural defects in mechanically ground graphite,* Carbon, 1999, 37, pp 947 - 952.

178 Parker W E, Merk R W and Woodriff E M, *Use of additives for graphite densification and improve neutron radiation stability*, Carbon, 1965, 2, p 395.

179 Marsh H, *Introduction to Carbon Science,* 1989, Permagon press, UK, pp 5 – 38.

180 Scaroni A W, Khan M R, Ljubisa S E and Randovic R*, Coal Pyrolysis,* 1980, *Vol*. A7, Pennsylvania State University, USA.

181 Madsen L D, Charavel R, Birch J and Svedberg E B, *Assessment of MgO (100) and (111) substrate quality by X-ray diffraction,* J Crystal Growth, 2000, 209, pp 91- 101.

182 Cottinett D, Couderc P and Romain J L S, *Raman microprobe study of heat-treated pitches,* Carbon, 1988, 26, pp 339 - 344.

183 Knight S D and White W B*, Characterisation of diamond films by Raman spectroscopy,* J Materials Research, 1989, 4, 1989, pp 385 – 392.

184 Jallad K N, Santhanam M, Cohen M D and Ben-Amotz D*, Chemical mapping of thaumasite in sulphate-attacked cement mortar using near-*

infrared Raman imaging microscopy, Cement and Concrete Research, 2002, 31, pp 953 –958.

185 *Laspade P, Marchand A, Couzi M and Cruege F, Caracterisation de materiaux carbon par micropectrometrie Raman,* Carbon, 1984, 22, pp 375 – 385.

186 Cuesta A, Dhamelincourt P, Laureyns J, Martinez-Alonzo A and Tascon J M D*, Raman microscope studies of carbon materials,* Carbon, 1994, 32, pp 1523 – 1532.

187 Dumont M, Chollon G, Dourges M A, Pailler R, Bourrat X, Naslain R, Bruneel J L and Couzi M*,* Chemical, microstructural and thermal analysis of a naphthalene-derived mesophase pitch, Carbon, 2002, 40, pp 1475 – 1486.

188 Wakayama H, Mizuno J, Fukushima Y, Nagano K, Fukunaga T and Mizutani U*, Structural defects in mechanically ground graphite,* Carbon, 1999, 37, pp 947-952

189 Knight D S and White W B, *Characterisation of diamond films by Raman spectroscopy,* J Materials Research, 1989, 4, pp 385-392.

190 Merck*, Reagent Diagnostic Chemicals, 1992/93*.

191 Aldrich, *Catalogue Handbook of Fine Chemicals*, 1994-1995.

192 Fluka, *Scientific Research*, 2003/2004.